

Observational Constraints on the Formation and Evolution of Binary Stars

R. J. White¹ and A. M. Ghez

UCLA Division of Astronomy and Astrophysics, Los Angeles, CA 90095-1562

ABSTRACT

We present a high spatial resolution multi-wavelength survey of 44 young binary star systems in Taurus-Auriga with separations of 10 - 1000 AU. These observations, which were obtained using the Hubble Space Telescope and the NASA Infrared Telescope Facility, quadruple the number of close (< 100 AU) binary stars with spatially resolved measurements from 0.3 to 2.2 μm and are the first 3.6 μm measurements for the majority of the companion stars in the sample.

Masses and ages are estimated for the components observed at optical wavelengths. The relative ages of binary star components are more similar than the relative ages of randomly paired single stars within the same star forming region. This is the first statistically significant evidence for coeval formation. Only one of the companion masses is substellar, from which we conclude that the apparent overabundance of T Tauri star companions relative to main-sequence star companions is not due to a wealth of substellar secondaries that would have been missed in main-sequence surveys.

The circumstellar environments of binary star systems are studied in this work through three diagnostics - the infrared color $K - L$, the ultraviolet excess ΔU , and H α emission. Several conclusions are drawn. First, the mass accretion rates for primary stars are similar to single stars, which suggests that companions as close as 10 AU have little effect on the mass accretion rate. Second, although most classical T Tauri star binaries retain both a circumprimary and a circumsecondary disk, there are several systems with only a circumprimary disk. Systems with only a circumsecondary disk are rare. This suggests that circumprimary disks survive longer than circumsecondary disks. Third, primary stars accrete at a higher rate, on average, than secondary stars. This is most likely because of their larger stellar mass, since the mass accretion rates for both single and binary T Tauri stars exhibit a moderate mass dependence. Fourth, approximately 10% of T Tauri binary star components have very red near-infrared colors ($K - L > 1.4$) and unusually high mass accretion rates. This phenomenon does not appear to be restricted to binary systems, however, since a comparable fraction of single T Tauri stars exhibit the same properties. These high accretion stars are probably not at an earlier stage of evolution, as has been proposed. Their semblance of younger protostars at optical and infrared wavelengths is most likely because of their similar

¹Present Address: McDonald Observatory, R.L.M. Hall 15.308, Austin, TX 78712-1083

high levels of accretion, which are above the norm for T Tauri stars, and not because of similar ages.

The stellar and circumstellar properties are also used to indirectly trace the evolution of circumbinary material. In contrast to single T Tauri stars, which have disk dissipation timescales comparable to their ages, the disk dissipation timescales for binary T Tauri stars are roughly 1/10 of their ages. Replenishment of the inner circumstellar disks may be necessary to explain the continuing disk accretion in these systems. The longer disk lifetimes of circumprimary disks, despite their higher depletion rates, suggests that circumprimary disks are being preferentially replenished, possibly from a circumbinary reservoir with low angular momentum relative to the binary. Further support for circumbinary reservoirs comes from the observed correlated presence of circumprimary and circumsecondary disks for binaries with separations of less than ~ 200 AU. The presence of disks appears uncorrelated for wider binaries. Additionally, binaries with separations of less than ~ 100 AU exhibit a higher fraction of high mass ratio (m_s/m_p) pairs than wider binaries. These separation dependent properties can be explained if the components are being replenished from a common circumbinary reservoir with low angular momentum. The components of the closest pairs are expected to be more equally replenished than the widest pairs, which consequently sustains both disks and drives their mass ratio toward unity. Overall, the results of this study corroborate previous work that suggests fragmentation is the dominant binary star formation mechanism; disk instabilities and capture seem unlikely.

Subject headings: binaries: visual — — stars: pre-main-sequence — stars: late-type — — circumstellar matter

1. Introduction

Surveys of young low mass stars in nearby star forming regions have established that the majority are members of binary star systems (e.g., Ghez et al. 1993; Leinert et al. 1993; Simon et al. 1995). More than half of these binary T Tauri stars have separations less than 100 AU, the characteristic size of a circumstellar disk (e.g., Beckwith et al. 1990). The ubiquity of these close companions has raised two important and related questions concerning the star formation process: “How do binary stars form?” and “How does a companion affect the distribution of circumstellar material?”. Unfortunately, obtaining the answers to these questions has been inhibited by the inherent difficulty of spatially resolving binaries with small angular separations. At the distance of nearby regions of star formation ($D \sim 150$ pc), the majority of these pairs have separations of less than 1 arcsecond and are unresolvable with standard ground-based observing techniques. Most T Tauri binary stars have only been spatially resolved at the one wavelength, typically $2.2 \mu\text{m}$, used in the high resolution lunar occultation or speckle imaging surveys that revealed their multiplicity (e.g., Ghez et al. 1993; Leinert et al. 1993; Simon et al. 1995). Extracting the stellar

and circumstellar properties (e.g., stellar temperature and luminosity, mass accretion rate) from this one resolved measurement is not possible since young stars have substantial excess emission and line-of-sight extinction. Determining these properties requires spatially resolved measurements over a broad range of wavelengths. A few studies have had some success accomplishing this for wide binaries, or for small samples of close binaries, and the combined results of these studies have been useful in understanding how binary stars form (Cohen & Kuhl 1979; Hartigan et al. 1994; Koresko 1995; Brandner & Zinnecker 1997; Ghez et al. 1997b; Woitas et al. 2001). Although the samples are small, the mass ratio and secondary mass distributions of T Tauri binary stars, as well as their comparable ages, tentatively suggest that core fragmentation (e.g., Boss 1988) is the dominant binary star formation process, while capture and disk instability scenarios seem unlikely (Ghez et al. 1997b).

Current models of the binary star formation process offer a framework with which we can begin to explore the distribution of circumstellar material in binary star systems. Numerical simulations of circumstellar material within a binary suggest that both circumprimary and circumsecondary disks are possible, as well as circumbinary structures (Artymowicz & Lubow 1994; Bate & Bonnell 1997). The inner disks are expected to be tidally truncated at roughly 1/3 of the semi-major axis of the binary (Artymowicz & Lubow 1994). Few observational constraints are available, however, to check these predications. Many spatially unresolved binary T Tauri stars exhibit strong H α emission and photospheric excesses suggesting the presence of an accreting inner circumstellar disk. However, it is in general not known whether this material is distributed in a circumprimary disk, a circumsecondary disk, or both. The presence of any accreting disks in systems with separations less than 100 AU is somewhat surprising given the small mass of these presumably truncated disks, as inferred from millimeter measurements of the unresolved pairs ($M_{\text{disk}} \lesssim 0.01 M_{\odot}$; Osterloh & Beckwith 1995; Dutrey et al. 1996; Jensen et al. 1996). If the accretion rates for these close binaries are similar to the rates for single T Tauri stars ($\sim 10^{-8} M_{\odot} \text{yr}^{-1}$; Gullbring et al. 1998), and if their ages are ~ 1 Myrs, many of these disks should have already dissipated. This potential timescale problem may be alleviated, however, if the inner circumstellar disks are being replenished from a circumbinary reservoir (Prato & Simon 1997).

Several spectroscopic studies have identified circumprimary disk and circumsecondary disk accretion signatures for relatively wide T Tauri binaries ($\gtrsim 100$ AU) resolvable with ground-based spectroscopy (Brandner & Zinnecker 1997; Prato & Simon 1997; Monin et al. 1998; Duchêne et al. 1999b; White et al. 1999). This work showed that at least for widely separated pairs, both circumprimary and circumsecondary disks can exist. A variety of high resolution studies have been carried out in order to resolve the properties of the closest and potentially most interesting pairs with separations of less than 100 AU. These studies are typically conducted at near-infrared (NIR) wavelengths where high resolution techniques such as speckle imaging or adaptive optics are more realizable. The majority of these studies, however, include only one or a few multiple systems and typically focus on peculiar systems with exceptionally NIR bright companions (e.g., T Tauri: Ghez et al. 1991; XZ Tau: Haas et al. 1990) or with extended circumstellar emission (GG Tau:

Roddier et al. 1996; UY Aur: Close et al. 1998). Only one extensive NIR survey of close (< 100 AU) binaries has been carried out (Woitas et al. 2001). While the components of many of these systems show signatures of retaining a circumstellar disk, details are difficult to interpret since the underlying stellar emission is unknown; the stellar properties are best extracted from optical measurements where the photospheric emission dominates and where the spectral types and colors of late-type stars are well established (e.g., Luhman 1999; White et al. 1999). A limited number of close binary T Tauri stars with signatures of accretion have been imaged with high resolution optical techniques (DD Tau: Bouvier et al. 1992; XZ Tau: Krist et al. 1997, 1999; FS Tau: Krist et al. 1998; DF Tau, GG Tau, UZ Tau: Ghez et al. 1997). No complete optical survey of close (< 100 AU) T Tauri binary stars has yet been conducted.

In this paper, we present spatially resolved observations of 44 T Tauri multiple star systems with projected separations of 10-1000 AU in the nearby star forming region Taurus-Auriga ($D = 140$ pc; Kenyon et al. 1994). These 0.3 to 3.6 μm observations represent the largest, most complete, broad-wavelength survey of multiple T Tauri stars to date. The source list, observations, and analysis are described in §2. The stellar and circumstellar properties are derived in §3 and then used in §4 to understand how circumstellar material is distributed in binary star systems. The results are also used to investigate the accretion rate’s dependence on the stellar mass, to determine the evolutionary state of infrared-bright, high accretion stars, to further constrain how binary stars form, and to confirm the over-abundance of T Tauri stellar companions in Taurus-Auriga relative to main-sequence stars.

2. Observations, Data Analysis, and Results

2.1. Sample Definition

The observational objective of this program was to observe a complete sample of multiple T Tauri star systems in the Taurus-Auriga star forming region with separations ranging from $0''.07 - 7''.0$ (10 - 1000 AU). The lower limit corresponds to the smallest separations resolvable with speckle imaging on a 3-m telescope at $2\mu\text{m}$ (i.e., $\lambda/2D$) and the upper limit insures a high probability of physical association ($\sim 99\%$, Reipurth & Zinnecker 1993). In this survey, binaries with separations of 10 - 100 AU are referred to as *close binaries* and those between 100 - 1000 AU are *wide binaries*. The initial target list, which was constructed in 1995, consists of 50 pairs in 47 systems; systems in this study are groups of stars with separations less than $10''.0$. The majority of the binaries were identified from the high resolution multiplicity surveys of Ghez et al. (1993), Leinert et al. (1993)², Richichi et al. (1994), and Simon et al. (1995). Additional wide binaries were extracted from Cohen & Kuhl (1979), Herbig & Bell (1988), and Hartmann et al. (1991). Of these 50 pairs, 46 have been

²The binary stars HBC 351 and HBC 358 were not included because their low Li I abundance (Walter et al. 1988; Martín 1994) suggests that they are not T Tauri stars (Martín 1998)

observed in this study (DI Tau, HBC 412, Haro 6-10, and HV Tau were not observed) and 43 were resolved (V410 Tau A-B is unresolved and RW Aur Ba-Bb and FY Tau A-B are probably not binary stars; see §2.3.2). Two additional companions discovered in these observations (V410 Tau C and FW Tau C) and supplemental measurements from the literature (including HV Tau and Haro 6-10) increase the total number of pairs resolved at multiple wavelengths to 47 (44 systems). More specifically, 41 pairs (39 systems) have been spatially resolved at both 2.2 and 3.6 μm (§2.2) and 28 pairs (25 systems) have been spatially resolved at optical wavelengths (§2.3; includes the T Tau system, although T Tau B was not detected). Table 1 provides a summary of the targets and observations included in this analysis.

Both classical T Tauri star (CTTS) systems and weak-lined T Tauri star (WTTS) systems are included in the larger sample of sources observed at NIR wavelengths, whereas the smaller sample of sources observed at optical wavelengths focuses primarily on the CTTS (Table 1). CTTSs are young stars that display signatures of active accretion such as strong $\text{H}\alpha$ emission and large UV excesses. In contrast, WTTSs are young stars that are not thought to be accreting. These stars exhibit only ‘weak’ $\text{H}\alpha$ emission and little if any UV excess, both of which can be attributed entirely to an active chromosphere (e.g., Walter et al. 1988). CTTS and WTTS systems are distinguished here based on the strength of $\text{H}\alpha$ emission, usually in the unresolved spectra of the pair, and a classical/weak dividing value set by Martín (1998). A negative equivalent width (EW) indicates emission. T Tauri stars are considered classical if their $\text{EW}(\text{H}\alpha) \leq -5 \text{ \AA}$ for K stars, $\leq -10 \text{ \AA}$ for M0-M2 stars and $\leq -20 \text{ \AA}$ for cooler stars. The T Tauri types of the components within these systems are discussed in §3.2.2.

The primary star, A, of each binary pair is defined to be the more massive component, if mass estimates based on spatially resolved optical measurements are available (§3.2). For systems without resolved optical measurements, the primary is assumed to be the component that is brighter at 2.2 μm . This assignment of primary and secondary is consistent with previous studies of these systems, except in the case of LkHa 332/G1. As will be shown in §3.2, the fainter component of this system (historically denoted as ‘B’) appears to be the more massive star. To avoid confusion in comparisons with previous measurements, the ‘A’ component of this system will always refer to the brighter component while the ‘B’ component is the true primary.

2.2. Near-Infrared Imaging

2.2.1. Observations

Observations at K (2.2 μm) and L (3.6 μm) of Taurus-Auriga binaries were obtained on 1996 Dec 5-6 and 1997 Dec 4-9 using the NASA Infrared Telescope Facility in Hawaii with NSFCAM (Rayner et al. 1993; Shure et al. 1994), which contains a 256×256 array. All images were obtained using the finest plate scale available. The plate scale ($0''.0532 \pm 0''.0010$ / pixel) and orientation with respect to the cardinal directions ($0.0^\circ \pm 1.0^\circ$) were established through observations of known

binaries. Systems with separations less than $1''.4$ were observed in a speckle imaging mode. These observations were conducted using only the central 128×128 pixels of the detector (for faster readout times), resulting in a field-of-view of $6''.8 \times 6''.8$. Typically, 1200 snapshots (0.1 second exposures) in sets of 400 were obtained for each source, interleaved with similar observations of a point source. Photometric standards were also observed regularly in the same manner for photometric calibration, weather permitting. Direct images of systems with separations greater than $1''.4$ were obtained on 1997 Dec 6 during photometric conditions using the full 256×256 array of NSFCAM, resulting in a field-of-view of $13''.6 \times 13''.6$. For each pair, dithered images with a total on-source integration time of 25-200 seconds were obtained, depending upon source brightness. Photometric standards and the single star SAO 76599 (Chen & Simon 1997) were also observed for photometric calibration and point spread function (PSF) fitting.

2.2.2. Data Analysis & Results

All the NIR images are first sky subtracted, flat fielded and bad pixel corrected. The speckle images are subsequently analyzed with both classical speckle analysis (Labeyrie 1970) and a shift-and-add technique (e.g., Bates & Cady 1980; Christou 1991; Ghez et al. 1998). The speckle analysis yields the diffraction-limited Fourier amplitudes of each object. The binary star flux ratio, separation, and orientation ($\pm 180^\circ$) are determined from a χ^2 minimization of a two-dimensional fit to the Fourier amplitudes (see Ghez et al. 1995 for details of the fitting procedure and the error analysis). The remaining 180° ambiguity in the position angle is eliminated on the basis of the shift-and-add images. The rapid sampling of the speckle imaging mode provides a useful check of the photometric conditions. When the count rate is constant over the ~ 1200 frames, the observations are calibrated relative to the photometric standards. These results are reported in Table 2.

The direct images for each of the wider pairs are registered and averaged to produce a high signal-to-noise ratio image. Photometry for the individual components of the multiple star systems is then obtained from these average images in two steps. First, the photometry of each system is determined by comparing the flux densities measured in large apertures to the flux densities of the photometric standards. Next, the relative flux densities and positions of each pair are determined by PSF fitting using the DAOPHOT package within IRAF³. Uncertainties in the system's magnitudes and flux ratios are calculated from the rms variations of the results from carrying out the same procedure on the original unregistered images. The uncertainties associated with the relative positions are estimated by combining the rms variations of the results from the unregistered images with the uncertainty in the plate scale and array orientation. System magnitudes and flux ratios for the pairs imaged directly are combined and the resulting component magnitudes and relative

³IRAF is distributed by the National Optical Astronomy Observatories, which are operated by the Association of Universities for Research in Astronomy, Inc., under cooperative agreement with the National Science Foundation.

positions for each pair are listed in Table 2.

The new speckle and direct imaging results provide the first spatially resolved L -band measurements for 32 of the 41 pairs resolved at both K and L . Since the new K and L speckle observations were not obtained simultaneously and often not photometrically, the results are combined with previous measurements to obtain component magnitudes. This is done by using the mean flux density (typically taken from the compilation of Kenyon & Hartmann 1995) and median flux ratio for each system. The resulting magnitudes for each component are given in Table 2, following any new observations reported here. Uncertainties in the component magnitudes are based on the standard deviations of multiple measurements, when available, and therefore should reflect the variability of the system as well as the measurement uncertainties; the references used are listed. Additionally, K and L measurements from the literature of Haro 6-10 and HV Tau (Leinert & Haas 1989; Ménard et al. 1993; Woitas et al. 1998), which were not observed here, are combined and listed in Table 2. Although many of the combined observations are non-simultaneous, this is not likely to compromise our interpretation since the variations of most young stars at NIR wavelengths tend to be relatively small ($\sigma_K < 0.2$ magnitudes), and variations of their near-infrared colors are even smaller (< 0.1 magnitudes; Kenyon & Hartmann 1995). The K and L component magnitudes used in the analysis (§3 and §4) are marked with asterisks in Table 2.

2.3. Optical and Ultra-Violet Imaging

2.3.1. Observations

Optical and UV measurements of 21 pairs plus 2 newly discovered components were obtained with the HST (Table 1). These observations were initiated in Cycle 4 (program ID 5395) of the HST mission (1994) with a pilot study of 4 CTTS and 2 WTTS systems (Ghez et al. 1997b). Here we present the results of a more extensive follow-up study, which was carried out in Cycle 6 (program ID 6735) of the HST mission (1997-1998) and which focused specifically on close CTTS binary systems. The systems observed in Cycle 6 were imaged through the same 5 broad-band filters used in Cycle 4: F336W, F439W, F555W, F675W, and F814W (filters that are the approximate equivalents to the Johnson-Cousins U , B , V , R_c and I_c passbands; Biretta et al. 1996), as well as the narrow-band $H\alpha$ filter F656N. In a total of 9 Cycle 6 pointings, 12 close and 1 wide binary stars were observed. For each pointing, the primary source was centered on the Planetary Camera of the WFPC2, which is an 800×800 CCD with a pixel size of $0''.0455$ and a field-of-view of $35'' \times 35''$ (Biretta et al. 1996). To improve the spatial resolution, the sources were imaged at two positions, offset by 10.5 pixels along the axes of the detector. To maximize the signal-to-noise ratio while allowing for possible source variability, the exposure times were set to achieve half-well counts in the CCD detector, based on ground-based measurements of the unresolved pairs. Specific details regarding these observations can be accessed from the Hubble Data Archive at the Space Telescope Science Institute (STScI).

In addition to the pairs observed with the HST, 8 other Taurus-Auriga binaries have spatially resolved optical measurements and are included in this study. Six wide binaries (Haro 6-37 Aa-B, UX Tau A-B, UX Tau A-C, HN Tau A-B, V710 Tau A-B, HV Tau A-C) have been resolved with direct imaging (Hartigan et al. 1994; Kenyon & Hartmann 1995; Magazzú & Martín 1994) and 2 close binaries (DD Tau and T Tau) were resolved with high resolution imaging techniques (Bouvier et al. 1992; Gorham et al. 1992; Stapelfeldt et al. 1997), although T Tau B was not detected. Together with measurements from the literature, the new HST observations provide spatially resolved measurements at optical wavelengths of the complete sample of CTTS binaries brighter than $V = 17$ magnitudes⁴ and with separations ranging from $0''.07$ to $0''.72$, that were known at the time the HST observations were proposed.

2.3.2. Data Analysis & Results

The STScI carried out the initial data processing through the ‘calibration pipeline’ (Holtzmann et al. 1995a). We further correct the data for the charge transfer efficiency problem associated with the WFPC2 detector using the relations of Whitmore et al. (1999). Since the 6 sources observed in Cycle 4 were initially analyzed before these corrections were available (Ghez et al. 1997b), these measurements are updated with the new calibrations. Although the majority of charge transfer efficiency corrections are less than 5 percent, some corrections for fainter systems observed through the F336W and F439W filters are 10 percent or more and dominate the photometric uncertainty. Cosmic ray events are removed by interpolating from neighboring pixels. Each set of images is registered and combined by centroiding on the brightest point sources.

Photometry for the widest components ($> 0''.5$) of the multiple star systems is carried out by summing the counts within 5 pixel ($0''.23$) radius apertures centered on the stars. The flux ratios are computed from the ratios of the components’ counts. System magnitudes in the Vega magnitude system are determined from the sum of the components’ counts, using the known filter zero points and aperture corrections (Holtzmann et al. 1995b; Keyes et al. 1997). Since the systems observed here typically have large source counts, the dominant source of uncertainty, in most cases, is the uncertainty in the charge transfer efficiency correction, which we estimate to be one half of the applied correction (Whitmore et al. 1999). The photometric uncertainties are determined by convolving this uncertainty with the ranges of the flux measurements from the original unregistered images.

Photometry for the individual components of the closest ($< 0''.5$) multiple star systems is accomplished in two steps. First, the Vega magnitudes of each system are determined from the total counts within 35 pixel ($1''.59$) radius apertures and the known filter zero points and aperture

⁴Haro 6-28 ($V = 17.30$ mag; Kenyon & Hartmann 1995) was the only known CTTS binary excluded because of its magnitude.

corrections. Uncertainties are computed in the same manner discussed above for the wider pairs. Next, the relative flux densities are determined using the PSF fitting routines of the DAOPHOT package within IRAF. The PSFs used in the fitting process are constructed from either isolated sources within the images (e.g., UZ Tau A) or from the PSF Archive available at the STScI. These PSFs are typically the average of three or more single stars that are positioned similarly on the chip as the target binary. The rms variations of the results from carrying out the same procedure on the original images using multiple PSFs provide estimates of the flux ratio uncertainties. The flux ratios and system magnitudes for all pairs imaged with the HST are reported in columns 3 and 4 of Table 3.

This photometry procedure works well for all systems except FS Tau. Extended emission in this system biases the stellar flux densities measured in large apertures as described above toward brighter values. Therefore the component magnitudes for this system are determined directly by using flux calibrated PSFs in the PSF fitting process. These values are combined into a flux ratio and total stellar magnitude and are listed in Table 3. These values may nevertheless still be biased because of the extended emission.

Columns 8 and 9 of Table 3 list the separations and position angles of the binary stars imaged with the HST. These are derived from the photometric centers of the components for pairs wider than $0''.5$, and from the results of the PSF fitting for closer pairs. The uncertainties associated with the relative positions are estimated by combining the rms variations of the results from the five broad-band filters with the uncertainty in the plate scale ($\sim 10^{-5}$ arcseconds per pixel) and spacecraft orientation ($\sim 0.03^\circ$) (Holtzmann et al. 1995a; Biretta et al. 1996).

Flux ratio lower limits are also given in Table 3 for the non-detections: FW Tau C in the F336W, F439W, and F555W filters and FV Tau/c B in the F336W and F439W filters. Since these two stars are detected through at least two filters, these positions are used to identify their locations in the other images. A scaled PSF is added at these positions to determine the minimum detectable flux densities using the DAOPHOT package within IRAF. No companion is detected to the ‘suspected binary’ FY Tau (Richichi et al. 1994). This missing companion is discussed below.

With system magnitudes and flux ratios, the magnitudes of each binary star component are determined. In order to better compare the HST broad-band measurements with previous ground-based observations and standard photospheric colors, the HST broad-band measurements of each resolved star are transformed to the more standard Johnson-Cousins filter system. These filter transformations are derived in Appendix A. The transformation values are typically small, with only weak dependencies on stellar temperature (spectral type) for stars hotter than about M5. The spectral types inferred in §3.1 are used to assign specific transformation values. Magnitudes in the Johnson-Cousins filter system for the T Tauri stars observed here are listed in columns 6 and 7 of Table 3 and are used in the analysis of the stellar and circumstellar properties (§3 and §4). The sums of the components’ flux densities for all pairs agree well with the ranges measured in previous lower resolution ground-based measurements (e.g., Herbst et al. 1994).

The measured F656N flux densities (F_{obs}) are converted to EW[H α] measurements, a common measure of H α emission. In order to estimate and remove the photospheric contribution to the narrow-band flux, F656N - F675W colors are derived from dwarf standard stars that have no appreciable H α emission (Appendix A). The observed F675W flux densities, attributable primarily to photospheric emission, are then converted to photospheric F656N flux densities (F_{phot}) using these colors. Since the F656N filter has an effective rectangular width of 28.3 Å and is centered on H α (Biretta et al. 1996), the EW[H α] values are approximated as $EW[H\alpha] = -28.3 \text{ \AA} \times (F_{obs} - F_{phot})/F_{phot}$ and are listed in Tables 3 and 4. Uncertainties are estimated from the convolution of the flux density uncertainties, the transformation uncertainty (0.02 magnitudes), and the filter width uncertainty (1 Å). Combining the flux densities for the components results in photometric EW[H α] estimates for the systems that are in reasonable agreement with previous spectroscopic measurements of the unresolved pairs (e.g., Herbig & Bell 1988). Specific differences are most likely because of variable H α emission, a common characteristic of classical T Tauri stars. However, for the strongest H α emission sources ($EW[H\alpha] > 100 \text{ \AA}$), the photometric estimates provide only lower limits since the emission-line will begin to contribute significantly to the F675W measurements. The photometric method for estimating EW[H α] is therefore, at the very least, sufficiently robust for distinguishing between CTTS and WTTS types.

Missing Companions

The suspected companion to FY Tau (separation $> 0''.15$; Richichi et al. 1994) is not detected in the HST images. Likewise, as discussed in Ghez et al. (1997b), the proposed companion of RW Aur B (Ghez et al. 1993) is not detected in the HST images. These suspected companions have only been reported once based on low signal-to-noise ratio NIR measurements. If the NIR measurements in question are used to estimate the photospheric flux at I_c (assuming no K excess emission, the same age and extinction as the primary, and dwarf colors, see §3.1), the predicted fluxes are 4.9 magnitudes (RW Aur C) and 4.2 magnitudes (FY Tau B) brighter than the I_c detection limits (~ 17.8 magnitudes in both cases). Under these assumptions, these companions should be easily seen in the HST images. It is possible that these missing companions are substantially more extinguished than their primary, but the considerable extinction differences required to reconcile the colors ($A_V[\text{sec}] > A_V[\text{prim}] + 8.0$ magnitudes) are inconsistent with the similar extinctions of binary star components (§3.1). We consider it more likely that the weak lunar occultation detection of FY Tau B was caused by scintillation, as considered possible by Richichi et al. (1994). The similarly weak detection of RW Aur C may also have been a false detection. We, hereafter, consider FY Tau to be a single star and RW Aur B to be a single star in a wide binary.

New Companions

New companions are discovered in the V410 Tau system (see Ghez et al. 1997b) and the FW Tau system in the HST images. The new companion to FW Tau, at a separation of $2''.3$, is particularly

intriguing as it is exceptionally bright in the narrow-band $H\alpha$ filter, but is very faint in the F675W and F814W filters and is not detected at shorter wavelengths. The strong Balmer series emission ($EW[H\alpha] > -454 \pm 224$; Table 3) is typical of non-stellar Herbig-Haro objects, which are knots of shocked gas that typically lie along the path of stellar jet (Schwartz et al. 1983). However, the emission comes from an isolated, unresolved point source and the nearby WTTS binary FW Tau A & B is an unlikely source for a jet. Since FW Tau C is detected through the F814W filter, which does not include many strong emission-lines commonly found in Herbig-Haro objects (Schwartz et al. 1983), a stellar interpretation is preferred.

The single star FZ Tau, at a separation of $17''.2$ from the suspected binary FY Tau (see above), was serendipitously observed but is not considered a companion. For completeness, the measurements of the single stars FY Tau and FZ Tau are provided in Appendix B.

Extended Emission

With the exception of FS Tau, none of the systems show evidence of extended nebulosity. Since the exposure times for all sources were scaled similarly to avoid saturation (§2.3.1), the sensitivity to extended emission is limited, but is nevertheless roughly uniform for the entire sample. Limiting surface brightnesses are estimated from the standard deviation of the counts per resolution element ($0''.09 \times 0''.09$ or 2×2 pixels) at a separation of $0''.5$ from the primary star’s position in the residual, PSF subtracted images (§2.3). Integrated over 0.008 arcsec^2 , the surface brightness is typically 7 magnitudes at F555W and 8 magnitudes at F814W below the magnitude of the primary. All but one (19/20) of the T Tauri star systems imaged with the HST in this program appear to be unresolved point sources at this resolution and dynamic range.

In contrast to the other systems, the FS Tau system reveals extended emission at all wavelengths observed with the HST. This is also seen in the long-exposure images obtained by Krist et al. (1998) with HST through the F555W and F814W filters. With our non-saturated images over a broader range of wavelengths, we analyze FS Tau’s extended emission by differencing the results of wide aperture photometry and the stellar flux densities derived above. In order to compare the results directly with those of Krist et al. (1998), a radius of $4''.0$ is used for the wide aperture photometry. A spectral type of M1, which was measured for the entire system by Cohen & Kuhi (1979), is adopted for the filter transformations. The resulting values are listed in Table 4 and, in the case of the wide aperture magnitudes, are fainter by 0.15 magnitudes at both V and I_c than the earlier measurements. Nonetheless, like the Krist et al. (1998) results, the nebulous emission appears bluer than the stellar emission ($V - I_c[\text{Nebula}] = 2.52$ versus $V - I_c[\text{Binary}] = 3.19$) as is expected for scattering by small dust grains. There is no evidence of $H\alpha$ emission from the nebulosity as might be expected from the interaction of a stellar jet with remnant cloud material (Eisloffel & Mundt 1998). The spatial distribution of the extended emission in the narrow-band $H\alpha$ image is the same as in the broad-band images, as expected for dust scattering. Additionally, the $EW[H\alpha]$ of the nebulosity ($-40.8 \pm 8.0 \text{ \AA}$) is actually diminished relative to the stellar pair

$(-72.1 \pm 3.5 \text{ \AA})$, suggesting a higher optical depth at $H\alpha$ due to H I gas in the nebulosity.

2.4. Optical Spectroscopy

2.4.1. Observations

The Faint Object Spectrograph (FOS) aboard the HST (program ID 6014) was used to obtain spatially separated spectra of the close binaries XZ Tau (1996 Feb 2), GH Tau (1996 Oct 6) and V955 Tau (1996 Dec 4). GG Tau A was also observed (1995 Nov 8) as part of this program, and its spectra were presented in White et al. (1999). These observations were conducted using the $0''.09 \times 0''.09$ aperture with the G570H (4600 - 6800 \AA) grating, which yielded a spectral resolution of $R \approx 1400$ (Keyes et al. 1995). Other observational details can be accessed from the Hubble Data Archive at STScI. The observations were carried out by first centering the $0''.09$ aperture on the brighter component, assumed to be the primary, and obtaining its spectrum and then offsetting to the known location of the secondary. This strategy worked well for GG Tau A and spectra of both components were obtained. For the XZ Tau system, the companion star was unexpectedly the brightest optical component at the time of the observations and consequently its spectrum was obtained first. The second spectrum obtained at the nominal offset resulted in a spectrum of the sky on the opposite side of the primary star. To avoid this incorrect source acquisition due to source variability again, the FOS acquisition strategy for GH Tau and V955 Tau was adjusted to obtain an offset spectrum at both plus and minus the separation of the companion. This strategy resulted in spectra of both components of the GH Tau system as well as a spectrum of the sky. While the measurement of V955 Tau A’s spectrum was successful, the attempt on V955 Tau B failed due to an unusual telescope error that offset the telescope to the wrong position. Altogether, these observations resulted in spatially resolved spectra for 6 components.

2.4.2. Data Analysis & Results

All HST spectra were initially calibrated by the FOS calibration pipeline (Keyes et al. 1997). However, flat fielding information for small apertures was not initially available, thus the spectra are flat fielded using the appropriate sensitivity functions provided by T. Keyes & E. Smith (private communication), which are now available in the calibration pipeline. The resulting spectra of XZ Tau B, GH Tau A & B and V955 Tau A are shown in Figure 1 (see White et al. 1999 for GG Tau A results). The spectra of all components show strong $H\alpha$ emission typical of classical T Tauri stars ($EW[H\alpha] = -76 \pm 4 \text{ \AA}$ for XZ Tau B, $-12 \pm 1 \text{ \AA}$ for GH Tau A, $-15 \pm 1 \text{ \AA}$ for GH Tau B, $-18 \pm 2 \text{ \AA}$ for V955 Tau A). Because of the limited resolution, no Li I at 6708 \AA is detected in any of the FOS spectra; approximate equivalent width upper limits to the detection of any features are 1 \AA . Of particular interest is the spectrum of XZ Tau B, which exhibits prominent Balmer series emission ($H\alpha$ and $H\beta$) and an array of strong emission-lines, including Fe I, Fe II, and Mg

I features. The spectrum and emission-line intensities are remarkably similar to those seen in the spectrum of DG Tau, a very high accretion single T Tauri star with prominent jet (Hessman & Guenther 1997), and suggests that XZ Tau B powers the jet in this system (Krist et al. 1999).

The primary goal of the spectroscopic analysis presented here is accurate spectral type classification of each component. Spectral types are established by comparison with spectral standards from Montes et al. (1997) over the temperature sensitive region 5700 - 6800 Å. This longer wavelength portion of each spectrum is used for spectral classification since it suffers the least from continuum excess emission common in classical T Tauri stars (Basri & Batalha 1990; Hartigan et al. 1991). The spectral types inferred from these comparisons are listed in Table 5. The best fit dwarf spectra are also shown in Figure 1.

While the majority of late-type T Tauri stars can be assigned spectral types with moderate resolution spectra, some T Tauri stars display a substantial continuum excess and strong emission-lines which can compromise the accuracy of this classification (e.g., XZ Tau B). The resolution of the FOS spectra is insufficient to determine the level of continuum excess emission, or veiling, which may be present in the spectra. This typically requires spectroscopy of sufficient spectral resolution ($R > 10,000$) to resolve individual atomic features. The strength of Balmer series emission, however, is correlated with continuum veiling (see §3.2.1; Basri & Batalha 1990). Since GH Tau A, GH Tau B, and V955 Tau A all show relatively weak $H\alpha$ emission ($< 20 \text{ \AA}$), at levels only modestly above the WTTS limit (§2.1), it is likely that they experience little or no optical veiling. In contrast, XZ Tau B clearly exhibits a continuum excess, although based on the available spectroscopic information there is no definitive way to accurately quantify this. Only the reddest portion of the spectrum shows any photospheric features. Both CaH absorption (6382 Å & 6389 Å) and the step-like features of TiO ($> 6600 \text{ \AA}$) are visible and indicate an underlying photosphere. Nevertheless, the depths of these temperature sensitive features are likely diminished because of continuum excess emission. While this region of the spectrum appears somewhat similar to the M1 standard shown in Figure 1, this spectral type is more likely an upper limit with respect to temperature.

3. Binary Star Property Results

3.1. Stellar Properties

3.1.1. Temperature, Extinction, and Luminosity Estimates

The standard method for deriving stellar temperatures and luminosities relies on both a spectroscopically derived spectral type and broad-band optical photometry. The latter is measured in this study for the component stars of the 25 systems described in §2.3. Only 8 of these systems, however, have spatially separated spectra and hence spectral types known for both components. For the remaining systems, the optically inferred spectral type of each unresolved system is assigned to

the component that is the brightest at optical wavelengths. This is the primary in all cases except for LkHa 332/G1. Uncertainties of one spectral subclass are assumed for all spectral types unless otherwise noted (Table 5). These spectral types are converted to temperatures using a temperature scale that is consistent with dwarf temperatures for M0 and hotter stars (Bessell & Brett 1988) and is moderately hotter than dwarf temperatures for cooler stars (Luhman 1999). In order to derive stellar luminosities, it is first necessary to estimate extinction values. These values are determined from the extinction law of Rieke & Lebofsky (1985) and a comparison of the $V - I_c$ colors observed with those corresponding to the from the spectral types, using the dwarf color relations of Bessell & Brett (1988) and Bessell (1991) for K7 and hotter stars and that of Kirkpatrick & McCarthy (1994) for M0 and cooler stars. Uncertainties in the extinctions are estimated by changing the spectral types by their uncertainties and rederiving the extinctions. Finally, the luminosities are derived from the dereddened I_c magnitudes, using a distance of 140 pc (Kenyon et al. 1994; Preibisch & Smith 1997). The I_c bandpass is chosen for calculating the stellar luminosities since it suffers the least contamination from UV excess. Bolometric corrections from Bessell (1991) are used for stars hotter than spectral type M3 and values from Monet et al. (1992) are used for spectral types of M3 and cooler. While bolometric corrections for early M stars are reasonably well established, their remains considerable uncertainty in the bolometric corrections for late-M stars (Monet et al. 1992; Kirkpatrick et al. 1993). The uncertainties in the adopted bolometric corrections are assumed to be 0.05 magnitudes for spectral types hotter than M5, 0.1 magnitudes for spectral types between M5 and M7, and 0.2 magnitudes for spectral types of M7 and cooler. These uncertainties are combined with the uncertainties in the photometry and the extinction estimates in order to determine the uncertainties in the stellar luminosities. The inferred properties are listed in Table 5.

For the companion stars without spectroscopic measurements of their spectral types, we assume that the extinction to the secondary is the same as to the primary. This assumption is checked by comparing the independently derived extinctions for the components of 14 fully resolved (photometrically and spectroscopically) T Tauri star systems with separations < 1000 AU, and with no known unresolved companions (Fig 2). The difference in extinction between the primary and secondary stars for these systems is consistent with no difference: mean $[A_V(\text{prim}) - A_V(\text{sec})] = -0.15$ magnitudes, with a standard deviation of 0.80 magnitudes. The standard deviation of these differences is reduced considerably if the most discrepant case, GG Tau Aa and Ab, is ignored: mean $[A_V(\text{prim}) - A_V(\text{sec})] = 0.01$ magnitudes, with a standard deviation of 0.54 magnitudes. Proceeding with the same extinction assumption, these extinction estimates are used to deredden the observed $V - I_c$ colors of the secondaries. The spectral types and corresponding temperatures of these stars are then estimated from their reddening corrected $V - I_c$ colors⁵. For GG Tau Bb, HN Tau B, and UX Tau C, $R_c - I_c$ colors are used since these stars have no V -band measurements. The uncertainties in the spectral types of the secondaries are estimated by changing the spectral types of the primaries by their uncertainties and then rederiving the extinctions and the colors of

⁵Although the transformations used to determine the Johnson-Cousins photometry depends on the spectral types (§2.3.2), this dependence is very weak and the solutions can be determined in one iteration.

the secondaries; a minimum uncertainty of 1 spectral subclass is assumed. The luminosities of the secondaries are derived from the dereddened I_c -band magnitudes as described above. The stellar properties for these companion stars are also listed in Table 5.

A few of the components measured photometrically have additional optically unresolved companions that need to be addressed individually. For the single-lined spectroscopic binaries UZ Tau E (Mathieu et al. 2000) and RW Aur A (Gahm et al. 1999, but see also Petrov et al. 2001), all the observed flux is attributed to the primary. For the double-lined spectroscopic binary V773 Tau A, the primary’s flux is estimated from the flux ratio at R and the observed spectral types (Welty 1995) as described in Ghez et al. (1997b). Four binary components - V807 Tau B, HV Tau A, Haro 6-37 A, and UX Tau B - each have an additional companion that has been resolved in NIR lunar occultation or speckle imaging measurements (Duchêne et al. 1999a; Ghez et al. 1993; Simon et al. 1992), but have no spatially resolved optical measurements. In order to correct for the emission from this companion, the magnitude difference at J ($1.25 \mu\text{m}$), if available (Haro 6-37 A and UX Tau B), or K is used to determine the approximate temperature and spectral type of the companion. First, the unresolved pair’s spectral type and corresponding temperature are assigned to the brighter star. Then the companion’s temperature is estimated from the absolute magnitude - temperature relations of the Baraffe et al. (1998) evolutionary models (§3.1.2), at an age of 3 Myrs. Finally, the companion’s contribution to each bandpass is then estimated and removed using the spectral type - color relations from the references listed above, normalized to the observed J (or K) magnitude. Only the flux corrected brighter star of each pair is included in the subsequent analysis.

For comparison with the components of multiple star systems, single stars in Taurus-Auriga are identified in Appendix B. The stellar properties of these stars are derived following the same procedure used for stars with both spectra and photometry, and these properties are reported in Table 7.

While the adopted methodology for determining luminosities, temperatures, and extinctions works well for the majority of T Tauri stars, this method is inadequate if the optical light is not predominately from the stellar photosphere. Young stars with exceptionally high levels of accretion are examples of this. In these cases, the optical light is dominated by continuum excess emission from the accretion shock (e.g., Gullbring et al. 2000). This is illustrated in the spectra of several component stars studied here such as XZ Tau B (Fig 1), HV Tau C (Magazzú & Martín 1994), and HN Tau A (Monin et al. 1998); the spectra show no or barely discernible photospheric features. An additional property that these high accretion stars have in common is that they are exceptionally red at near- and mid-infrared wavelengths. Since we have $K - L$ colors for the majority of binary star components studied here (Table 1), we use the well known correlation between $K - L$ color and optical excess emission (§3.2.1) to identify stars with abnormally high optical excess levels. A linear fit to this relation implies that stars with $K - L$ colors > 1.4 magnitudes have optical excess emission levels that are > 10 times that from the stellar photosphere (§3.2.1). This high level of excess emission is greater than the levels spectroscopically determined for all the CTTSs in Hartigan

et al. (1995), and thus we label stars with $K - L$ colors above this value as *high accretion stars*. This classification is further supported by optical spectroscopy. All stars with $K - L$ colors greater than 1.4 magnitudes display nearly featureless optical spectra, when available, while those with bluer $K - L$ colors typically show well defined photospheric features and consequently have better established spectral types. The list of high accretion stars includes the binary star components CZ Tau B, FS Tau A, FS Tau B, Haro 6-10 B, HV Tau C⁶, T Tau B, XZ Tau B, FV Tau/c B, and HN Tau A, and the single stars DG Tau, DR Tau, and HL Tau. Since the inferred luminosities and temperatures for these high accretion stars may be in error, the derived values are listed in Tables 5 and 7 in parentheses.

3.1.2. Absolute Age and Mass Estimates

Masses and ages of the binary star components are estimated by comparing the stellar luminosities and temperatures with the predictions of pre-main-sequence (PMS) evolutionary models. Although considerable uncertainties remain in the assumptions used to calculate these models, recent studies by White et al. (1999) and Simon et al. (2000) have shown that the evolutionary models of Baraffe et al. (1998) computed with a mixing length equal to nearly twice the pressure scale height are consistent with the available observational constraints. The Baraffe et al. (1998) models, however, are only computed for masses between $0.025 M_{\odot}$ and $1.20 M_{\odot}$. In order to extract masses and ages for the entire range of masses in this study, the low mass evolutionary models of Baraffe et al. (1998) are combined with the higher mass models of Palla & Stahler (1999), as was done by White (2001). These models agree reasonably well at the adopted transition mass of $1.00 M_{\odot}$.

In Figure 3, the components of binary systems with spatially resolved optical measurements are plotted on an H-R diagram along with the adopted models for PMS evolution. Single T Tauri stars (Appendix B) are also shown, and high accretion stars (both binary components and single stars) are distinguished and labeled. The inferred masses and ages for the binary star sample are listed in Table 5. Uncertainties are set by the ranges of masses and ages inferred by changing the temperature and luminosity estimates by their uncertainties (Table 5). Stars with a luminosity above the youngest isochrone are assigned an age upper limit of 1 Myrs. The ages derived for these binary star components, excluding the high accretion stars, range from < 1 Myrs to 19 Myrs, with a mean $\log[\text{age}]$ of 6.43 ± 0.05 dex (~ 2.7 Myrs; includes 45 stars, $\sigma = 0.35$ dex). The masses range from $0.042 M_{\odot}$ to $2.11 M_{\odot}$, with only one component, GG Tau Bb, below the hydrogen burning minimum mass (i.e. a brown dwarf; White et al. 1999). These values are consistent with the overall population of single T Tauri stars in Taurus-Auriga (Appendix B). The combined sample of singles and binary components have a mean $\log[\text{age}]$ of 6.44 ± 0.04 dex (includes 94 stars, $\sigma = 0.37$

⁶Although HV Tau C has not been detected at L , it is classified as a high accretion star because of its featureless optical spectrum and its exceptionally red $K - N$ color (Magazzú & Martín 1994; Woitas et al. 1998).

dex). The non-physical luminosity and temperature estimates derived for the high accretion stars are illustrated by their systematically under-luminous locations on the H-R diagram relative to the majority of T Tauri stars. Since the optical measurements for these stars are insufficient to determine their stellar properties, it is not possible to confidently determine which component is the true primary (i.e., more massive). Consequently, these objects are excluded from the following discussion of relative masses and ages, but are revisited in §4.3.

3.1.3. *Relative Ages and Masses of Binary Star Components*

The component ages listed in Table 5 are used to test the coevality of binary star components. GG Tau B is omitted from this analysis since it was used to define the temperature scale with the assumption of coevality imposed on it (Luhman 1999; White et al. 1999). As shown in Figure 4, the components of binary stars are, on average, consistent with being coeval. If the four components with age upper limits are assigned an age of 1 Myrs (1 primary star and 3 secondary stars), the differences in the components’ $\log[\text{age}]$ have a mean of 0.07 ± 0.07 dex and a standard deviation of 0.31 ± 0.05 dex. This standard deviation is comparable to the average uncertainty in the ages (~ 0.30 dex). We therefore conclude that the observed spread in relative ages is dominated by measurement uncertainties, and estimate a 3σ upper limit to the intrinsic $\log[\text{age}]$ differences to be 0.15 dex. For a typical T Tauri star age (3 Myrs; §3.1.2), this implies that binary stars are coeval to ~ 1 Myrs. Divided into two sets, the close and wide pairs, this sample shows that close pairs have a slightly smaller spread in age compared with wider pairs ($\sigma = 0.27 \pm 0.05$ dex versus $\sigma = 0.39 \pm 0.11$ dex), but the difference is not statistically significant.

An additional test of coevality that is less dependent on accurately converting measurement uncertainties to age uncertainties is a comparison of the relative ages of the binary star components and randomly paired single T Tauri stars. An ensemble of random pairings of 49 single T Tauri stars in Taurus-Auriga (Appendix B) leads to a median standard deviation in $\log[\text{age}]$ of 0.54 dex, which is considerably larger than that of the binary sample (0.31 ± 0.05 dex). An example set of randomly paired single stars is shown in Figure 4 for comparison with the binary star sample. Although the $\log[\text{age}]$ differences of the binary star sample appear to be significantly less than the $\log[\text{age}]$ differences of the randomly paired single star sample, effects other than a larger spread of intrinsic ages could, in principle, produce apparently larger age differences. For example, larger measurement uncertainties for the single stars could have this effect. However, the stellar properties of the single stars are actually more accurately determined since they all have spectral types from spectra and multi-epoch photometry. Uncertainties in the evolutionary models and temperature scale could also produce a larger age spread, and this effect would be the most significant for pairs with the largest differences in temperature. If binary stars and randomly paired single stars with similar temperature differences are compared, however, the binary stars are more coeval than the single stars over all ranges of temperature differences. Another possibility is that our method of equating the A_V ’s for some of the binary star components biases the binary star pairs toward similar

ages. To check this, we analyze the sub-set of the binaries for which both components have been measured spectroscopically and photometrically. This set has a standard deviation of 0.34 ± 0.08 dex, similar to the whole binary star sample, suggesting that the method has not affected our analysis. We therefore conclude that the components of T Tauri binary stars are significantly more coeval than randomly paired single T Tauri stars within the same star forming region.

The component mass estimates are used to study the distribution of binary star mass ratios (m_s/m_p). Mass ratios for 21 pairs with optically resolved measurements (Table 5) are plotted versus binary separations in Figure 5 (*top left*). As shown in Figure 5 (*top right*), the mass ratios are correlated with the K magnitude differences between the primaries and the secondaries. Thus we use this empirical relation ($m_s/m_p = 1 - 0.328\Delta K$) to estimate mass ratios for the 20 additional binaries with spatially resolved K -band measurements (§2.1). Pairs with a high accretion star are excluded from both samples. Figure 5 (*bottom left*) shows that the mass ratio distributions determined from the optical measurements and from K magnitude differences are similar and are both peaked near unity. Combining both samples, Figure 5 (*bottom right*) shows that the majority of high mass ratio pairs are in close systems. Here the definition of 'close' is extended slightly to 110 AU to include FQ Tau; this separation shows the clearest break in the distribution of mass ratios versus separation (Fig 5, *top left*). A K-S test shows that these distributions are different at the 95% level, a 2σ difference. One limiting observational bias is that faint, low mass ratio binaries are more difficult to detect at close separations than at wide separations. However, an identical significance (95%) is determined if the K-S test is conducted on close and wide pairs excluding binaries with K magnitude differences of 3.0 or more (1 close, 1 wide). A similar mass ratio dependence on separation, as traced by K flux ratio, was reported in the Taurus-Auriga binary study of Köhler & Leinert (1998), which consisted of 85 pairs, 34 of which are X-ray identified systems (Wichmann et al. 1996) and thus are not included in the sample studied here. Thus, although multiplicity surveys that are more sensitive to close, low mass companions are needed to minimize observational biases and confirm this tentative suggestion, it appears that high mass ratio pairs are slightly more common among close (~ 10 -110 AU) binaries than among wide (~ 110 -1000 AU) binaries in Taurus-Auriga.

3.2. Circumstellar Properties

Standard accretion disk diagnostics are used to study the circumstellar disks associated with the components of the binary T Tauri stars studied here. Specifically, UV excesses, $K-L$ colors, and the EW[H α]s are used to identify circumstellar accretion disks, and the strengths of these diagnostics are used to characterize mass accretion rates. Since these accretion disk diagnostics have been discussed extensively in the literature (e.g., Hartmann 1998), in §3.2.1 we very briefly summarize their effectiveness through correlations with independently determined, optical continuum excesses extracted from high resolution spectra, a direct tracer of the mass accretion rate (Hartigan et al. 1995). These relations are explored using the single T Tauri star sample (Appendix B), which is

free of biases introduced by unresolved companions. In §3.2.2, the T Tauri types (CTTS versus WTTS) of the binary star components are assigned and the effectiveness and consistency of the diagnostics used for type classification are discussed. The circumstellar properties of the binary star systems are presented in §3.2.3.

3.2.1. Signatures of Circumstellar Disks

Ultra-Violet Excesses and Mass Accretion Rates

The accretion of circumstellar material produces substantial excess UV luminosity due to the dissipation of the accreting material’s kinetic energy as it impacts the stellar surface. Although this excess luminosity is most accurately measured from high resolution spectroscopy (e.g., Basri & Batalha 1990), it can also be confidently inferred from broad-band UV measurements. Figure 6 (*top left*) shows the correlation between the excess emission measured in the U -band filter⁷ and the optical continuum excess emission, or optical veiling, measured in high resolution spectra (Hartigan et al. 1995). Stars with the largest U -band excesses have the largest levels of optical veiling. In a similar but more useful comparison, Gullbring et al. (1998) quantified the relation between U -band excess measurements and the total accretion luminosity determined from optical veiling. Following their empirically determined relation, we estimate accretion luminosities for single CTTSs (Appendix B) from U -band excesses. These values are then converted to mass accretion rates following the model of Gullbring et al. (1998), in combination with stellar radii ($L_{\star} = 4\pi R_{\star}^2 \sigma T_{\star}^4$) and mass estimates. The accretion rates, listed in Table 7, range from $3 \times 10^{-10} M_{\odot} \text{ yr}^{-1}$ to $7 \times 10^{-8} M_{\odot} \text{ yr}^{-1}$ (mean $\log[\dot{M}] = -8.33$, $\sigma = 0.67$), and are consistent with the range of accretion rates inferred from spectroscopic data (Gullbring et al. 1998). The limitation of this method is that the moderate U -band excesses common in WTTSs and attributable to their active chromospheres give the impression of low level accretion. The observed U -band excesses for the single WTTSs are used to determine upper limits to their mass accretion rates (Table 7), adopting the same methodology described above. A mass accretion rate upper limit of $10^{-10} M_{\odot} \text{ yr}^{-1}$ is assumed for LkCa 19 and LkCa 5, which both have slightly negative U -band excesses. Chromospheric excesses can give the appearance of accretion rates of up to a few $\times 10^{-9} M_{\odot} \text{ yr}^{-1}$.

The Near Infrared Color $K - L$

The amount of NIR excess emission is known to be correlated with the rate of circumstellar accretion. Larger accretion rates must dissipate angular momentum more quickly in the viscous disk and this leads to a warmer, more luminous disk (Bertout et al. 1988; Kenyon & Hartmann 1990). The

⁷The U -band excess is quantified as ΔU , which is 2.5 times the logarithm of the ratio of the total U -band flux and the photospheric U -band flux, where both quantities are reddening corrected ($\Delta U = 2.5 \times \log [F_{tot}/F_{phot}]$).

increase in disk emission produces larger NIR excesses and redder NIR colors. The $K - L$ color is a particularly useful NIR accretion diagnostic since the underlying photospheric color exhibits little spectral type dependence ($K - L[\text{K0}] = 0.06$ versus $K - L[\text{M5}] = 0.29$) and it is not significantly affected by the moderate extinction ($A_V \sim 1 - 2$ magnitudes) associated with most T Tauri stars. In Figure 6 (*bottom left*), the observed $K - L$ colors for single T Tauri stars are compared to their optical excesses. All sources with $K - L$ colors larger than ~ 0.3 magnitudes have detectable optical excesses, while those with normal photospheric $K - L$ colors ($\sim 0.1 - 0.3$) have no detectable optical excesses. The $K - L$ color is also correlated with the level of optical excess emission, and this relation is quantified with a linear least squares fit⁸ ($\log[r] = 2.199(K - L) - 2.148$) in Figure 6 (*bottom left*).

H α Emission

Balmer series emission, especially $\text{H}\alpha$, is the most common diagnostic of circumstellar accretion onto young stars. The large emission-line fluxes are believed to be generated in the partially optically thin channeled accretion flow (e.g., Muzerolle et al. 1998), although some chromospheric emission is likely to be present. In order to account for the spectral type dependence of the possible underlying chromospheric $\text{H}\alpha$ emission, we define a 'normalized' $\text{EW}[\text{H}\alpha]$ as $\text{nEW}[\text{H}\alpha] = \text{EW}[\text{H}\alpha] - \text{EW}[\text{H}\alpha]_{w/c}$, where $\text{EW}[\text{H}\alpha]_{w/c}$ is the equivalent width value used to distinguish CTTSs from WTTSs (§2.1). This definition yields a more convenient distinction between WTTSs and CTTSs since WTTSs have a positive $\text{nEW}[\text{H}\alpha]$ and CTTSs have a negative $\text{nEW}[\text{H}\alpha]$. In Figure 6 (*top right*) the $\text{nEW}[\text{H}\alpha]$ s of the single T Tauri stars are compared to their optical excesses. All sources with strong $\text{H}\alpha$ emission ($\text{nEW}[\text{H}\alpha] < 0$) have detectable optical excesses, and the emission and excesses are modestly correlated. One possible concern is that larger continuum excesses may lead to smaller $\text{EW}[\text{H}\alpha]$ s since the $\text{EW}[\text{H}\alpha]$ is simply a ratio of $\text{H}\alpha$ to continuum flux. Calculating the luminosity of $\text{H}\alpha$ emission eliminates the continuum dependence. In Figure 6 (*bottom right*), the $\text{H}\alpha$ luminosities are also compared to their optical excesses for the same sample of T Tauri stars. The continuum levels used to determine the $\text{H}\alpha$ luminosities are estimated from reddening corrected R_c magnitudes. Although the $\text{H}\alpha$ luminosities are modestly correlated with the levels of optical excess emission, there is still considerable scatter in the relation and there is an observable overlap in the $\text{H}\alpha$ luminosities for systems with and without optical excesses. In the following analysis, only the $\text{nEW}[\text{H}\alpha]$ is used as a tracer of circumstellar accretion.

⁸ $K - L$ colors greater than 1.4 imply continuum excesses that are nearly 10 times that of the stellar continuum, and this $K - L$ color is therefore chosen to identify high accretion stars (§3.1.1).

3.2.2. Assigning T Tauri Types

The $nEW[H\alpha]$ s and the $K - L$ colors show the most distinct distributions of values for systems with optical excesses compared to systems without optical excesses (Fig 6). Thus, both could be used for classifying T Tauri types (CTTS versus WTTS; §2.1). We adopt the $nEW[H\alpha]$ for distinguishing CTTSs and WTTSs since it is the more commonly used determinant. High accretion stars, however, are distinguished from CTTSs with more moderate accretion rates by their red $K - L$ colors (§3.1.1). The assigned T Tauri types for the components of the binary sample are listed in Table 5. In the absence of spatially resolved $H\alpha$ measurements, $K - L$ colors are used to assign the T Tauri types: $K - L < 0.4$ are WTTSs (V410 Tau A), $0.4 < K - L < 1.4$ are CTTSs (UZ Tau Ba & Bb). These types are marked in Table 5 with a colon. The T Tauri types of the components without spatially resolved $H\alpha$ or $K - L$ measurements are assigned based on UV excesses (Fig 6): $\Delta U < 0.8$ magnitudes are WTTSs (V773 Tau A & C, V410 Tau C), $\Delta U > 0.8$ magnitudes are CTTSs (DF Tau A & B). These types are marked with a double colon in Table 5. The types assigned from $K - L$ colors and U -band excesses are consistent with the T Tauri types assigned to the unresolved systems as determined from $H\alpha$ emission (Table 1).

One single star (IQ Tau) and several binary star components (IS Tau B, LkHa 332/G1 A, LkHa 332/G1 B, FV Tau/c A) have weak $H\alpha$ emission (i.e. below the CTTS limit), but red $K - L$ colors (> 0.5 magnitudes). Conversely, a few stars (GM Aur, FP Tau, FO Tau B) have strong $H\alpha$ emission, but photospheric $K - L$ colors. The T Tauri types assigned to these peculiar stars therefore depends on whether the $nEW[H\alpha]$ s or $K - L$ colors are used; here the $nEW[H\alpha]$ s are used. In the majority of cases, however (40/43 = 93% of single stars; 33/38 = 87% of binary star components), the T Tauri types assigned by the $nEW[H\alpha]$ s and the $K - L$ colors are consistent. For the two stars GM Aur and FP Tau with $K - L$ colors typical of WTTSs, their CTTS type assigned from the strength of $H\alpha$ emission are supported by their optically veiled spectra (Hartigan et al. 1995). No optical veiling measurements are available for the other peculiar stars.

3.2.3. The Observed Circumstellar Properties of Binary Star Components

Mass accretion rates for the components of the binary systems resolved optically are calculated following the same methodology used for the single T Tauri stars. For high accretion stars, these values are very uncertain because of the considerable uncertainty in the stellar parameters (§3.1.1). Accretion rates determined for WTTSs are assumed to be upper limits; an upper limit of $10^{-10} M_{\odot} \text{ yr}^{-1}$ is assigned to V773 Tau A, which has a small negative U -band excess. The ΔU s and mass accretion rates are listed in Table 5, along with the $K - L$ colors and $EW[H\alpha]$ measurements.

In Figure 7, the mass accretion rates, the $K - L$ colors, and the $nEW[H\alpha]$ s of primary stars within both CTTS and WTTS systems are plotted versus the projected separation of their companion. Systems with a high accretion star are not included since it is unclear which component is the true primary (§3.1.3). For comparison, the corresponding accretion diagnostics of single CTTSs

and single WTTSs (Appendix B) are plotted with arbitrary separations. For all three accretion diagnostics, the CTTS primaries have distributions that are indistinguishable from the single CTTS distributions. This is true independent of the binary separation. The presence of a companion star, even as close as ~ 10 AU, does not appear to disrupt the distribution of inner circumstellar material sufficiently to diminish or enhance the mass accretion rate. The majority of WTTS primaries have accretion diagnostics that are consistent with the single WTTS sample, and indicative of little or no accretion.

In Figure 8, the mass accretion rates, the $K - L$ colors, and the $\text{nEW}[\text{H}\alpha]$ s of secondary stars are compared to their more massive companions. Pairs are distinguished based on the T Tauri type of the system (Table 1) and binary separation (close versus wide). These comparisons suggest that, independent of the accretion diagnostic used, primary stars generally have accretion signatures that are comparable to or larger than that of their associated companion, implying a higher mass accretion rate. Ghez et al. (1997b), Duchêne et al. (1999b), and Prato & Monin (2001) have reported similar results. We find this to be true for both close and wide pairs; the distributions of relative accretion diagnostics (primary versus secondary) for close and wide pairs are not significantly different. The dominance of the primaries’ accretion signatures is the most pronounced in systems with small mass ratios (i.e. systems with the most discrepant masses). This is illustrated in Figure 9, which plots the differences in the mass accretion rates, the $K - L$ colors, and the $\text{nEW}[\text{H}\alpha]$ s between primaries and secondaries versus their mass ratios. Although the small number of low mass ratio systems limits the interpretation, a general trend is evident considering all 3 diagnostics. In comparable mass systems ($m_s/m_p > 0.8$), either component can have the dominant accretion signatures. In smaller mass ratio systems ($m_s/m_p < 0.8$), however, primaries systematically have the dominant accretion signatures. Although pairs with high accretion components are not included in these comparisons, these pairs would be a strong exception to this result if high accretion stars are lower mass components. However, Koresko et al. (1997) have shown that many high accretion stars are, bolometrically, the more luminous component and thus may be the more massive component.

The presence of circumprimary and circumsecondary disks is investigated using the spatially resolved accretion disk signatures of the binary sample (Fig 8). As discussed in §3.2.2, both the $\text{nEW}[\text{H}\alpha]$ and the $K - L$ color have relatively clean breaks between accreting (CTTS) and non-accreting (WTTS) stars. We therefore identify circumstellar disks based on $\text{nEW}[\text{H}\alpha]$ s less than zero or $K - L$ colors greater than 0.4 magnitudes. As shown in Figure 8, systems which support a circumsecondary disk, but no circumprimary disk are rare. Only 1 of 35 systems with $K - L$ measurements and 0 of 16 systems with $\text{nEW}[\text{H}\alpha]$ measurements show this configuration. In contrast, there are many systems (7 of 35 based on $K - L$ and 5 of 16 based on $\text{nEW}[\text{H}\alpha]$) with a circumprimary disk but no circumsecondary disk. Thus, if only one circumstellar disk exists, it is almost always associated with the more massive star. The existence of a component’s disk, however, appears to be correlated with the existence of its companion’s disk for close systems. In this more general comparison in which mass is not relevant, high accretion stars are included as CTTSs. The correlation of disk existence, or equivalently of T Tauri type, holds out to a separation of ~ 210

AU. Of the 16 pairs with separations less than 210 AU and with spatially separated nEW[H α] measurements (2 WTTS and 14 CTTS systems), only three systems are mixed types (FV Tau/c, IS Tau, V807 Tau). Of the 30 pairs with separations less than 210 AU and with spatially separated $K - L$ measurements (21 CTTS and 9 WTTS systems), only 4 are mixed types (FO Tau, FQ Tau, VY Tau, V807 Tau). Assuming a fixed distribution of primaries (WTTS or CTTS) and an equal probability of having either a WTTS or a CTTS companion (Hartmann et al. 1991), the probability to get the observed number of mixed systems from each of the two samples is 6×10^{-4} ($C_{16}^3 (\frac{1}{2})^{16}$) and 3×10^{-5} ($C_{30}^4 (\frac{1}{2})^{30}$), respectively. These low probabilities strongly suggest that the relative T Tauri types are correlated. In contrast, of the 8 pairs with separations greater than 210 AU and with spatially separated nEW[H α] measurements (2 WTTS and 6 CTTS systems), 5 are mixed types. Similarly, of the 11 wider pairs with spatially separated $K - L$ measurements (10 CTTSs and 1 WTTSs), 4 are mixed types. The circumstellar disks in systems wider than 210 AU are more consistent with random pairing.

4. Discussion

4.1. Circumstellar Disks in Binary Star Systems

Millimeter observations of binary T Tauri stars suggest that the circumprimary and circumsecondary disk masses of close binary (< 100 AU) systems may be diminished relative to the disk masses of single T Tauri stars (Osterloh & Beckwith 1995; Dutrey et al. 1996; Jensen et al. 1996). The diminished masses are attributed to disk truncation by the companion star. Since it is statistically unlikely that these binary stars have disks that are just on the verge of complete depletion, the disk mass estimates and the disk accretion rates can be used to calculate a characteristic disk lifetime (M_{disk}/\dot{M}). Following this simple procedure, several binary star studies have found that the disk lifetimes for binary stars, calculated from the best available accretion rates and age estimates, are typically less than the ages of the stars (Mathieu et al. 1994; Prato & Simon 1997; Duchêne et al. 1999b). Thus, it is somewhat surprising that these binary stars are still actively accreting. However, Prato & Simon (1997) found that single stars typically have disk lifetimes that are also less than their ages, which may imply systematic errors in their assumed stellar ages and/or circumstellar properties. The new mass accretion rates and stellar ages calculated self-consistently here for single stars and for binary star components using spatially resolved measurements will allow us to more carefully investigate this potential timescale problem.

In the left-hand panel of Figure 10, the measured mass accretion rates are combined with disk masses from the literature to calculate the disk lifetimes, which are then compared to the stellar ages for both single and binary T Tauri stars. Disk masses are taken from Osterloh & Beckwith (1995), Beckwith et al. (1990), Dutrey et al. (1996) for UZ Tau A and B, and Guilloteau et al.

(1999) for GG Tau A⁹. Although these millimeter studies do not spatially resolve circumprimary and circumsecondary disks, the disk mass estimates for each system should nevertheless be a reasonable approximation of the combined circumstellar disk mass. The mass accretion rates for the binary systems are the sums determined for all components and the ages are the averages of all components. Systems with a high accretion star are not included because of the uncertainty in their ages and mass accretion rates. As this figure illustrates, the single stars are distributed evenly about the line that represents disk lifetimes equal to stellar ages. In contrast, the binaries are systematically below this line, implying that the binary star disk lifetimes are significantly shorter than their stellar ages. For the binary stars, this effect shows no significant dependence on separation, although only 2 of the 12 binary stars have separations larger than 100 AU.

To quantify the comparison of disk lifetimes and stellar ages for single and binary T Tauri stars, the right-hand panel of Figure 10 shows histograms of the logarithm ratios of stellar ages to disk lifetimes. Limits are treated as actual values; single stars have only a slightly smaller fraction of disk lifetime estimates that are based on disk mass upper limits than binary stars (36% for singles, 42% for binaries). Single stars have disk lifetimes that are, on average, comparable to their ages (mean $\log[\text{Age}/\text{Disk Lifetime}] = -0.04 \pm 0.18$ dex), while binary stars have disk lifetimes that are, on average, less than their ages by nearly a factor of 10 (mean $\log[\text{Age}/\text{Disk Lifetime}] = 0.95 \pm 0.34$ dex; a 2.8σ difference from zero). However, a direct comparison of the $\log[\text{Age}/\text{Disk Lifetime}]$ distributions for singles and binaries using a K-S test implies that they differ only at the 80% confidence level, a 1.2σ difference (Figure 10). The discrepancy between the disk lifetimes and the ages of binary stars, as well as discrepancy between the distributions of $\log[\text{Age} / \text{Disk Lifetime}]$ for binaries and singles increase substantially, though, if high accretion stars are included by assuming that the mass accretion rates determined for DG Tau and DR Tau from *IUE* spectra are typical for high accretion stars (§4.3; Gullbring et al. 2000) and that they have their companions’ or an average age. In this case, the mean $\log[\text{Age}/\text{Disk Lifetime}]$ for binaries increases to 1.47 ± 0.37 dex, while for singles it remains at 0.11 ± 0.18 dex, and the $\log[\text{Age}/\text{Disk Lifetime}]$ distributions differ at the 99% level according to a K-S test. Thus, although the properties of high accretion stars are uncertain, their properties support the trends identified for other T Tauri stars. We conclude that while single T Tauri stars have disk lifetimes comparable to their ages, close binary T Tauri stars have disk lifetimes that are roughly 1/10 of their ages.

One solution to this timescale problem is that the circumstellar disks are being replenished from circumbinary reservoirs. In support of this, the close binaries GG Tau and UY Aur are known to be surrounded by substantial circumbinary material (Dutrey et al. 1994; Roddier et al. 1996; Guilloteau et al. 1999; Close et al. 1998; Duvert et al. 1998), while other systems show spatially extended circumbinary nebulosity (e.g., FS Tau, T Tau, CoKu Tau 1; §2.3.2, Stapelfeldt et al. 1998a; Padgett et al. 1999). The majority of these reservoirs, however, are not likely to

⁹The circumstellar disk mass estimate for GG Tau A is based on measurements which spatially resolve the circumstellar disk emission from the circumbinary emission (Guilloteau et al. 1999).

be very massive since the millimeter upper limits of many of the close binaries correspond to circumbinary mass upper limits of $\sim 0.005 M_{\odot}$, assuming optically thin emission (Jensen et al. 1996). Nevertheless, the addition of mass in this amount to the circumstellar disks of close binaries would be enough to bring the disk lifetimes to within 2σ of the ages, and possibly reconcile the discrepancy. We therefore consider the possibility that some circumbinary material is present and is replenishing the circumstellar disks. Numerical simulations have demonstrated how this may occur (Artymowicz & Lubow 1996; Bate & Bonnell 1997). For example, replenishment from a circumbinary disk can successfully explain the episodic accretion characteristics of DQ Tau, a 16 day spectroscopic binary in which replenishment from a circumbinary reservoir must be occurring in order to sustain the observed accretion rates (Mathieu et al. 1997; Basri et al. 1997). Although the binaries studied here have orbital periods which are too long to observe such episodic effects, the consequence of replenishment in these systems may explain their long disk lifetimes.

The flow of circumbinary material onto the individual circumstellar disks depends to a large extent on its angular momentum relative to the binary star. If the circumbinary material has sufficient angular momentum to form a circumbinary disk, then the lower mass object is expected to be preferentially replenished (Artymowicz & Lubow 1994); this component has closer encounters with the reservoir of circumbinary material. Alternatively, if the angular momentum of the surrounding material is insufficient to form a circumbinary disk, then the in-falling material is expected to preferentially replenish the circumprimary disk; this material will fall toward the center of mass (Bonnell & Bastien 1992; Bate & Bonnell 1997). Thus if replenishment is occurring for close (10 - 100 AU) binaries as suggested by their delayed depletion, the angular momentum of this material may be constrained by studying the relative circumstellar properties in binary systems.

The result that there are many systems with only circumprimary disks, but that systems with only circumsecondary disks are very rare, implies that circumprimary disks are longer lived. This finding is in contrast to the predictions of the high angular momentum, circumbinary disk replenishment scenario. This scenario preferentially replenishes the circumsecondary’s disk and this, in conjunction with the secondary’s lower accretion rate due to its lower mass (§4.2), should result in the secondary having a longer disk lifetime. The observations are in better agreement with the low angular momentum replenishment scenario. In this case, the circumprimary’s disk will be preferentially replenished, allowing it to survive longer than the circumsecondary’s disk. The higher accretion rates of primary stars (Fig 8) further strengthens the case for preferential primary replenishment, since otherwise they would deplete their disk first, assuming equal disk masses. We note, however, that Armitage et al. (1999) have proposed an alternative explanation for the longer disk lifetimes of primary stars in which neither disk is replenished. The more massive component within a binary system is capable of supporting a more massive circumstellar disk due to its larger Roche lobe. This disk will consequently survive longer than the circumsecondary disk, presuming similar accretion rates. Replenishment scenarios are nevertheless a likely possibility for close binary T Tauri stars given their apparently short disk dissipation timescales and the direct evidence of circumbinary material in some systems.

The relative T Tauri types and binary mass ratios provide additional support for replenishment from a circumbinary reservoir. As suggested by Prato & Simon (1997), replenishment from a common reservoir (e.g., circumbinary) may co-regulate the evolution of the binary star components (e.g., Bate & Bonnell 1997) and may result in circumprimary and circumsecondary disk dissipation timescales that are similar. Both components would be replenished, with perhaps a modest preference for the primary as noted above, until the circumbinary reservoir is depleted. In such a scenario, CTTS primaries should preferentially have CTTS secondaries. This prediction is supported by the relative T Tauri types of binaries with separations less than 210 AU, which are strongly correlated (§3.2.3). Prato & Simon (1997) and Duchêne et al. (1999b) have found a similar correlation of T Tauri type. Although they suggest this correlation may extend to wider separations than 200 AU, their samples of wider binaries are small and, in the latter study, biased by stars that are not currently believed to be of the T Tauri class (e.g. HBC 352, HBC 355, HBC 360; Martín 1994). The mixed pairing of wider systems studied here suggests a maximum binary separation for this correlation. Pairs with a separation of up to ~ 200 AU appear to be regulated by the same circumbinary reservoir, while wider pairs are not.

This separation limit is only slightly larger than the separation at which a slight break occurs in the distribution of mass ratios (~ 100 AU; Fig 5). Accretion from a circumbinary reservoir can also explain this. Under the assumption of formation by fragmentation (§4.4), only a small fraction ($\lesssim 10\%$) of the final stellar masses are contained in the initial protobinary fragments for systems of separation less than ~ 100 AU (Boss 1988; Bate 2000). For these systems the majority of the mass of the stellar components is accreted from circumbinary material (Bate & Bonnell 1997). Consequently, Bate (2000) predict that close binary systems are more likely to have high mass ratios than wide binary systems; the closer the components are to the center of mass of the system, the more equally they will receive accreted mass. This effect is not expected to yield a strong mass ratio dependence on separation over the range of separations explored here (10 - 1000 AU), and thus is consistent with the weak trend seen in Figure 5.

4.2. Evidence for a Mass Dependent Accretion Rate

As Figures 8 and 9 illustrate, primaries generally have dominant accretion signatures, and their dominance is the most significant in systems with small mass ratios. Since the presence of a close companion appears to have little effect on the mass accretion rate (Fig 7), this suggests that the higher relative accretion rates of primary stars may simply be a consequence of their higher relative mass. To investigate this, in Figure 11 the mass accretion rates, $K - L$ excesses¹⁰, and $n\text{EW}[\text{H}\alpha]$ s of CTTS binary components are plotted versus their stellar mass. Only components with

¹⁰A $K - L$ excess is used here in order to eliminate the small spectral type dependence of the underlying photosphere, since this information is available for all stars with mass estimates. The $K - L$ excess is defined as the difference between the observed $K - L$ color and the reddened photospheric $K - L$ color (§3.1.1).

masses derived from optical measurements are shown; high accretion stars are excluded. Primary and secondary stars are distinguished, but close and wide pairs are not since both sets have similar distributions of mass accretion rates, $K-L$ colors, and $\text{nEW}[\text{H}\alpha]$ s (Fig 8). The accretion diagnostics of the single CTTS sample are also included.

The mass accretion rates shown in Figure 11 show a general trend of decreasing mass accretion rate with decreasing stellar mass. The Spearman rank correlation coefficient between $\log[\dot{M}]$ and $\log[\text{mass}]$ is 0.57, with a probability of $< 0.1\%$ of being drawn from a random distribution. Nevertheless, stars near the median mass ($\sim 0.7 M_{\odot}$) experience mass accretion rates which span 2.5 orders of magnitude. Thus, although the mass accretion rate appears to be correlated with stellar mass, it is not a one-to-one relation. The $K-L$ color excesses and $\text{nEW}[\text{H}\alpha]$ s also plotted in Figure 11 are not as well correlated with stellar mass. Although the $K-L$ excesses and the $\text{nEW}[\text{H}\alpha]$ measurements for stars less massive than $0.3 M_{\odot}$ ($\log[M] < 0.5$) are below the average value for higher mass stars, the small number of low mass T Tauri stars with accretion diagnostics limits the statistical significance of this comparison. For all 3 accretion diagnostics however, the distribution of primaries, secondaries, and single stars with similar masses are indistinguishable. The dominant mass accretion signatures of primary stars relative to their companions is therefore most likely because of their higher relative mass, and not a consequence of being in a binary system.

4.3. High Accretion T Tauri Stars

Of the 82 binary star components in Table 1 with spatially resolved NIR measurements, 9 (11%) are classified as high accretion stars based on their very red NIR colors (§3.1.1). This fraction is similar to previous estimates. Zinnecker & Wilking (1992) estimate that approximately 5% of binary star components (within 10% of binary systems) have similar red colors, although in these previous studies they have usually been referred to as ‘infrared companions’ (see also Ghez et al. 1997a). We have not adopted this terminology here, however, since the word ‘infrared’ has come to imply that these sources are optically invisible, which is often not the case, and the word ‘companion’ implies that this phenomenon occurs only within binary star systems, although there is no convincing evidence to support this. Of the 52 single stars in Table 7, 3 (6%) are classified as high accretion stars. Although this fraction is slightly less than the fraction in the binary sample studied here, there is an observational bias toward finding these optically faint stars near a known T Tauri star because of directed companion searches at NIR wavelengths (e.g., Ghez et al. 1993; Leinert et al. 1993; Simon et al. 1995). This bias may also explain why the known single high accretion stars are the brightest members of this class; isolated high accretion stars would typically be too faint, for their optical colors, to be distinguished from the background population in optical photometric surveys (e.g., Briceño et al. 1998). Deep NIR surveys, ideally including L -band measurements, offer the best hope of identifying these peculiar young stars (e.g., Haisch et al. 2000; Lada et al. 2000).

The similarities in the spectral energy distributions of Class I sources, which are believed to be at an earlier stage of evolution than T Tauri stars (Lada & Wilking 1984), and some high

accretion stars like T Tau B have led many astronomers to speculate that some high accretion companions are also protostars at an earlier stage of evolution than the T Tauri stage (e.g., Dyck et al. 1982). This scenario, however, is inconsistent with the coeval ages of binary stars presented in this study, and the favored binary star formation mechanism that produces them (§4.4). It is more likely that the high accretion stars are relatively normal T Tauri stars experiencing unusually high accretion. For example, Gullbring et al. (2000), using *IUE* archival spectra, estimate the mass accretion rates for the single high accretion stars DG Tau and DR Tau to be $3\text{--}5 \times 10^{-7} M_{\odot}\text{yr}^{-1}$, which is nearly a factor of 100 (2.9σ in $\log[\dot{M}]$) above the mean accretion rates of CTTSs (§3.2.1). The similar properties of Class I sources thus likely stem from their similar high levels of accretion that are above the norm for T Tauri stars (Kenyon et al. 1998). In several cases, the optical spectra of high accretion stars strikingly resemble those of Class I sources (e.g., HV Tau C versus IRAS 04264+2433; Magazzú & Martín 1994; Kenyon et al. 1998), especially the prominence and strength of forbidden line-emission. The red $K - L$ colors of both high accretion stars and Class I sources demonstrate that it is not possible to unambiguously identify Class I sources based solely on $K - L$ colors as is sometimes done (e.g., Haisch et al. 2000; Lada et al. 2000). Approximately 10% of a T Tauri population may be high accretion stars. If the enhanced accretion of these stars is an episodic phenomenon (Ghez et al. 1991; Koresko et al. 1997), this fraction of high accretion stars would then suggest that T Tauri stars spend approximately 10% of their T Tauri life in this enhanced accretion phase.

With such large levels of excess emission, one would expect high accretion stars to appear over-luminous relative to the majority of T Tauri stars. Surprisingly, the optical measurements reveal the opposite. Figure 3 illustrates that high accretion stars are, on average, systematically under-luminous relative to other T Tauri stars of similar temperature and/or color. The most likely explanation for these low luminosity estimates is that the extinction estimates are too low. There are two reasons to expect this. First, the substantial UV excesses associated with high accretion rate stars may extend considerably into the V -band, giving the systems a bluer, less extinguished appearance. Second, several high accretion stars display considerable extended emission (e.g., HL Tau, HV Tau, FS Tau; Stapelfeldt et al. 1995; Monin & Bouvier 2000; Krist et al. 1998) and in some cases are highly polarized sources (DG Tau, HL Tau; Bastien 1982). If much of the optical flux from high accretion stars is attributable to scattered light, the preferential blue scattering from small dust grains will again give the system a bluer and less extinguished appearance. We emphasize, however, that the high accretion star phenomenon can not be explained simply as an edge-on disk orientation effect. For example, the spatially resolved edge-on disk system HK Tau B (Stapelfeldt et al. 1998b; Koresko 1998) is a borderline CTTS/WTTS ($n\text{EW}[\text{H}\alpha] = +2.5 \text{ \AA}$; Monin et al. 1998) with a modestly reddened photospheric $K - L$ color (0.46 magnitudes; Table 2). Nevertheless, the properties of high accretion stars imply that high levels of accretion are correlated with high levels of extinction and scattered light emission. In light of this correlation, we consider the optically faint CTTSs FW Tau C (Table 5), LkHa 358 (Table 7), and ITG 33a (Itoh et al. 1996; Martín 2000), which have no L -band measurements, to be candidate high accretion stars.

4.4. Implications for Binary Star Formation

As summarized by Clarke et al. (1995), the proposed binary star formation scenarios typically fall into three main categories: disk instabilities, capture, and core fragmentation. Each of these scenarios produces binary star populations with distinct stellar and circumstellar properties that can in principle be tested, and this has been the goal of many young binary star studies (Cohen & Kuhl 1979; Hartigan et al. 1994; Koresko 1995; Brandner & Zinnecker 1997; Ghez et al. 1997b; Woitas et al. 2001). The combined results of these studies favor fragmentation (e.g., Boss 1988) as the dominant binary star formation mechanism. As summarized in Ghez et al. (1997b), the observations that binary star components are coeval, that secondary star mass and mass ratio distributions are independent of the primary star mass, that secondary star masses are typically much greater than T Tauri star disk masses, and that GG Tau A retains a well defined circumbinary disk, all uphold a model in which the systems form via fragmentation. The properties of the larger sample of systems with resolved optical measurements presented here strengthen the arguments for the fragmentation scenario. In particular, the relative ages of binary star components in Taurus-Auriga are shown to be more similar than the relative ages of randomly paired single T Tauri stars in Taurus-Auriga. Although the observed coevality of these components ($\lesssim 1$ Myrs) is still considerably larger than typical collapse timescales (~ 0.1 Myrs), this is the first statistically significant evidence that demonstrates that the components of binary stars are related in a way that single stars are not. Secondly, the survival of circumstellar disks in close binary systems, the correlation of T Tauri types, and the tentative suggestion of a mass ratio dependence on separation, all provide additional support for circumbinary structures. Capture encounters are thought to preclude the formation of stable circumbinary material (Hall et al. 1996), but these structures are believed to be a natural consequence of core fragmentation. Altogether, the stellar and circumstellar properties of binary stars strongly support the conclusion that fragmentation, as opposed to disk instabilities or capture, is the dominant binary star formation mechanism.

4.5. The Overabundance of T Tauri Companions

The secondary star mass estimates can be used to eliminate one proposed explanation for the overabundance of T Tauri star companions. Over the separation range considered here (10 - 1000 AU), T Tauri stars are 2-3 times more likely to have a companion star than solar-type main-sequence stars (Ghez 1995). One suggested explanation for this is that the surveys of young stars are more sensitive to low mass companions and therefore detect low mass stars (or possibly substellar objects) that are missed in surveys of older main-sequence stars. Since most main-sequence surveys have detection limits near the stellar/substellar boundary ($0.08 M_{\odot}$; Duquennoy & Mayor 1991), this explanation would require that nearly half of T Tauri companions have masses at or below the substellar limit. In contrast to this, all of the companion masses determined here except for GG Tau Bb (1/21) are above the substellar limit. Thus the overabundance of T Tauri companions cannot be explained by a substantially higher fraction of very low mass companions. The high

binary fraction of T Tauri stars may instead be a consequence of the star formation process in low density T Associations. The star formation process in giant molecular clouds (e.g., Orion), which is believed to be the birthplace for the majority of solar-type stars (Miller & Scalo 1978), appears to produce a binary fraction than that is consistent with solar-type main-sequence stars (Petr et al. 1998; Duchêne et al. 1999a).

5. Summary and Conclusions

We have carried out an extensive high spatial resolution survey of multiple T Tauri star systems in Taurus-Auriga. Three sets of *new* observational data are presented: (1) high resolution speckle and direct imaging measurements at K and L of nearly all binary systems with separations of $0''.14 - 7''.0$ (20 - 1000 AU), (2) high resolution space-based optical, UV, and narrow-band $H\alpha$ observations of 11 binaries with separations of $0''.07 - 0''.7$ (10 - 100 AU), and (3) spatially separated, moderate resolution ($R \sim 1500$) optical spectra of four close binaries (GG Tau, GH Tau, V955 Tau, and XZ Tau; separations 35 - 50 AU). In addition to the previously known components, these observations revealed a new companion in the FW Tau system (separation = $2''.29$), making this a triple star system. The new observations presented here, in combination with previous measurements, are used to determine the stellar and circumstellar properties of the components of binary stars in Taurus-Auriga. A carefully selected sample of single T Tauri stars in this region is also identified for comparison (Appendix B).

Masses and ages for the components with optical measurements are determined from comparisons with PMS evolutionary models. The ages derived for the binary star components range from < 1 Myrs to 19 Myrs and the stellar masses range from $0.042 M_{\odot}$ to $2.11 M_{\odot}$. The distributions of these ages and masses are indistinguishable from the distributions of single T Tauri stars in Taurus-Auriga. Except for GG Tau Bb, the secondary star masses are all above the substellar limit, and this result eliminates one proposed explanation for the high frequency of companions to T Tauri stars relative to main-sequence stars. The overabundance of T Tauri companions cannot be explained by a substantially higher fraction of very low mass companions that would have been missed in main-sequence surveys.

The circumstellar accretion disks within binary star systems are studied in this work through three diagnostics - the infrared color $K - L$, UV excess, and $H\alpha$ emission. The strength of these accretion signatures for primary stars are similar to single stars, which suggests that companions as close as 10 AU have little effect on the mass accretion rate. The inferred accretion rates are used in combination with disk mass estimates from the literature to compare the disk lifetimes and the stellar ages for both single and binary T Tauri stars. Although single stars have disk lifetimes comparable to their ages, binary stars have disk lifetimes that are roughly 1/10 of their ages. Thus, the continuing disk accretion in binary systems suggests that the supposedly truncated circumprimary and circumsecondary disks are being replenished.

The circumstellar properties are used to compare circumprimary and circumsecondary disks. While there are several systems that contain only a circumprimary disk, systems that contain only a circumsecondary disk are rare. This suggests that, on average, circumprimary disks survive longer than circumsecondary disks. Primary stars also appear to accrete at a higher rate than their lower mass companions. The longer disk lifetime of circumprimary disks, despite their higher accretion rates, suggests that circumprimary disks are being preferentially replenished, possibly from a circumbinary reservoir that has low angular momentum relative to the binary. This replenishment scenario is further supported by the high mass ratios of close pairs ($\lesssim 100$ AU) as well as the similar T Tauri types of binaries with separations of less than ~ 200 AU. Bate (2000) predict that the majority of the final stellar mass for the closest systems is accreted from circumbinary material and that the closest systems will accrete more equally than wider systems. Consequently, the closest pairs are driven toward mass ratios of unity and have components with comparable disk lifetimes, consistent with the observations.

The higher mass accretion rates of primary stars relative to secondary stars are most likely due to their larger masses. Primary, secondary, and single stars of similar mass have similar mass accretion rates, but higher mass stars generally have larger accretion rates than lower mass stars. Approximately 10% of T Tauri stars, including both single stars and binary star components, can be distinguished as high accretion stars by their uncharacteristically red near- and mid-infrared colors. Optically, high accretion stars are, on average, distinctively faint and exhibit heavily veiled spectra with unusually strong forbidden-line emission; high extinction and scattered light emission appear to be correlated with enhanced accretion. High accretion stars are probably not at an earlier stage of evolution as has been proposed. The similarities they share with younger protostars at optical and infrared wavelengths stem from their similar accretion rates, which are above the norm for T Tauri stars, as opposed to their ages.

Both the stellar and circumstellar properties of this large binary star sample favor fragmentation (e.g., Boss 1988) as the dominant binary star formation process. The relative ages of binary stars, which are currently limited by measurement uncertainties, imply that binary star components are coeval to ~ 1 Myrs. These relative ages, however, still only offer weak constraints on the details of the formation since they are considerably larger than typical collapse timescales (~ 0.1 Myrs). Nevertheless, binary stars are shown to be more coeval than randomly paired single T Tauri stars within the same star forming region, which implies that they are related in a way that other stars within the same region are not (i.e. through formation). Additionally, the case for formation via fragmentation is strengthened by the direct detection of circumbinary structures (e.g. GG Tau), and the indirect evidence for circumstellar disk replenishment from a circumbinary reservoir for close pairs (e.g. short disk lifetimes, correlations in T Tauri type, high mass ratios). Circumbinary disks and/or envelopes are a natural outcome of the fragmentation process, but are difficult to retain in alternative formation scenarios such as capture. Overall, the stellar and circumstellar properties of binary T Tauri star components offer many powerful constraints on the formation and evolution of binary stars and their associated circumstellar material.

Support for this work was provided by the Packard Foundation and NASA through grants NAGW-4770 NAG5-6975 under the Origins of Solar Systems Program and grant numbers G0-06014.01-94A and G0-06735.01-95A from the Space Telescope Science Institute, which is operated by AURA, Inc., under NASA contract NAS5-26555. The authors are grateful to G. Duchêne, J. Patience, L. Prato, and R. Webb for helpful comments and discussions and appreciate the assistance provided by the FOS instrument scientists T. Keyes and E. Smith. In addition, an anonymous referee carefully reviewed this paper and provided much appreciated comments and suggestions.

A. HST Broad-Band Filter Transformations

In order to compare the HST broad-band measurements in the Vega magnitude system with standard photospheric colors and previous ground-based observations, the broad-band measurements are transformed to the more standard Johnson-Cousins filter system. These transformations, which are a function of spectral type, are calculated with STScI’s SYNPHOT package within IRAF using the dwarf spectral standards of Gunn & Stryker (1983). These transformations are listed in Table 6 for spectral types G8 through M8. Table 6 also lists the transformation values to change F675W magnitudes to F656N (narrow-band $H\alpha$) magnitudes in the Vega magnitude system. These transformation are derived in the same way that the broad-band transformations are derived, and are used to estimate the photospheric contribution to the narrow-band $H\alpha$ flux (see §2.3.2). The last column in Table 6 lists the ID numbers from Gunn & Stryker (1983) of the stars used to establish the transformations. If multiple stars are listed, the values are their average; if no stars are listed, the values are interpolated with respect to temperature from hotter and cooler spectral types. Uncertainties are estimated to be 0.02 magnitudes for U -F336W, B -F439W, and F656N-F675W transformations and 0.01 magnitudes for V -F555W, R_c -F675W, and I_c -F814W transformations for spectral types earlier than M5. These uncertainty estimates are based on variations of the transformation values for stars with similar or the same spectral type. Because of insufficient spectral standards, more conservative values of 0.05 and 0.02 magnitudes, respectively, should be adopted for the uncertainty in the transformation of cooler spectral types.

The F336W filter has a red leak, which for unextincted K and M dwarfs is typically 10% of the observed flux (Holtzmann et al. 1995b). However, by transforming the flux measurements to the Johnson-Cousins system using transformation derived from the filter throughput curves, the read leak is accounted for.

B. Single T Tauri Stars in Taurus-Auriga

In order to understand the effects of a close companion star and the binary star formation process, it is useful to have a comparison sample of single stars. Table 7 lists single T Tauri stars in Taurus-Auriga with spectral types later than K0, with both V and I_c photometry, and with strong

Li I (6708 Å; Martín 1998) absorption. These single stars were selected from the high resolution imaging studies of Ghez et al. (1993, 2001), Leinert et al. (1993), Simon et al. (1995), Sartoretti et al. (1998), and Bertout et al. (1999)¹¹. Spectroscopic binaries and radial velocity variables were also excluded when radial velocity measurements were available (Hartmann et al. 1986, 1987; Walter et al. 1988; Mathieu et al. 1997). We also report that CoKu Tau 4, FN Tau, Haro 6-13, and JH 108 are single stars (Ghez et al. 1993; Leinert et al. 1993; Simon et al. 1995) that have insufficient optical photometry to be included (Kenyon & Hartmann 1995). Although all stars in Table 7 have no known companions within 10''0, some small fraction of these 'single' stars may nevertheless have a companion at a separation less than the survey resolution (typically 0''.1) or with a brightness below the detection limit (typically 2-3 magnitudes fainter than the target star at 2.2 μm). Additionally, near several stars listed here as single are additional T Tauri stars at separations just above 10''0 (DH Tau & DI Tau; GI Tau & GK Tau; Hartigan et al. (1994)). These wide pairs may be associated.

The HST transformed, Johnson-Cousins photometry for the two single T Tauri stars imaged in this program, FY Tau and FZ Tau, are listed here for completeness. FY Tau: $U = 17.37 \pm 0.04$, $B = 17.11 \pm 0.05$, $V = 15.18 \pm 0.02$, $R_c = 13.67 \pm 0.03$, $I_c = 12.31 \pm 0.02$. FZ Tau: $U = 15.98 \pm 0.02$, $B = 16.40 \pm 0.06$, $V = 15.05 \pm 0.07$, $R_c = 13.60 \pm 0.08$, $I_c = 12.26 \pm 0.04$. The star near FW Tau, at a separation of 12''20 and position angle of 246.8° from the primary, exhibits Hα absorption ($EW[H\alpha] = +6.5 \pm 0.6$) and is assumed to be a background star.

The stellar and circumstellar properties of the single stars are derived following the methodology outlined in §3. These values are listed Table 7 along with the optical photometry and spectral type references. The values inferred for the high accretion stars should be used with caution (§3.1.1). The single star sample is plotted on an H-R diagram in Figure 3. The inferred ages range from < 1 Myrs to 19 Myrs and the inferred masses range from 0.087 M_⊙ to 1.24 M_⊙ (Table 7). The WTTs and CTTSs have similar distributions of masses and ages. If stars with an age upper limit are assigned an age of 1 Myrs, the mean log[age] of the 29 CTTSs is 6.46 ($\sigma = 0.40$) and the mean log[age] of the 20 WTTs is 6.29 ($\sigma = 0.35$). The combined sample of 49 stars has a mean log[age] of 6.39 ($\sigma = 0.39$).

REFERENCES

- Armitage, P. J., Clarke, C. J. & Tout, C. A. 1999, MNRAS, 304, 425
- Artymowicz, P. & Lubow, S., H. 1994, ApJ, 421, 651
- Artymowicz, P. & Lubow, S., H. 1996, ApJ, 467, L77

¹¹Although stars have been detected close to GK Tau and HO Tau (Hartigan et al. 1994), optical photometry demonstrate that they are unlikely to be associated and too faint to bias the inferred properties.

- Baraffe, I., Chabrier, G., Allard, F., & Hauschildt, P. H. 1998, *A&A*, 337, 403
- Basri, G. & Batalha, C. 1990, *ApJ*, 363, 654
- Basri, G., Johns-Krull, C. M., & Mathieu, R. D. 1997, *AJ*, 114, 781
- Basri, G. & Marcy, G. W. 1995, *AJ*, 109, 762
- Bastien, P. 1982, *A&AS*, 48, 153
- Bate, M. R. 2000, *MNRAS*, 314, 33
- Bate, M. R. & Bonnell, I. A. 1997, *MNRAS*, 285, 33
- Bates, R. H. T., & Cady, F. M. 1980, *Opt. Commun.*, 32, 365
- Beckwith, S. V. W., Sargent, A. I., Chini, R. S., & Guesten, R. 1990, *AJ*, 99, 924
- Bertout, C., Basri, G., & Bouvier, J. 1988, *ApJ*, 330, 350
- Bertout, C., Robichon, N., & Arenou, F. 1999, *A&A*, 352, 574
- Bessell, M. S. 1991, *AJ*, 102, 303
- Bessell, M., & Brett, J. M. 1988, *PASP*, 100, 1134
- Biretta, J. A., et al. 1996, *WFPC2 Instrument Handbook, Version 4.0* (Baltimore: STScI)
- Bonnell, I. & Bastien, P. 1992, *ApJ*401, L31
- Boss, A. P. 1988, *Comments Astrophys.*, 12, 169
- Boss, A. P. 1993, *ApJ*, 410, 157
- Bouvier, J., Tessier, E., & Cabrit, S. 1992, *A&A*, 261, 451
- Brandner, W. & Zinnecker, H. 1997, *A&A*, 321, 220
- Briceño, C., Hartmann, L. W., Stauffer, J., Gagné, M., Stern, R. A., & Caillault, J. 1997, *AJ*, 113, 740
- Briceño, C., Hartmann, L. W., Stauffer, J., & Martín, E. 1998, *AJ*, 115, 2074
- Chen, W. P. & Simon, M. 1997, *AJ*, 113, 752
- Chen, W. P., Simon, M., Longmore, A. J., Howell, R. R., & Benson, J. A. 1990, *ApJ*, 357, 224
- Christou, J. C. 1991, *PASP*, 103, 1040
- Clarke, C. J. 1995, in *Evolutionary Processes in Binary Stars*, eds. R. A. M. J. Wijers, M. B. Davies & C. A. Tout (Dordrecht:Kluwer), 477

- Close, L. et al. 1998, ApJ, 499, 883
- Cohen, M. & Kuhi, L. V. 1979, ApJS, 41, 743
- Duchêne, G. 1999a, A&A, 341, 547
- Duchêne, G., Monin, J. -L., Bouvier, J., & Ménard, F. 1999b, A&A, 351, 954
- Duquennoy, A. & Mayor, M. 1991, A&A, 248, 485
- Dutrey, A., Guilloteau, S., Duvert, G., Prato, L., Simon, M., Schuster, K., & Ménard, F. 1996, A&A, 309, 493
- Dutrey, A., Guilloteau, S., Prato, L., Simon, M., Duvert, G., Schuster, K., & Ménard, F. 1998, A&A, 338, L63
- Dutrey, A., Guilloteau, S., & Simon, M. 1994, A&A, 286, 149
- Duvert, G., Dutrey, A., Guilloteau, S., Ménard, F., Schuster, K., Prato, L., Simon, M. 1998, A&A, 332, 867
- Dyck, H. M, Simon, T., & Zuckerman, B. 1982 ApJ, 255, 103
- Eisloffel, J. & Mundt, R. 1998, AJ, 115, 1554
- Gahm, G. F., Petrov, P. P., Duemmier, R., Gameiro, J. F., & Lago, M. T. V. T. 1999, A&A, 352, L95
- Ghez, A. M. 1995, in Evolutionary Processes in Binary Stars, eds. R. A. M. J. Wijers, M. B. Davies & C. A. Tout (Dordrecht:Kluwer), 477
- Ghez, A. M., Weinberger, A. J., Neugebauer, G., Matthews, K., McCarthy, Jr., D. W. 1995, AJ, 110, 753
- Ghez, A. M., McCarthy, D. W., Patience, J. L., Beck, T. L. 1997a, ApJ, 481, 378
- Ghez, A. M., Klein, B. L., Morris, M., Becklin, E. E. 1998, ApJ, 509, 678
- Ghez, A. M., Neugebauer, G., & Matthews, K. 1993, A&A, 106, 2005
- Ghez, A. M., Neugebauer, G., Gorham, P. W., Haniff, C. A., Kulkarni, S. R., Matthews, K., Koresko, C., & Beckwith, S. 1991, AJ, 102, 2066
- Ghez, A. M., White, R. J., & Simon, M. 1997b, ApJ, 490, 353
- Ghez, A. M., Sand, D., & White, R. J. 2001, in prep.
- Gorham, P. W., Ghez, A. M., Haniff, S. R., Kulkarni, K., Matthews, K & Neugebauer, G. 1992, AJ, 103, 953

- Guenther, E. & Hessman, F. V. 1993, *A&A*, 268, 192
- Guilloteau, S. & Dutrey, A. 1994, *A&A*, 291, L23
- Guilloteau, S., Dutrey, A., & Simon, M. 1999, *A&A*, 348, 570
- Gullbring, E., Hartmann, L. W., Briceño, C., & Calvet, N. 1998, *ApJ*, 492, 323
- Gullbring, E., Calvet, N., Muzerolle, J., & Hartmann, L. 2000, *ApJ*, 544, 927
- Gunn, J. E. & Stryker, L. L. 1983, *ApJS*, 52, 121
- Haisch, K. E., Lada, E. A., & Lada, C. J. 2000, *AJ*, 120, 1396
- Haas, M., Leinert, Ch., & Zinnecker, H. 1990, *A&A*, 230, L1
- Hall, S. M., Clarke, C. J., & Pringle, J. E. 1997, *MNRAS*, 278, 303
- Hartigan, P., Edwards, S., Ghandour, L. 1995, *ApJ*, 452, 736
- Hartigan, P., Kenyon, S. J., Hartmann, L. W., Strom, S. E., Edwards, S., Welty, A. D., & Stauffer, J. 1991, *ApJ*, 382, 617
- Hartigan, P., Strom, K. M., & Strom, S. E. 1994, *ApJ*, 427, 961
- Hartmann, L. 1998, *Accretion Processes in Star Formation* (Cambridge: Cambridge University Press)
- Hartmann, L. W., Cassen, P., & Kenyon, S. J. 1997, *ApJ*, 475, 770
- Hartmann, L., Stauffer, J. R., Kenyon, S. J., & Jones, B. F. 1991, *AJ*, 101, 1050
- Hartmann, L., Hewett, R., Stahler, S., & Mathieu, R. D., 1986, *ApJ*, 309, 275
- Hartmann, L., Soderblom, D. R., & Stauffer, J. R. 1987, *AJ*, 93, 907
- Henry, T. J. & McCarthy, D. W. 1993, *AJ*, 106, 773
- Herbig, G. H. & Bell, K. R. 1988, *Lick Obs. Bull.*, 1111, 1
- Herbst, W., Herbst, D. K., & Grossman, E. J. 1994, *AJ*, 108, 1906
- Hessman, F., V. & Guenther, E., W. 1997, *A&A*, 321, 497
- Hillenbrand, L. A., Strom, S. E., Calvet, N., Merrill, K. M., Gatley, I., Makindon, R. B., Meyer, M. R., & Skrutskie, M. F. 1998, *AJ*, 116, 1816
- Holtzmann, J. A. et al. 1995a, *PASP*, 107, 156

- Holtzmann, J. A., Burrows, C. J., Casterno, S., Hester, J. J., Trauger, J. T., Watson, A. M., & Worthy, G. 1995b, *PASP*, 107, 1065
- Itoh, Y., Tamura, M., & Gatley, I. 1996, *ApJ*, 465, L129
- Jensen, E., L., N., Mathieu, R., D., & Fuller, G., A. 1994, *ApJ*, 429, L29
- Jensen, E., L., N., Mathieu, R., D., & Fuller, G., A. 1996, *ApJ*, 458, 312
- Jensen, E., L., N., Koerner, D. W., & Mathieu, R., D. 1996, *AJ*, 111, 2431
- Kenyon, S. J. & Hartmann, L. W. 1990, *ApJ*, 349, 197
- Kenyon, S. J. & Hartmann, L. W. 1995, *ApJS*, 101, 117
- Kenyon, S. J., Hartmann, L. W., Strom, K. M., & Strom, S. E. 1990, *AJ*, 99, 869
- Kenyon, S. J., Dobrzycka, D., & Hartmann, L. W. 1994, *AJ*, 108, 1872
- Kenyon, S. J., Brown, D. I., Tout, C. A., & Berlind, P. 1998, *AJ*, 115, 2491
- Keyes, C. D. 1997, *HST Data Handbook*, ed. C. D. Keyes, version 3.0, Vol. 2, (Baltimore: STScI)
- Keyes, C. D., Koratkar, A. P., Dahlem, M., Hayes, J., Christensen, J., & Martin, S. 1995, *Faint Object Spectrograph Instrument Handbook*, version 6.0, (Baltimore: STScI)
- Kirkpatrick, J. D., Kelly, D. M., Rieke, G. H., Liebert, J., Allard, F., & Wehrse, R. 1993, *ApJ*, 402, 643
- Kirkpatrick, J. D. & McCarthy, D. W. Jr. 1994, *AJ*, 107, 333
- Köhler, R. & Leinert, Ch. 1998, *A&A*, 331, 977
- Königl, A. 1991, *ApJ*, 370, L39
- Koresko, C. D. 1995, *ApJ*, 440, 764
- Koresko, C. D. 1998, *ApJ*, 507, L145
- Koresko, C. D. 2000, *ApJ*, 531, L147
- Koresko, C. D., Herbst, T. M., & Leinert, Ch. 1997, *ApJ*, 480, 741
- Krist, J. E., et al. 1997, *ApJ*, 481, 447
- Krist, J. E., et al. 1998, *ApJ*, 501, 841
- Krist, J. E., et al. 1999, *ApJ*, 515, L35

- Lada, C. J., Muench, A. A., Haisch, K. E. Jr., Lada, E. A., Alves, J. F., Tollestrup, E. V., & Willner, S. P. 2000, *AJ*, 120, 3162
- Lada, C. J. & Wilking, B. A. 1984, *ApJ*, 287, 610
- Labeyrie, A. 1970, *A&A*, 6, 85
- Lavalley, C., Cabrit, S., Dougados, C., Ferruit, P., & Bacon, R. 1997, *A&A*, 327, 671
- Leinert, Ch. & Haas, M. 1989, *ApJ*, 342, L39
- Leinert, Ch., Haas, M., Richichi, A., Zinnecker, H., & Mundt, R. 1991, *A&A*, 250, 407
- Leinert, Ch., Zinnecker, H., Weitzel, N., Christou, J., Ridgway, S. T., Jameson, R., Haas, M., & Lenzen, R. 1993, *A&A*, 278, 129
- Luhman, K. L., Briceño, C., Rieke, G. H., & Hartmann, L. W. 1998, *ApJ*, 493, 909
- Luhman, K. L. 1999, *ApJ*, 525, 466
- Magazzú, A. & Martín, E. L. 1994, *A&A*, 1994, 287
- Martín, E. L. 1998, *AJ*, 115, 351
- Martín, E. L. 2000, *AJ*, 120, 2114
- Martín, E. L., Rebolo, R., Magazzú, A., & Pavlenko, Ya. V. 1994, *A&A*, 282, 503
- Mathieu, R. D. 1994, *ARA&A*, 32, 465
- Mathieu, R. D., Ghez, A. M., Jensen, E. L. N., & Simon, M. 2000, in *Protostars and Planets IV*, ed. V. Mannings, A. P. Boss, S. S. Russell (Tucson: University of Arizona), in press
- Mathieu, R. D., & Stassun, K., Basri, G., Jensen, E. L. N., Johns-Krull, C. M., Valenti, J. A., Hartmann, L. W. 1997, *AJ*, 113, 1841
- Mathieu, R. D., Walter, F. M., & Myers, P. C. 1989, *AJ*, 98, 987
- McDonald, J., M. & Clarke, C., J. 1995, *MNRAS*, 275, 671
- Ménard, F., Monin, J., -L., Angelucci, F., & Rouan, D. 1993, *ApJ*, 414, L117
- Meyer, M. R., Calvet, N., & Hillenbrand, L. A. 1997, *AJ*, 114, 288
- Miller, G. E. & Scalo, J. M. 1978, *PASP*, 90, 506
- Monet, D. G., Dahn, C. C., Vrba, F. J., Harris, H. C., Pier, J. R., Luginbuhl, C. B., & Ables, H. D. 1992, *AJ*, 103, 638
- Moneti, A. & Zinnecker, H. 1991, *A&A*, 242, 428

- Monin, J. -L., & Bouvier, J. 2000, *A&A*, 356, 75
- Monin, J. -L., Menard, F., & Duchêne, G. 1998, *A&A*, 339, 113
- Montes, D., Martín, E. L., Fernández-Figueroa, M. J., Cornide, M. & De Castro, E. 1997, *A&AS*, 123, 473
- Mundt, R., & Giampapa, M. S. 1982, *ApJ*, 256, 156
- Myers, P. C., Fuller, G. A., Goodman, A. A., & Benson, P. J. 1991, *ApJ*, 376, 551
- Myers, P. C., Fuller, G. A., Mathieu, R. D., Beichman, C. A., Benson, P. J., Schild, R. E., & Emerson, J. P. 1987, *ApJ*, 319, 340
- Muzerolle, J., Calvet, N., & Hartmann, L. 1998, *ApJ*, 492, 743
- Osterloh, M. & Beckwith, S. V. W. 1995, *ApJ*, 439, 288
- Padgett, D. L., Brandner, W., Stapelfeldt, K. R., Strom, S. E., Terebey, S., & Koerner, D. 1999, *AJ*, 117, 1490
- Palla, F. & Stahler, S. 1999, *ApJ*, 525, 772
- Petr, M. G., Coude Du Foresto, V., Beckwith, S. V. W., Richichi, A., McCaughrean, M. J. 1998, *ApJ*, 500, 825
- Petrov, P. P., Gahm, G. F., Gameiro, J. F., Duemmler, R., Ilyin, I. V., Laakkonen, T., Lago, M. T. V. T., Tuominen, I. 2001, *A&A*, in press
- Prato, L. & Simon, M. 1997, *ApJ*, 474, 455
- Prato, L. & Monin, J. -L. 2001, in 'The Formation of Binary Stars', ed. H. Zinnecker & R. Mathieu, in press
- Preibisch, T. & Smith, M. D. 1997, *A&A*, 322, 825
- Pringle, J. E. 1989, *MNRAS*, 239, 361
- Rayner, J., et al. 1993, *Proc. SPIE*, 1946, 490
- Rieke, G. H. & Lebofsky, M. J. 1985, *ApJ*, 288, 618
- Reipurth, B. & Zinnecker, H. 1993, *A&A*, 278, 81
- Rice, J. B. & Strassmeier, K. G. 1996, *A&A*, 316, 164
- Richichi, A., Leinert, Ch., Jameson, R., & Zinnecker, H. 1994, *A&A*, 287, 145
- Roddier, C., Roddier, F., Northcott, M. J., Graves, J. E., & Jim, K. 1996, *ApJ*, 463, 326

- Sartoretti, P., Brown, R. A., Latham, D. W., & Torres, G. 1998, *A&A*, 334, 592
- Schwartz, R. D. 1983, *ARA&A*, 21, 209
- Shu, F. H., Adams, F. C., & Lizano, S. 1987, *ARA&A*, 25, 23
- Shu, F. H., Tremaine, S., Adams, F. C., & Ruden, S. P. 1990, *ApJ*, 358, 495
- Shure, M., et al. 1994, *Exp. Astron.*, 3, 239
- Simon, M., Chen, W. P., Howell, R. R., Benson, J. A., Slowick, D. 1992, *ApJ*, 384, 212
- Simon, M., Ghez, A. M., Leinert, Ch., Cassar, L., Chen, W. P., Howell, R. R., Jameson, R. F., Matthews, K., Neugebauer, G., & Richichi, A. 1995, *ApJ*, 443, 625
- Simon, M., Dutrey, A., & Guilloteau, S. 2000, *ApJ*, in press
- Stapelfeldt et al. 1995, *ApJ*, 449, 888
- Stapelfeldt et al. 1997, *ApJ*, 508, 736
- Stapelfeldt, K. R. et al. 1998a, *ApJ*, 508, 736
- Stapelfeldt, K. R., Krist, J. E., Ménard, F., Bouvier, J., Padgett, D. L., Burrows, C. J. 1998b, *ApJ*, 502, L65
- Stahler, S. W. 1983, *ApJ*, 274, 822
- Stahler, S. W. 1988, *ApJ*, 332, 804
- Stapelfeldt, K. R., Krist, J. E., Menard, F., Bouvier, J., Padgett, D., L., & Burrows, C. J. 1998 *ApJ*, 502, L65
- Strom, K. M., Strom, S. E., Edwards, S. Cabrit, S., & Skrutskie, M. F. 1989, 97, 1451
- Strom, K. M. & Strom, S. E. 1994, *ApJ*, 424, 237
- Walter, F. M., Brown, A., Mathieu, R. D., Myers, P. C., & Vrba, F. J. 1988, *AJ*, 96, 297
- Welty, A., D. 1995, *AJ*, 110, 776
- White, R. J. 2001, in 'The Formation of Binary Stars', ed. H. Zinnecker & R. Mathieu, in press
- White, R. J., Ghez, A. M., Reid, N. I., & Schultz, G. 1999, *ApJ*, 520, 811
- Whitney, B. A., Kenyon, S. J., & Gomez, M. 1997, *ApJ*, 485, 703
- Whitmore, B., Heyer, I. & Casertano, S. 1999, *PASP*, 111, 1559
- Wichmann, R. et al. 1996, *A&A*, 312, 439

Woitas, J. & Leinert, Ch. 1998, *A&A*, 338, 122

Woitas, J., Leinert, Ch., & Köhler, R. 2001, *A&A*, submitted

Zinnecker, H. & Wilking, B. A. 1992, in 'Binary Stars as Tracers of Stellar Formation,' ed. A. Duquennoy & M. Mayor (Cambridge: Cambridge Univ. Press)

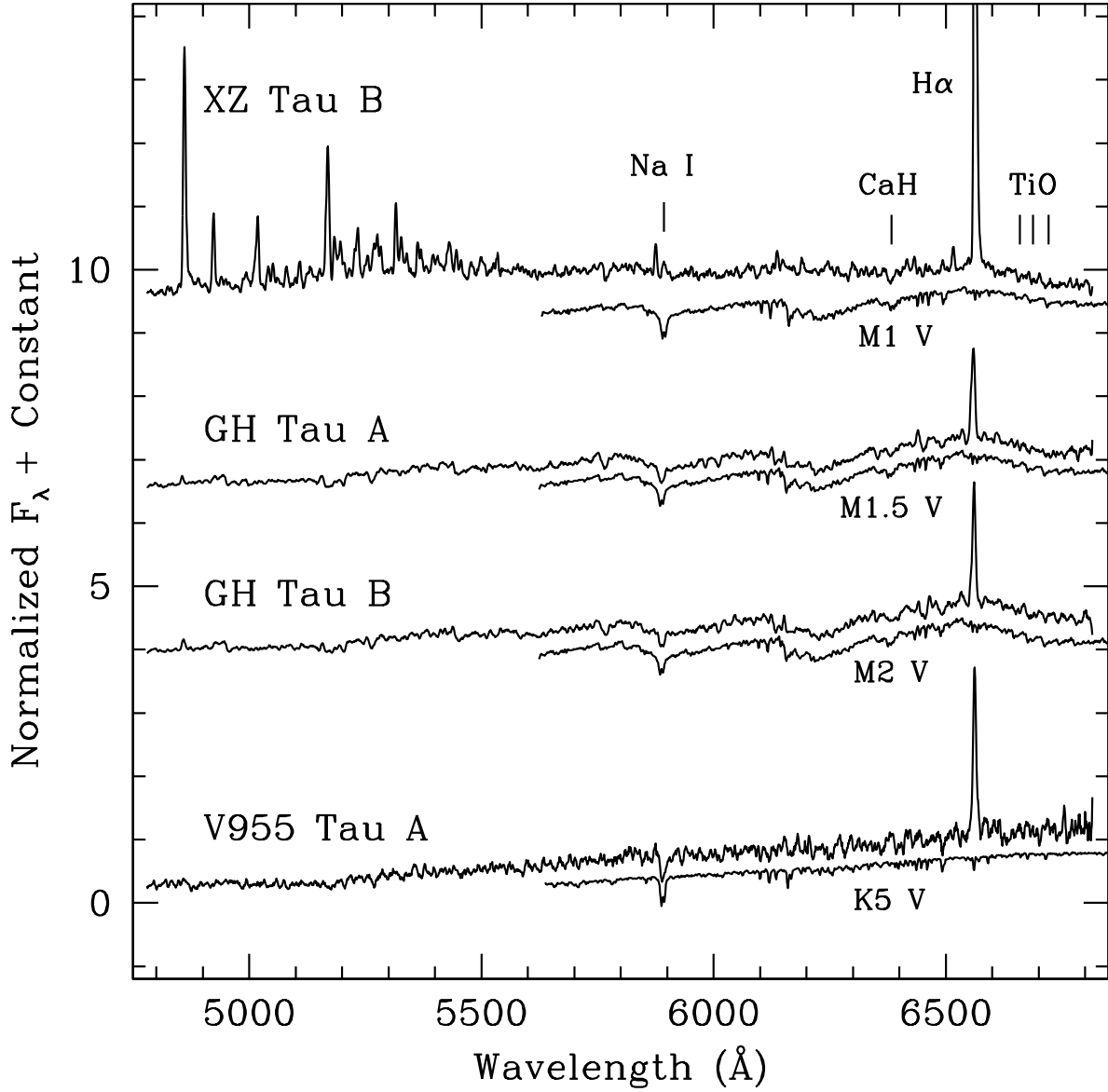


Fig. 1.— Hubble Space Telescope / Faint Object Spectrograph spectra of XZ Tau B, GH Tau A, GH Tau B, and V955 Tau A, normalized at 6500 Å. The spectra have been offset vertically for clarity, but have the same relative scaling. Dwarf spectra of similar spectral type are also shown, displaced vertically, over the wavelength region used for spectral classification. The XZ Tau B spectrum is heavily veiled, but nevertheless shows faint TiO absorption near 6700 Å.

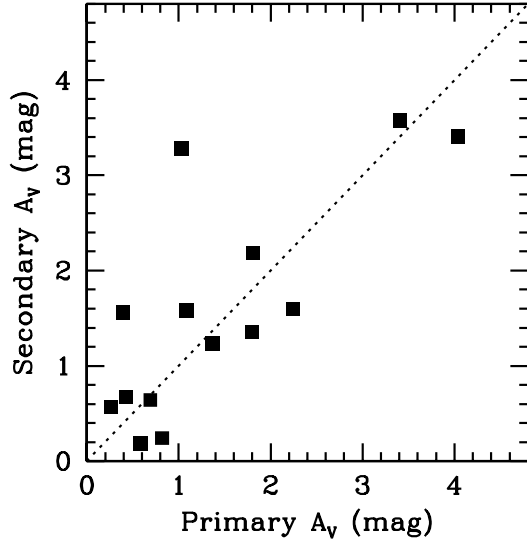


Fig. 2.— The visual extinctions of secondary stars are plotted versus the visual extinctions of primary stars for binary systems in which the extinction of each component is determined independently. Six pairs are from Taurus-Auriga (Table 5); eight pairs are from Chamaeleon, Lupus, and Ophiuchus (Brandner & Zinnecker 1997). The components of a binary system typically have similar visual extinctions.

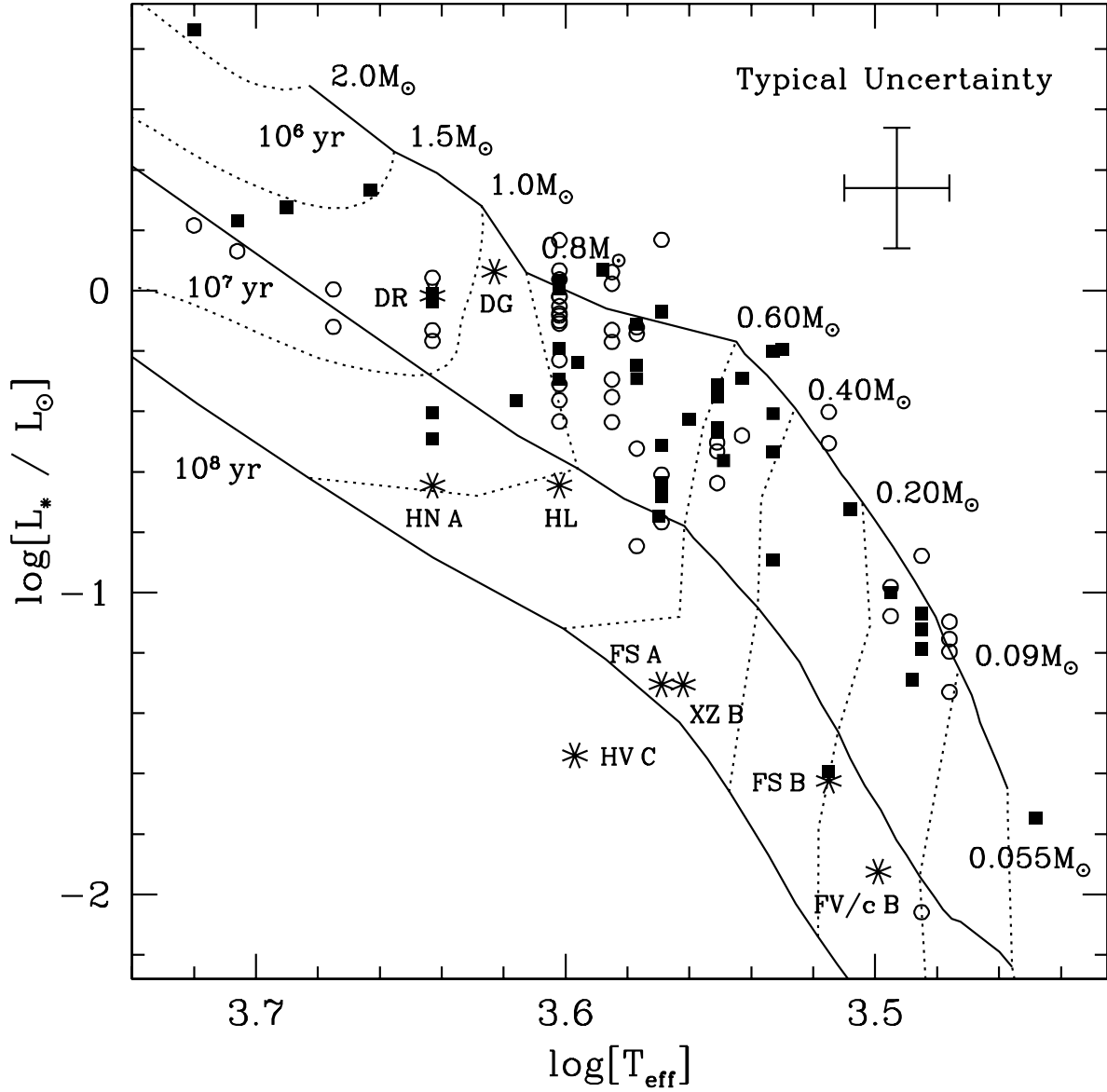
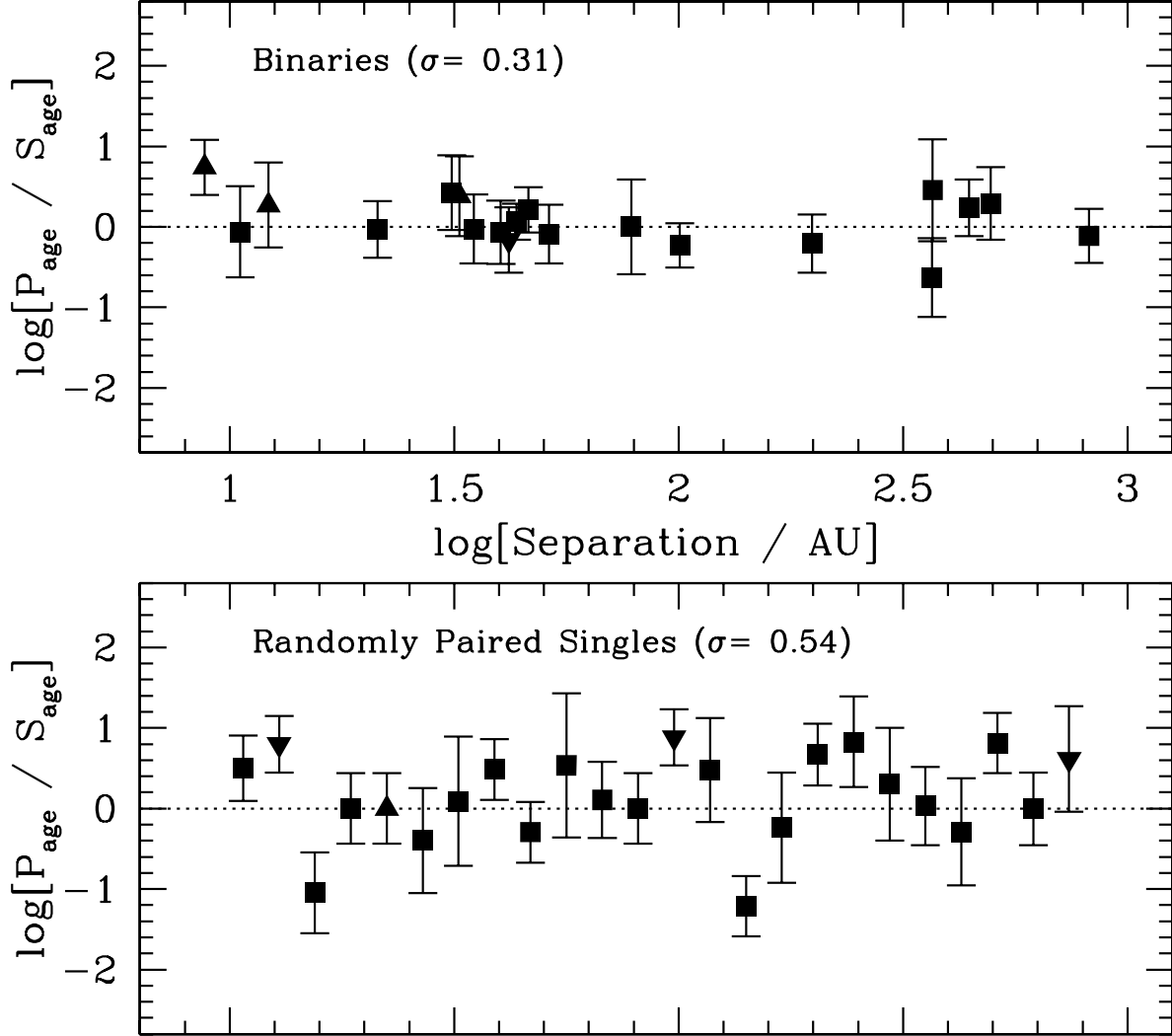


Fig. 3.— The components of the multiple star systems (*squares*) and single stars (*circles*) are plotted on an H-R diagram along with adopted PMS evolutionary models of Baraffe et al. (1998; $M < 1.0 M_\odot$) and Palla & Stahler (1998; $M > 1.0 M_\odot$). Since the adopted method for deriving luminosities and temperatures is inadequate for high accretion stars (§3.1.1), these objects are distinguished as *asterisks* and labeled.



Arbitrary Distribution

Fig. 4.— The relative ages of binary star components are plotted versus their projected separations. The *triangles* represent systems with either primary age upper limits (*downward pointing*) or secondary age upper limits (*upward pointing*). There is no statistically significant difference in age between primaries and secondaries over all separation ranges. The bottom panel shows the relative ages for a sample of randomly paired single stars, plotted with arbitrary separations. The components of binary stars are generally more coeval than single stars within the same star forming region.

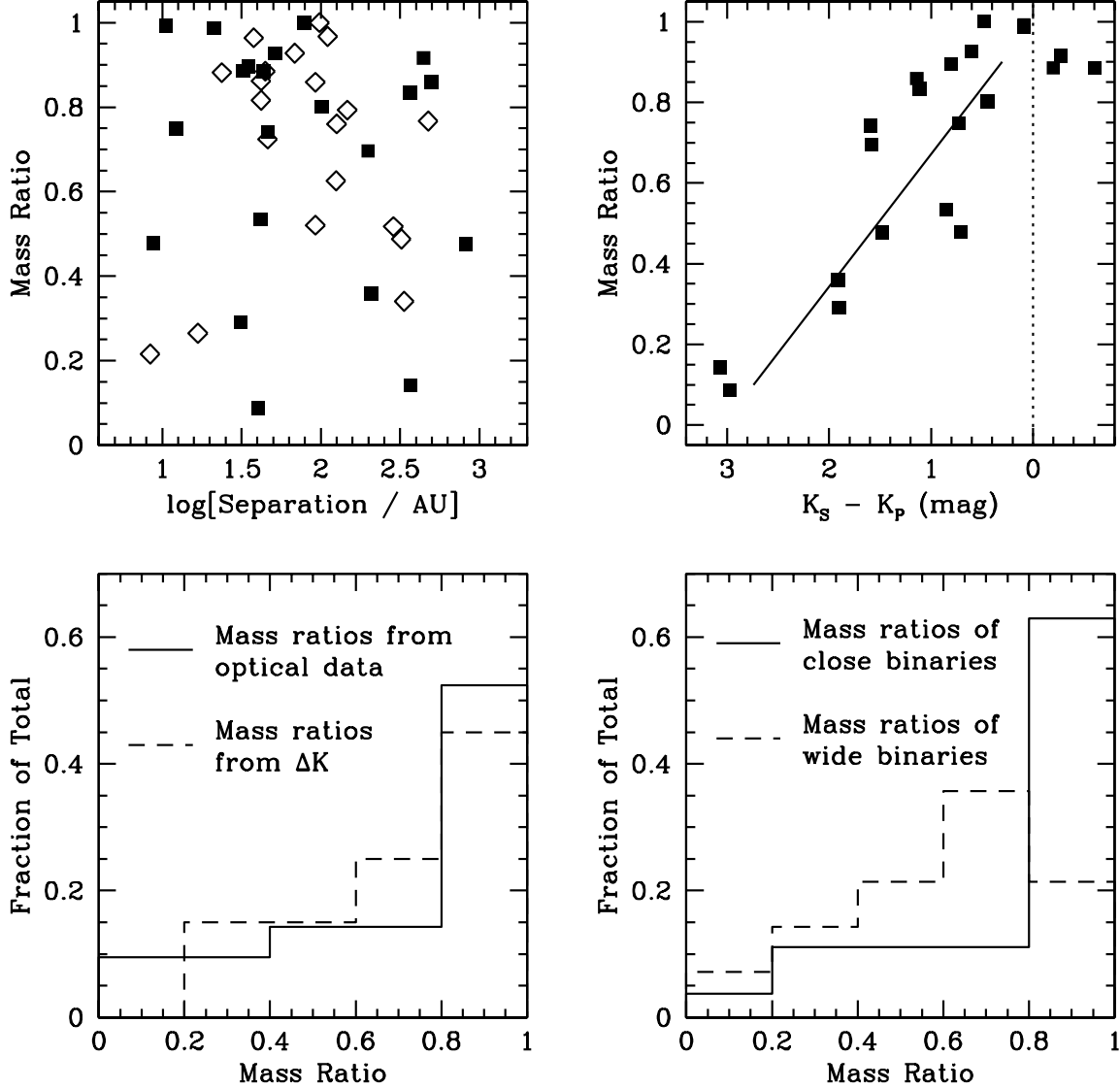


Fig. 5.— In the top left panel, the mass ratios (m_s/m_p) of pairs are plotted versus the their projected separations. *Solid squares* represent mass ratios computed from optically resolved measurements (Table 5). *Open diamonds* represent mass ratios computed from K magnitude differences, following the linear relation shown in the top right panel ($m_s/m_p = 1 - 0.328\Delta K$). The bottom left panel shows that mass ratios computed from optical measurements (*solid histogram*) and from K magnitude differences (*dashed histogram*) are similar and are peaked toward unity. Combining mass ratios computed from both methods, the bottom right panel shows that close pairs (*solid histogram*) have a higher fraction of high mass ratio binaries than wide pairs (*dashed histogram*).

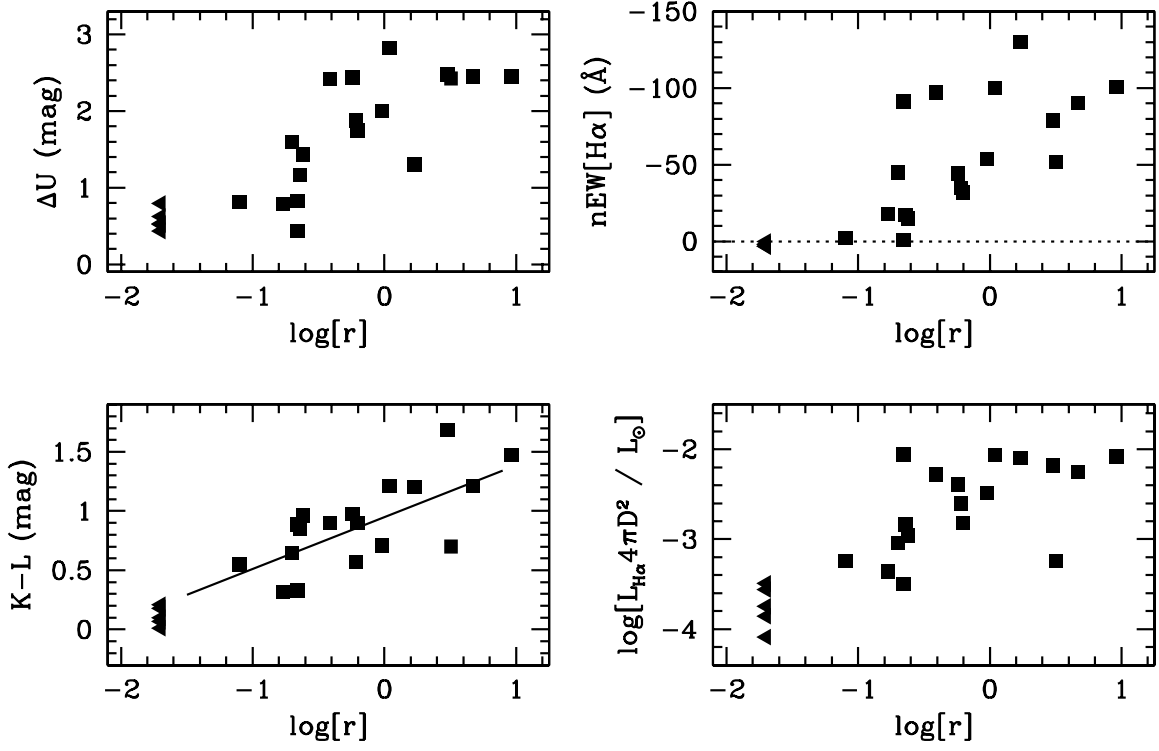


Fig. 6.— The ΔU s, $K - L$ colors, $nEW(H\alpha)$ s, and $H\alpha$ luminosities (§3.2.1) of single T Tauri stars are compared to their levels of optical excess emission ($r = F_{ex}/F_{phot}$) measured in high resolution optical spectra (Hartigan et al. 1995). *Triangles* represent stars with optical excess upper limits. All diagnostics are at least modestly correlated with the level of optical excess. A linear least squares fit to the $K - L$ versus $\log[r]$ relation is also shown ($\log[r] = 2.199(K - L) - 2.148$).

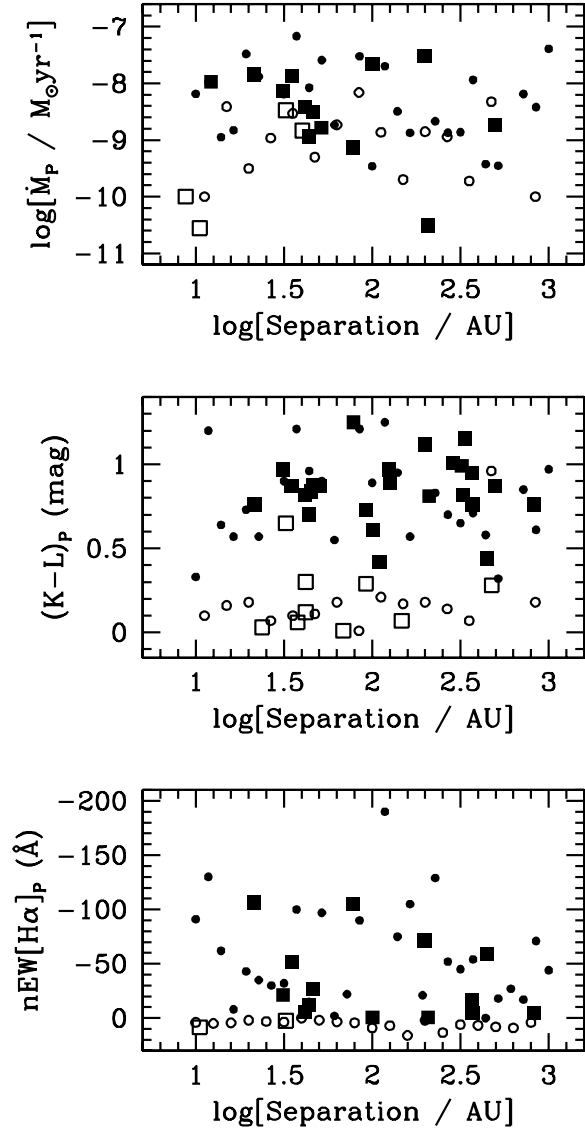


Fig. 7.— The mass accretion rates, the $K - L$ colors, and the $n\text{EW}[\text{H}\alpha]_P$ s of the CTTS primaries (*large filled squares*) and WTTS primaries (*large open squares*) are plotted versus the projected separations of their companions. The corresponding accretion diagnostics of single CTTSs (*small filled circles*) and WTTSs (*small open circles*) are also plotted with an arbitrary distribution of separations for comparison. The accretion signatures of primaries and singles are similar.

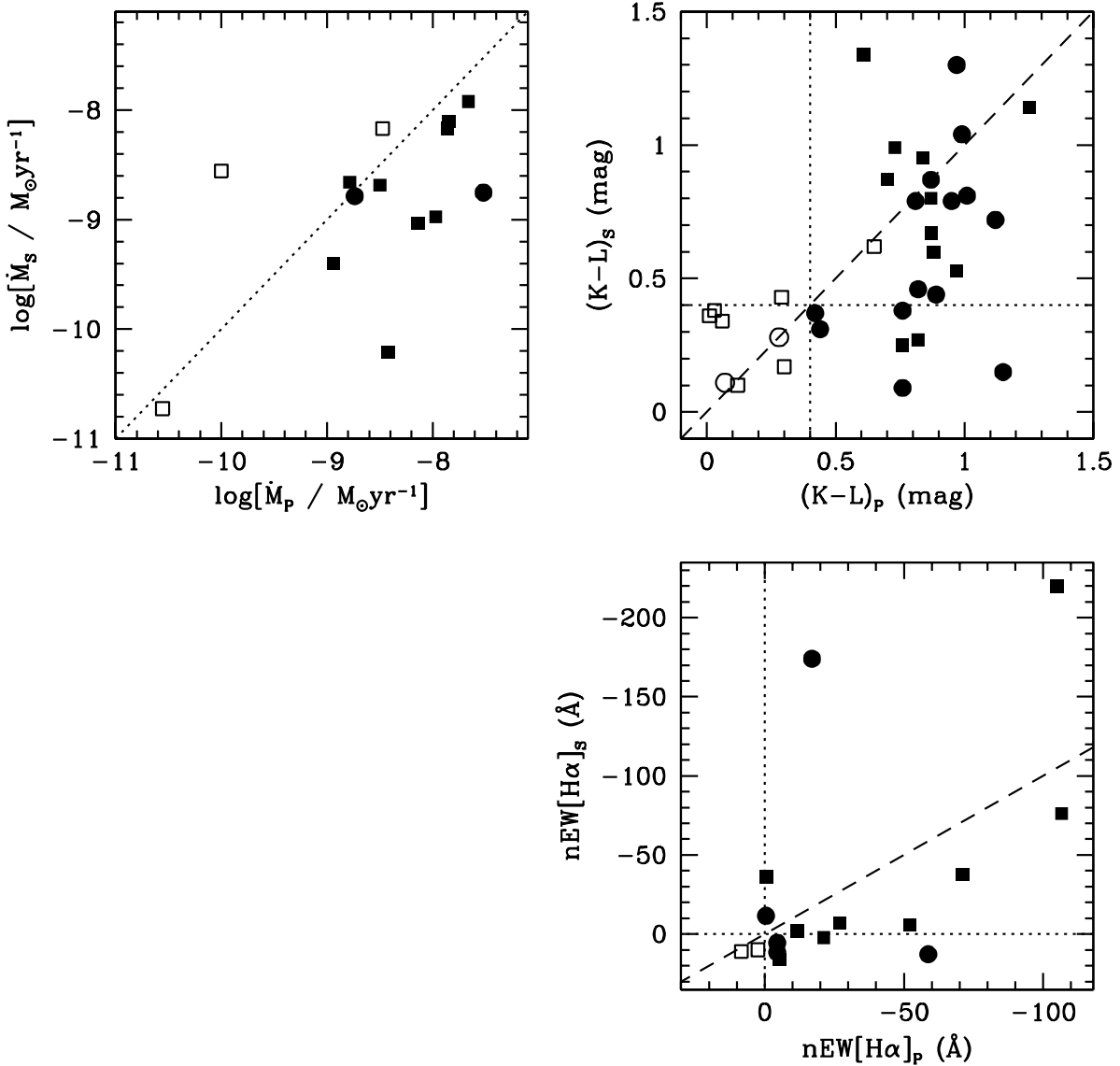


Fig. 8.— The mass accretion rates, the $K - L$ colors, and the $nEW[H\alpha]_s$ of secondary stars are compared to primary stars. CTTS systems (*filled symbols*) are distinguished from WTTS systems (*open symbols*) and close pairs (10-100 AU; *squares*) are distinguished from wide pairs (100-1000 AU; *circles*). $K - L$ colors greater than 0.4 magnitudes and $nEW[H\alpha]_s$ greater than zero imply the existence of a circumstellar disk. Primary stars appear to have, on average, accretion signatures that are comparable to or larger than those of their companions. Although several systems appear to harbor a circumprimary disk and no circumsecondary disk, systems with only a circumsecondary disk are much more rare.

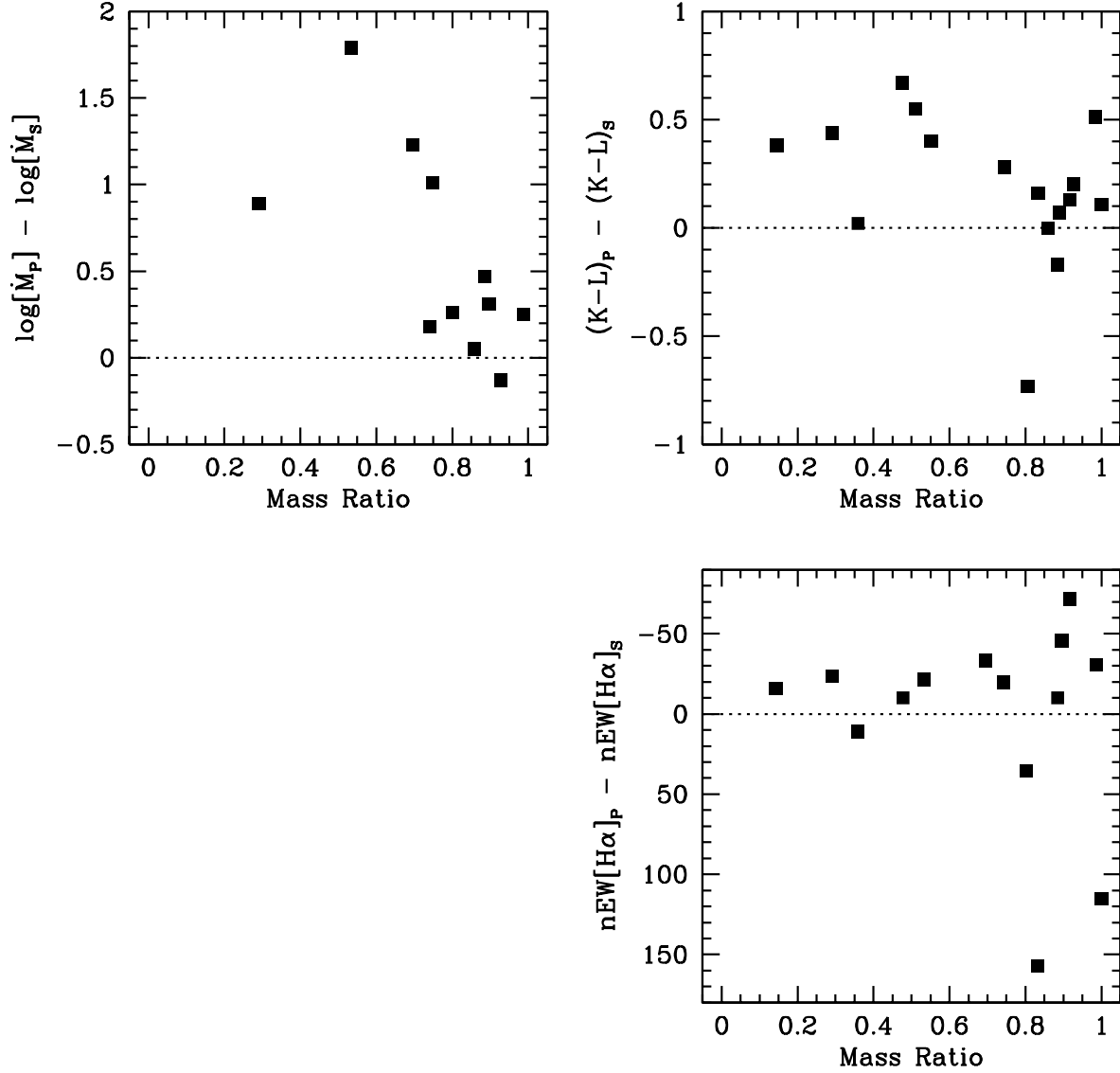


Fig. 9.— The differences in the mass accretion rates, the $K - L$ colors, and the $nEW[H\alpha]$ s of primaries and secondaries are plotted versus the binary mass ratios (m_s/m_p). For pairs with comparable masses ($m_s/m_p > 0.8$), the primaries and secondaries have accretion signatures of comparable strength. For systems with small mass ratios ($m_s/m_p < 0.8$), the primaries generally have the dominant accretion signatures.

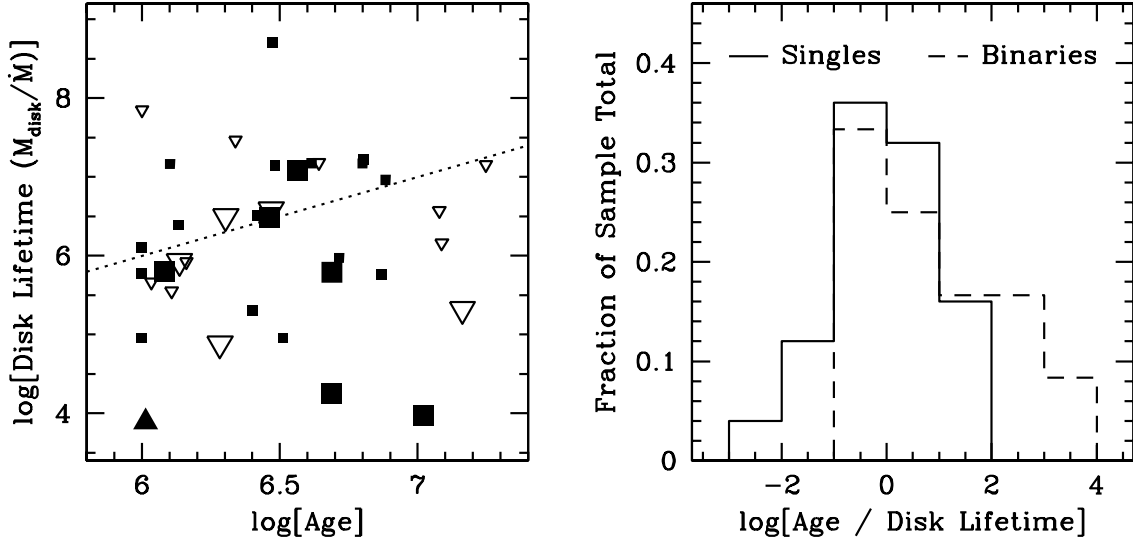


Fig. 10.— In the left panel, the disk lifetimes (M_{disk}/\dot{M}) of single (*small symbols*) and binary (*large symbols*) T Tauri stars are compared to their stellar ages. *Solid squares* are calculated from disk mass estimates, *solid triangles* are calculated from disk mass lower limits, and *open triangles* are calculated from disk mass upper limits (Osterloh & Beckwith 1995; Beckwith et al. 1990; Dutrey et al. 1996; Guilloteau et al. 1999). The *dotted line* represents disk lifetimes equal to stellar ages. In the right panel, the distributions of $\log[\text{Age}/\text{Disk Lifetime}]$ for singles and binaries are shown. Single stars have, on average, disk lifetimes comparable to their ages, and binary stars have, on average, disk lifetimes that are roughly 1/10 of their ages, but the distributions of $\log[\text{Age}/\text{Disk Lifetime}]$ for singles and binaries are only marginally different.

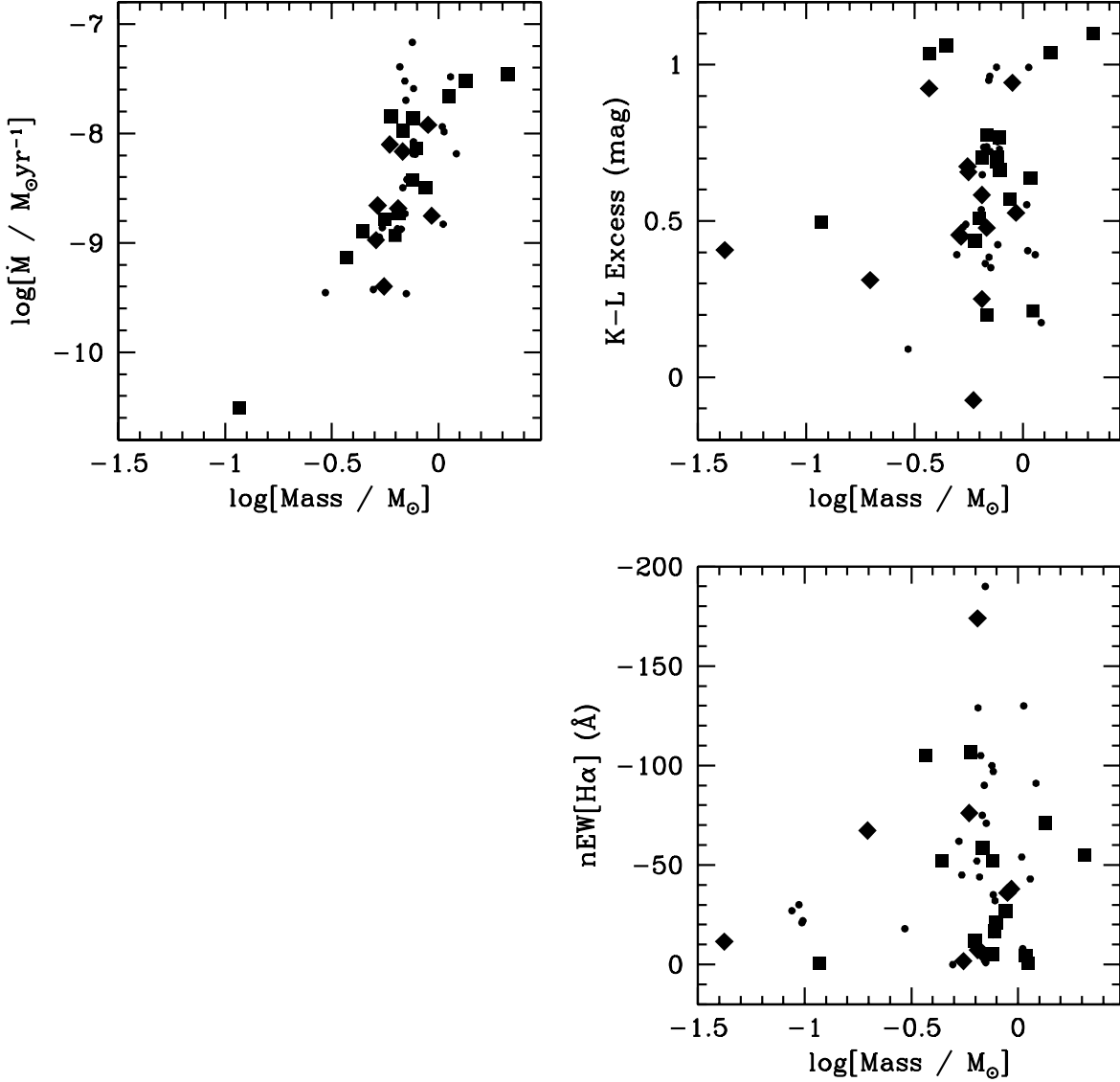


Fig. 11.— The mass accretion rates, the $K - L$ color excesses ($((K - L)_{obs} - (K - L)_{phot})$, and the $n\text{EW}[\text{H}\alpha]$ s of CTTSs are plotted versus their stellar mass. Primaries (*large squares*) are distinguished from secondaries (*large diamonds*) and from single stars (*small circles*). The distribution of mass accretion rates shows a general trend of decreasing mass accretion rates with decreasing stellar masses. Although the $K - L$ colors and $n\text{EW}[\text{H}\alpha]$ s of the lowest mass stars are below the mean of higher mass stars, these trends are suggestive, but not statistically significant.

Table 1. Summary of Sample and Measurements

Source ^a	Pair ^b	Sep	Type ^c	Optical ^d	NIR ^d
Close Binary Stars					
V773 Tau	A [†] -B	0 ^{''} 07	W	<i>UBVRI</i>	<i>K</i>
V410 Tau	A-B	0 ^{''} 07	W	<i>[UBVRI]</i>	<i>K</i>
FW Tau	A-B	0 ^{''} 08	W	<i>UBVRI, Hα</i>	<i>K</i>
DF Tau	A-B	0 ^{''} 09	C	<i>UBVRI</i>	<i>K</i>
(RW Aur)	(Ba-Bb)	(0 ^{''} 09)	C	<i>[UBVRI]</i>	<i>K</i>
(FY Tau)	(A-B)	(> 0 ^{''} 15)	C	<i>[UBVRI]</i>	<i>K</i>
FO Tau	A-B	0 ^{''} 15	C	<i>UBVRI, Hα</i>	<i>KL</i>
V928 Tau	A-B	0 ^{''} 19	W	...	<i>KL</i>
IS Tau	A-B	0 ^{''} 22	C	<i>UBVRI, Hα</i>	<i>KL</i>
FS Tau	A-B	0 ^{''} 23	C	<i>UBVRI, Hα</i>	<i>KL</i>
LkHa 332/G2	A-B	0 ^{''} 23	W	...	<i>KL</i>
LkHa 332/G1	A-B	0 ^{''} 23	W	<i>UBVRI, Hα</i>	<i>KL</i>
GG Tau	Aa-Ab	0 ^{''} 25	C	<i>UBVRI</i>	<i>KL</i>
V410 Tau	A-C	0 ^{''} 27	W	<i>[UB]VRI</i>	<i>K</i>
V927 Tau	A-B	0 ^{''} 27	W	...	<i>KL</i>
IW Tau	A-B	0 ^{''} 29	W	...	<i>KL</i>
V807 Tau	A-B [†]	0 ^{''} 30	C	<i>UBVRI, Hα</i>	<i>KL</i>
XZ Tau	A-B	0 ^{''} 30	C	<i>UBVRI, Hα</i>	<i>KL</i>
GH Tau	A-B	0 ^{''} 31	C	<i>UBVRI, Hα</i>	<i>KL</i>
CZ Tau	A-B	0 ^{''} 32	W	...	<i>KL</i>
V955 Tau	A-B	0 ^{''} 33	C	<i>UBVRI, Hα</i>	<i>KL</i>
GN Tau	A-B	0 ^{''} 33	C	...	<i>KL</i>
UZ Tau	Ba-Bb	0 ^{''} 37	C	<i>UBVRI</i>	<i>KL</i>
LkCa 3	A-B	0 ^{''} 50	W	...	<i>KL</i>
DD Tau	A-B	0 ^{''} 56	C	<i>VRI, Hα</i>	<i>KL</i>
VY Tau	A-B	0 ^{''} 66	W	...	<i>KL</i>
Haro 6-28	A-B	0 ^{''} 66	C	...	<i>KL</i>
T Tau	A-B [†]	0 ^{''} 70	C	<i>[VRI]</i>	<i>KL</i>
FV Tau/c	A-B	0 ^{''} 71	C	<i>UBVRI, Hα</i>	<i>KL</i>
FV Tau	A-B	0 ^{''} 72	C	<i>UBVRI, Hα</i>	<i>KL</i>

Table 1—Continued

Source ^a	Pair ^b	Sep	Type ^c	Optical ^d	NIR ^d
<u>Wide Binary Stars</u>					
FQ Tau	A-B	0 ^{''} .76	C	...	KL
UY Aur	A-B	0 ^{''} .88	C	...	KL
FX Tau	A-B	0 ^{''} .89	C	...	KL
LkCa 7	A-B	1 ^{''} .07	W	...	KL
Haro 6-10	A-B	1 ^{''} .20	C	...	KL
RW Aur	A [†] -B	1 ^{''} .42	C	<i>UBVRI, Hα</i>	KL
GG Tau	Ba-Bb	1 ^{''} .48	C	<i>[UBV]RI</i>	KL
CoKu Tau 3	A-B	2 ^{''} .05	C	...	KL
FW Tau	A-C	2 ^{''} .29	W	<i>[UBV]RI, Hα</i>	...
DK Tau	A-B	2 ^{''} .30	C	...	KL
HK Tau	A-B	2 ^{''} .34	C	...	KL
IT Tau	A-B	2 ^{''} .39	C	...	KL
Haro 6-37	A [†] -B	2 ^{''} .62	C	<i>UBVRI, Hα</i>	KL
UX Tau	A-C	2 ^{''} .63	C	<i>RI, Hα</i>	KL
HN Tau	A-B	3 ^{''} .11	C	<i>RI, Hα</i>	KL
V710 Tau	A-B	3 ^{''} .17	C	<i>BVRI, Hα</i>	KL
J1-4872	A [†] -B [†]	3 ^{''} .40	W	...	KL
UZ Tau	A [†] -Ba	3 ^{''} .54	C	<i>UBVRI</i>	KL
HV Tau	A [†] -C	3 ^{''} .98	W	<i>VRI, Hα</i>	<i>K[L]</i>
UX Tau	A-B [†]	5 ^{''} .86	C	<i>BVRI, Hα</i>	KL

^a RW Aur Ba-Bb and FY Tau A-B are listed in parentheses because we have concluded they are not binary stars (§2.3.2).

^b A dagger ([†]) indicates an unresolved companion star from Welty (1995, V773 Tau), Gahm et al. (1999, RW Aur), Ghez et al. (2001, J1-4872 B), Duchêne et al. (1999a, Haro 6-37, J1-4872 A, UX Tau B), Mathieu et al. (2000, UZ Tau A), Simon et al. (1995, HV Tau, V807 Tau) and Koresko (2000, T Tau).

^c T Tauri type of the system (C=CTTS and W=WTTS).

^d Filters listed in italics denote measurements obtained from the literature (§2.3.1 & §2.3.3). Filters listed in brackets denote measurements in which the targeted companion was not resolved or detected.

Table 2. Near Infrared Measurements of TTSs

Source	Flt	Obs Date	Flux Ratio ^a	System (mag)	Primary (mag)	Secondary (mag)	Sep (arcsec)	PA (degrees)	Ref
DF Tau A-B	K	1996 Dec 6	1.62 ± 0.17	0.0896 ± 0.0079	290.2 ± 1.2	1
FO Tau A-B	K	1996 Dec 5	1.000 ± 0.010	0.1499 ± 0.0069	193.7 ± 1.0	1
	L	1996 Dec 6	1.74 ± 0.49	0.160 ± 0.010	188.4 ± 5.9	1
					$8.89 \pm 0.14^*$	$8.98 \pm 0.15^*$			1,2,3,4
							1
					$8.13 \pm 0.12^*$	$8.73 \pm 0.20^*$			1,4
V928 Tau A-B	K	1997 Dec 9	1.055 ± 0.037	0.1967 ± 0.0037	117.2 ± 1.2	1
	L	1997 Dec 8	1.009 ± 0.002	7.95 ± 0.05	$8.64 \pm 0.09^*$	$9.00 \pm 0.12^*$	0.1851 ± 0.0035	118.7 ± 1.8	1
					8.70 ± 0.05	8.71 ± 0.05			1
					$8.61 \pm 0.05^*$	$8.62 \pm 0.05^*$			1,4
IS Tau A-B	K	1996 Dec 5	5.73 ± 0.13	0.2223 ± 0.0043	95.4 ± 1.4	1
	L	1996 Dec 6	8.6 ± 1.7	0.265 ± 0.045	98 ± 15	1
					$8.85 \pm 0.05^*$	$10.75 \pm 0.12^*$			1,2,3,4
					$7.88 \pm 0.05^*$	$10.22 \pm 0.20^*$			1,4
FS Tau A-B	K	1996 Dec 5	7.0 ± 1.7	0.253 ± 0.013	85.9 ± 1.4	1
		1997 Dec 5	7.02 ± 0.12	0.2266 ± 0.0045	87.9 ± 1.2	1
	L	1997 Dec 5	5.54 ± 2.1	0.230 ± 0.013	97.1 ± 2.4	1
					$7.88 \pm 0.27^*$	$10.00 \pm 0.46^*$			1,4,5,6
							1
					$6.44 \pm 0.13^*$	$8.30 \pm 0.37^*$			1,4
332/G2 A-B ^b	K				$8.39 \pm 0.08^*$	$8.95 \pm 0.09^*$			3,4
	L	1997 Dec 8	1.89 ± 0.19	7.98 ± 0.05	8.44 ± 0.06	9.13 ± 0.09	0.2341 ± 0.0045	244.8 ± 2.9	1
					$8.09 \pm 0.06^*$	$8.78 \pm 0.09^*$			1,4
332/G1 A-B	K				$8.66 \pm 0.04^*$	$9.29 \pm 0.38^*$			2,3,4
	L	1997 Dec 8	1.741 ± 0.028	7.68 ± 0.04	8.17 ± 0.04	8.77 ± 0.04	0.2381 ± 0.0045	90.7 ± 1.3	1
					$8.04 \pm 0.05^*$	$8.64 \pm 0.05^*$			1,4
GG Tau Aa-Ab	K	1996 Dec 6	1.95 ± 0.16	0.2436 ± 0.0046	354.9 ± 1.3	1
	L	1996 Dec 6	2.226 ± 0.011	0.2487 ± 0.0046	357.2 ± 1.0	1
					$7.76 \pm 0.15^*$	$8.56 \pm 0.24^*$			1,7,8,9,10
					$6.89 \pm 0.15^*$	$7.76 \pm 0.15^*$			1,4
V927 Tau A-B	K	1997 Dec 4	1.56 ± 0.10	0.2670 ± 0.0068	289.4 ± 2.5	1
	L	1997 Dec 9	1.50 ± 0.25	8.57 ± 0.07	$9.24 \pm 0.03^*$	$9.66 \pm 0.05^*$	0.2684 ± 0.0050	103.88 ± 1.0	1
					9.12 ± 0.10	9.56 ± 0.13			1,3,4
					$9.12 \pm 0.08^*$	$9.56 \pm 0.11^*$			1,4
IW Tau A-B	K				$9.05 \pm 0.03^*$	$9.16 \pm 0.03^*$			3,4
	L	1997 Dec 9	0.847 ± 0.050	8.15 ± 0.07	8.99 ± 0.08	8.82 ± 0.08	0.2899 ± 0.0055	178.9 ± 1.0	1
					$8.99 \pm 0.04^*$	$8.82 \pm 0.04^*$			1,4
V807 Tau A-B	K	1997 Dec 4	2.62 ± 0.27	0.3089 ± 0.0054	323.2 ± 1.0	1

Table 2—Continued

Source	Flt	Obs Date	Flux Ratio ^a	System (mag)	Primary (mag)	Secondary (mag)	Sep (arcsec)	PA (degrees)	Ref
XZ Tau A-B	L	1996 Dec 6	5.58 ± 0.52	...	$7.36 \pm 0.05^*$	$8.21 \pm 0.10^*$	0.3149 ± 0.0056	323.3 ± 1.0	1,2,3,4 1
	K	1996 Dec 5	0.599 ± 0.022	...	$6.54 \pm 0.14^*$	$7.94 \pm 0.14^*$	0.2998 ± 0.0057	324.5 ± 1.0	1,4 1
					$9.23 \pm 0.59^*$	$8.50 \pm 0.57^*$			1,2,4,11
GH Tau A-B	L	1996 Dec 5	0.300 ± 0.048	0.299 ± 0.029	322.1 ± 1.1	1
	K	1996 Dec 5	0.826 ± 0.060	...	$7.90 \pm 0.34^*$	$6.59 \pm 0.31^*$	0.3049 ± 0.0058	114.8 ± 1.1	1,4 1
					$8.64 \pm 0.23^*$	$8.44 \pm 0.21^*$			1,2,3,4
CZ Tau A-B	L	1996 Dec 5	0.710 ± 0.059	0.3119 ± 0.0067	115.3 ± 1.6	1
	K				$7.94 \pm 0.10^*$	$7.57 \pm 0.10^*$			1,4 3,4
					$9.69 \pm 0.04^*$	$10.53 \pm 0.06^*$			
V955 Tau A-B	L	1997 Dec 9	1.15 ± 0.22	8.59 ± 0.07	9.27 ± 0.12	9.42 ± 0.13	0.3170 ± 0.0058	88.1 ± 1.1	1
	K	1996 Dec 5	4.12 ± 0.43	...	$8.87 \pm 0.25^*$	$9.02 \pm 0.26^*$	0.3231 ± 0.0075	204.0 ± 1.2	1,4 1
					$8.06 \pm 0.08^*$	$9.65 \pm 0.09^*$			1,3,4
GN Tau A-B	L	1996 Dec 6	5.58 ± 0.52	0.341 ± 0.026	208.8 ± 1.1	1
	K	1996 Dec 5	1.171 ± 0.026	...	$7.18 \pm 0.05^*$	$9.05 \pm 0.10^*$	0.3348 ± 0.0063	124.1 ± 1.0	1,4 1
					$8.57 \pm 0.11^*$	$8.92 \pm 0.12^*$			1,4,6
UZ Tau Ba-Bb	L	1997 Dec 5	1.248 ± 0.031	0.3336 ± 0.0063	124.0 ± 1.2	1
	K	1996 Dec 06	1.65 ± 0.10	...	$7.73 \pm 0.08^*$	$7.97 \pm 0.08^*$	0.3602 ± 0.0069	0.8 ± 1.0	1,4 1
					$8.70 \pm 0.13^*$	$9.30 \pm 0.16^*$			1,4,6,8,10
LkCa 3 A-B	L	1996 Dec 6	5.58 ± 0.52	0.3686 ± 0.0070	3.4 ± 1.1	1
	K	1997 Dec 5	1.230 ± 0.049	...	$7.83 \pm 0.12^*$	$8.63 \pm 0.17^*$	0.4792 ± 0.0091	72.8 ± 1.0	1,4 1
					$8.17 \pm 0.10^*$	$8.39 \pm 0.11^*$			1,2,3,4
DD Tau A-B	L	1997 Dec 9	0.895 ± 0.036	7.34 ± 0.07	8.16 ± 0.07	8.03 ± 0.07	0.4777 ± 0.0089	73.0 ± 1.4	1
	K	1996 Dec 5	1.173 ± 0.059	...	$8.16 \pm 0.06^*$	$8.03 \pm 0.06^*$	0.555 ± 0.010	182.3 ± 1.0	1,4 1
					1.448 ± 0.046	...			0.555 ± 0.010
VY Tau A-B	L	1996 Dec 6	1.72 ± 0.13	...	$8.41 \pm 0.13^*$	$8.89 \pm 0.19^*$	0.557 ± 0.011	182.7 ± 1.1	1,2,3,4 1
	K				$7.16 \pm 0.21^*$	$7.75 \pm 0.22^*$			1,4
					$9.22 \pm 0.16^*$	$10.68 \pm 0.17^*$	3,4		

Table 2—Continued

Source	Flt	Obs Date	Flux Ratio ^a	System (mag)	Primary (mag)	Secondary (mag)	Sep (arcsec)	PA (degrees)	Ref
Haro 6-28 A-B	L	1997 Dec 9	3.37 ± 0.79	8.76 ± 0.10	9.04 ± 0.12	10.36 ± 0.22	0.665 ± 0.013	316.6 ± 1.0	1
	K	1997 Dec 7	1.396 ± 0.014	...	$8.93 \pm 0.27^*$	$10.25 \pm 0.33^*$	0.647 ± 0.012	245.2 ± 1.0	1,4
					$9.83 \pm 0.14^*$	$10.26 \pm 0.15^*$			1,3,4
L	1997 Dec 7	1.174 ± 0.017	0.644 ± 0.012	245.1 ± 1.0	1	
T Tau A-B	K	1997 Dec 4	5.34 ± 0.16	0.685 ± 0.013	179.5 ± 1.0	1
		1997 Dec 6	5.79 ± 0.26	0.698 ± 0.013	179.1 ± 1.0	1
	L	1997 Dec 6	0.730 ± 0.010	0.698 ± 0.015	179.4 ± 1.0	1,2,4,8,12
FV Tau/c A-B	K	1996 Dec 5	7.66 ± 0.20	...	$4.32 \pm 0.18^*$	$3.98 \pm 0.18^*$	0.701 ± 0.014	293.3 ± 1.0	1,4
					$8.95 \pm 0.03^*$	$11.03 \pm 0.13^*$			1,3,4
	L	1996 Dec 6	2.91 ± 0.15	0.703 ± 0.014	293.8 ± 1.0	1
FV Tau A-B	K	1996 Dec 5	1.485 ± 0.010	...	$8.43 \pm 0.05^*$	$9.59 \pm 0.07^*$	0.704 ± 0.013	271.6 ± 1.0	1,4
					$7.92 \pm 0.11^*$	$8.37 \pm 0.13^*$			1
	L	1996 Dec 5	0.687 ± 0.019	0.712 ± 0.014	271.9 ± 1.0	1,2,4,7
FQ Tau A-B	K	1997 Dec 9	1.083 ± 0.019	9.29 ± 0.07	$7.31 \pm 0.19^*$	$7.03 \pm 0.19^*$	0.752 ± 0.014	66.80 ± 1.0	1,4,7
					10.00 ± 0.07	10.09 ± 0.07			1
	L	1997 Dec 8	1.154 ± 0.013	8.89 ± 0.09	$10.17 \pm 0.31^*$	$10.27 \pm 0.31^*$	0.757 ± 0.014	67.17 ± 1.0	1,3,4
UY Aur A-B	K	1997 Dec 8	2.02 ± 0.10	7.21 ± 0.04	9.57 ± 0.09	9.72 ± 0.09	0.878 ± 0.017	227.1 ± 1.0	1
					$9.75 \pm 0.31^*$	$9.90 \pm 0.31^*$			1,4
	L	1997 Dec 8	2.100 ± 0.017	6.18 ± 0.05	7.65 ± 0.04	8.41 ± 0.05	0.878 ± 0.017	227.1 ± 1.0	1,2,3,4
FX Tau A-B	K	1997 Dec 7	2.201 ± 0.016	...	6.60 ± 0.05	7.41 ± 0.05	0.890 ± 0.017	289.0 ± 1.0	1
					$6.23 \pm 0.12^*$	$7.04 \pm 0.12^*$			1,4
	L	1997 Dec 7	2.969 ± 0.034	7.17 ± 0.10	$8.59 \pm 0.14^*$	$9.32 \pm 0.16^*$	0.885 ± 0.017	289.0 ± 1.0	1,2,3,4
LkCa 7 A-B	K	1997 Dec 9	1.729 ± 0.093	8.20 ± 0.08	7.49 ± 0.10	8.67 ± 0.10	1.021 ± 0.019	24.30 ± 1.0	1
					$7.70 \pm 0.21^*$	$8.88 \pm 0.21^*$			1,4
	L	1997 Dec 9	1.729 ± 0.093	8.20 ± 0.08	$8.84 \pm 0.03^*$	$9.47 \pm 0.04^*$	1.021 ± 0.019	24.30 ± 1.0	3,4
Haro 6-10 A-B	K	1997 Dec 9	1.729 ± 0.093	8.20 ± 0.08	8.70 ± 0.08	9.29 ± 0.09	1.021 ± 0.019	24.30 ± 1.0	1
	L				$8.77 \pm 0.04^*$	$9.36 \pm 0.05^*$			1,4
	K				$7.92 \pm 0.79^*$	$10.23 \pm 0.79^*$			4,13,14
	L				$6.41 \pm 0.11^*$	$7.10 \pm 0.21^*$			4,13,14

Table 2—Continued

Source	Flt	Obs Date	Flux Ratio ^a	System (mag)	Primary (mag)	Secondary (mag)	Sep (arcsec)	PA (degrees)	Ref
RW Aur A-B	K	1996 Dec 6	4.20 ± 0.16	1.397 ± 0.026	254.6 ± 1.0	1
	L	1996 Dec 6	6.16 ± 0.24	...	7.06 ± 0.17*	8.64 ± 0.36*	1.396 ± 0.026	254.5 ± 1.0	1,3,4,10
GG Tau Ba-Bb	K	1997 Dec 6	5.81 ± 0.47	9.94 ± 0.03	10.11 ± 0.03*	12.02 ± 0.07*	1.515 ± 0.060	131.7 ± 2.2	1
	L	1997 Dec 6	5.92 ± 0.83	9.13 ± 0.03	9.30 ± 0.03*	11.23 ± 0.15*	1.483 ± 0.089	133.1 ± 5.5	1
CoKu 3 A-B	K	1997 Dec 6	3.87 ± 0.21	8.25 ± 0.03	8.50 ± 0.03*	9.97 ± 0.05*	2.051 ± 0.058	172.7 ± 1.2	1
	L	1997 Dec 6	4.66 ± 0.35	7.28 ± 0.04	7.49 ± 0.04*	9.16 ± 0.07*	2.079 ± 0.063	172.2 ± 2.1	1
DK Tau A-B	K	1997 Dec 6	4.21 ± 0.30	7.20 ± 0.03	7.43 ± 0.03*	8.99 ± 0.07*	2.304 ± 0.045	117.6 ± 1.2	1
	L	1997 Dec 6	4.02 ± 0.13	6.20 ± 0.02	6.44 ± 0.02*	7.95 ± 0.03*	2.337 ± 0.056	117.6 ± 1.3	1
HK Tau A-B	K	1997 Dec 6	21.3 ± 1.1	8.63 ± 0.03	8.68 ± 0.03*	12.00 ± 0.05*	2.342 ± 0.061	170.4 ± 1.1	1
	L	1997 Dec 6	29.6 ± 3.1	7.82 ± 0.02	7.86 ± 0.02*	11.54 ± 0.11*	2.284 ± 0.053	168.8 ± 2.4	1
IT Tau A-B	K	1997 Dec 6	6.37 ± 0.76	7.85 ± 0.05	8.01 ± 0.05*	10.02 ± 0.12*	2.39 ± 0.11	223.4 ± 2.8	1
	L	1997 Dec 6	16.0 ± 4.4	6.79 ± 0.08	6.86 ± 0.08*	9.87 ± 0.29*	2.69 ± 0.14	226.6 ± 6.8	1
Haro 6-37 A-B	K	1997 Dec 6	2.78 ± 0.22	7.24 ± 0.04	7.57 ± 0.05*	8.68 ± 0.07*	2.620 ± 0.051	37.6 ± 1.0	1
	L	1997 Dec 6	3.22 ± 0.11	6.33 ± 0.02	6.62 ± 0.02*	7.89 ± 0.03*	2.653 ± 0.051	37.1 ± 1.1	1
UX Tau A-C	K	1997 Dec 6	16.9 ± 1.6	7.44 ± 0.06	7.50 ± 0.06*	10.57 ± 0.08*	2.632 ± 0.027	180.2 ± 1.0	1
	L	1997 Dec 6	24.0 ± 2.0	6.70 ± 0.02	6.74 ± 0.02*	10.19 ± 0.09*	2.634 ± 0.033	180.2 ± 1.0	1
HN Tau A-B	K	1997 Dec 6	30.8 ± 2.4	7.98 ± 0.03	8.01 ± 0.03*	11.73 ± 0.08*	3.109 ± 0.082	219.1 ± 1.1	1
	L	1997 Dec 6	65 ± 12	6.58 ± 0.03	6.60 ± 0.03*	11.14 ± 0.20*	3.15 ± 0.33	219.2 ± 2.5	1
V710 Tau A-B	K	1997 Dec 6	0.780 ± 0.030	7.86 ± 0.02	8.76 ± 0.03*	8.49 ± 0.03*	3.168 ± 0.062	176.2 ± 1.1	1
	L	1997 Dec 6	0.879 ± 0.034	7.50 ± 0.02	8.32 ± 0.03*	8.18 ± 0.03*	3.178 ± 0.064	176.5 ± 1.2	1
J4872 A-B	K	1997 Dec 6	1.92 ± 0.20	8.14 ± 0.06	8.59 ± 0.08*	9.30 ± 0.08*	3.401 ± 0.068	233.3 ± 1.1	1
	L	1997 Dec 6	1.92 ± 0.20	7.86 ± 0.06	8.31 ± 0.08*	9.02 ± 0.08*	3.365 ± 0.080	232.7 ± 1.2	1
UZ Tau A-Ba	K				7.56 ± 0.02*	8.70 ± 0.13*	1,15,16
	L				6.69 ± 0.10*	7.83 ± 0.16*	1,4
HV Tau A-C	K				7.92 ± 0.06*	12.14 ± 0.07*	3.98 ± 0.03	43.5 ± 0.4	17
	L				7.56 ± 0.06*	> 9.27*	3.98 ± 0.03	43.5 ± 0.4	17
UX Tau A-B	K	1997 Dec 6	3.91 ± 0.31	7.25 ± 0.05	7.50 ± 0.06*	8.98 ± 0.06*	5.86 ± 0.11	269.4 ± 1.0	1
	L	1997 Dec 6	7.24 ± 0.19	6.60 ± 0.02	6.74 ± 0.02*	8.89 ± 0.02*	5.86 ± 0.11	269.3 ± 1.0	1

Note. — The K and L magnitudes used in the analysis (§3 & §4) are marked with asterisks and are the combined values from the listed references.

^a Flux ratios are calculated as A/B, where A and B are defined in §2.1. This is equivalent to primary/secondary for all pairs except LkHa 332/G1.

^b The brighter component of LkHa 332/G1, listed under the column labeled Primary, is actually the less massive component, but is treated as component A here to avoid confusion with previous measurements (see §2.1).

References. — (1) this work; (2) Ghez et al. (1993); (3) Leinert et al. (1993); (4) Kenyon & Hartmann (1995); (5) Chen et al. (1990); (6) Simon et al. (1992); (7) Leinert et al. (1991); (8) Ghez et al. (1995); (9) Roddier et al. (1996); (10) Ghez et al. (1997b); (11) Haas et al. (1990); (12) Ghez et al. (1991); (13) Leinert & Haas (1989); (14) Ménard et al. (1993); (15) Hartigan et al. (1994); (16) Moneti & Zinnecker (1991); (17) Woitas et al. (1998)

Table 3. HST/WFPC2 Observations of Binary T Tauri Stars

Source (Obs Date)	HST Flt	Flux Ratio ^a	System (mag)	Trans- formed to	Primary (mag -or- Å)	Secondary (mag -or- Å)	Mean Sep (arcsec)	Mean PA (degrees)
V773 Tau A-B (1994 Oct 29)	F336W	5.7 ± 4.1	13.36 ± 0.03	<i>U</i>	13.60 ± 0.12	15.49 ± 0.67	0.0628 ± 0.0024	321.9 ± 2.7
	F439W	13 ± 11	12.38 ± 0.02	<i>B</i>	12.31 ± 0.07	15.10 ± 0.85		
	F555W	4.9 ± 2.0	10.84 ± 0.03	<i>V</i>	11.03 ± 0.08	12.76 ± 0.37		
	F675W	3.5 ± 1.2	9.76 ± 0.01	<i>R_c</i>	10.13 ± 0.08	11.49 ± 0.29		
	F814W	3.0 ± 1.5	9.03 ± 0.03	<i>I_c</i>	9.34 ± 0.14	10.53 ± 0.41		
V410 A-B (1994 July 31)	F336W	> 207	12.84 ± 0.01	<i>U</i>	12.91 ± 0.02	> 16.2	0.2871 ± 0.0050	132.34 ± 0.81
	F439W	> 780	12.05 ± 0.02	<i>B</i>	11.88 ± 0.02	> 15.6		
	F555W	> 1140	10.77 ± 0.03	<i>V</i>	10.76 ± 0.03	> 13.7		
	F675W	> 1870	9.93 ± 0.03	<i>R_c</i>	10.04 ± 0.03	> 13.8		
	F814W	> 760	9.35 ± 0.03	<i>I_c</i>	9.35 ± 0.03	> 14.0		
FW Tau A-B (1997 Mar 18)	F336W	1.25 ± 0.16	18.22 ± 0.06	<i>U</i>	19.09 ± 0.11	19.33 ± 0.13	0.0754 ± 0.0050	3.4 ± 3.0
	F439W	1.44 ± 0.26	17.73 ± 0.04	<i>B</i>	17.94 ± 0.13	18.33 ± 0.17		
	F555W	1.21 ± 0.19	16.02 ± 0.03	<i>V</i>	16.64 ± 0.11	16.85 ± 0.13		
	F675W	1.153 ± 0.053	14.27 ± 0.03	<i>R_c</i>	15.06 ± 0.05	15.22 ± 0.05		
	F814W	1.13 ± 0.18	12.38 ± 0.04	<i>I_c</i>	13.07 ± 0.12	13.20 ± 0.13		
	F656N	1.23 ± 0.11	13.56 ± 0.05	EW[H α]	-11.6 ± 3.4	-9.0 ± 3.6		
DF Tau A-B (1994 July 27)	F336W	8.5 ± 2.4	12.56 ± 0.05	<i>U</i>	12.75 ± 0.06	15.06 ± 0.28	0.0871 ± 0.0038	301.2 ± 2.0
	F439W	3.37 ± 0.51	13.13 ± 0.04	<i>B</i>	13.18 ± 0.05	14.47 ± 0.13		
	F555W	1.87 ± 0.24	11.97 ± 0.04	<i>V</i>	12.43 ± 0.06	13.10 ± 0.10		
	F675W	1.33 ± 0.13	10.79 ± 0.02	<i>R_c</i>	11.53 ± 0.05	11.84 ± 0.06		
	F814W	1.020 ± 0.038	9.86 ± 0.01	<i>I_c</i>	10.59 ± 0.02	10.61 ± 0.02		
FO Tau A-B (1997 Mar 6)	F336W	1.634 ± 0.044	16.50 ± 0.16	<i>U</i>	17.08 ± 0.17	17.61 ± 0.17	0.1525 ± 0.0029	194.70 ± 0.43
	F439W	0.964 ± 0.044	17.07 ± 0.02	<i>B</i>	17.59 ± 0.05	17.55 ± 0.05		
	F555W	1.070 ± 0.038	15.21 ± 0.05	<i>V</i>	15.91 ± 0.05	15.98 ± 0.05		
	F675W	1.102 ± 0.010	13.42 ± 0.03	<i>R_c</i>	14.26 ± 0.04	14.36 ± 0.04		
	F814W	1.071 ± 0.051	11.85 ± 0.03	<i>I_c</i>	12.56 ± 0.05	12.63 ± 0.05		
	F656W	1.397 ± 0.027	11.43 ± 0.04	EW[H α]	-116.6 ± 8.8	-86.1 ± 7.0		
IS Tau A-B (1997 Nov 7)	F336W	18.7 ± 4.5	18.01 ± 0.10	<i>U</i>	18.14 ± 0.11	21.35 ± 0.28		
	F439W	16.3 ± 2.3	17.83 ± 0.11	<i>B</i>	17.66 ± 0.12	20.61 ± 0.19		
	F555W	13.82 ± 0.92	15.63 ± 0.07	<i>V</i>	15.69 ± 0.07	18.52 ± 0.10		
	F675W	7.74 ± 0.37	14.02 ± 0.07	<i>R_c</i>	14.28 ± 0.07	16.49 ± 0.09		

Table 3—Continued

Source (Obs Date)	HST Flt	Flux Ratio ^a	System (mag)	Trans- formed to	Primary (mag -or- Å)	Secondary (mag -or- Å)	Mean Sep (arcsec)	Mean PA (degrees)
	F814W	3.577 ± 0.080	12.55 ± 0.03	I_c	12.81 ± 0.03	14.15 ± 0.04		
	F656N	9.14 ± 0.37	13.08 ± 0.02	EW[H α]	-26.2 ± 3.9	-17.8 ± 4.4	0.2228 ± 0.0024	98.81 ± 0.80
FS Tau A-B ^b (1997 Mar 7)	F336W	7.6 ± 2.5	18.75 ± 0.10	U	18.95 ± 0.13	21.16 ± 0.37		
	F439W	6.33 ± 0.56	19.26 ± 0.03	B	19.18 ± 0.04	21.19 ± 0.10		
	F555W	5.09 ± 0.56	17.54 ± 0.05	V	17.72 ± 0.06	19.49 ± 0.12		
	F675W	3.98 ± 0.39	15.86 ± 0.05	R_c	16.23 ± 0.08	17.73 ± 0.11		
	F814W	2.47 ± 0.13	14.35 ± 0.03	I_c	14.71 ± 0.04	15.69 ± 0.06		
	F656N	6.52 ± 0.63	14.17 ± 0.06	EW[H α]	-81 ± 12	38.1 ± 9.3	0.2276 ± 0.0071	87.43 ± 0.32
332/G1 A-B ^c (1997 Mar 3)	F336W	1.127 ± 0.067	18.66 ± 0.39	U	19.41 ± 0.39	19.56 ± 0.39		
	F439W	0.964 ± 0.018	17.72 ± 0.06	B	18.25 ± 0.07	18.23 ± 0.07		
	F555W	0.937 ± 0.010	15.42 ± 0.05	V	16.20 ± 0.05	16.13 ± 0.05		
	F675W	1.0836 ± 0.0090	13.65 ± 0.02	R_c	14.49 ± 0.02	14.58 ± 0.02		
	F814W	1.412 ± 0.013	12.01 ± 0.02	I_c	12.58 ± 0.03	12.96 ± 0.03		
	F656N	1.181 ± 0.050	13.29 ± 0.06	EW[H α]	-2.6 ± 2.1	0.0 ± 2.0	0.2320 ± 0.0027	86.88 ± 0.31
GG Tau Aa-Ab (1994 July 25)	F336W	50.2 ± 2.1	13.65 ± 0.03	U	13.75 ± 0.03	17.99 ± 0.05		
	F439W	22.2 ± 1.7	13.81 ± 0.01	B	13.63 ± 0.02	16.99 ± 0.08		
	F555W	14.8 ± 1.2	12.23 ± 0.02	V	12.29 ± 0.02	15.22 ± 0.08		
	F675W	9.33 ± 0.58	11.07 ± 0.01	R_c	11.31 ± 0.01	13.73 ± 0.06		
	F814W	4.91 ± 0.16	10.25 ± 0.02	I_c	10.44 ± 0.02	12.16 ± 0.04	0.2502 ± 0.0026	358.79 ± 0.45
V410 A-C (1994 July 31)	F336W	> 1310	12.84 ± 0.01	U	12.91 ± 0.02	> 20.9		
	F439W	> 1360	12.05 ± 0.02	B	11.88 ± 0.02	> 19.5		
	F555W	659 ± 260	10.77 ± 0.03	V	10.76 ± 0.03	17.79 ± 0.43		
	F675W	265 ± 65	9.93 ± 0.03	R_c	10.04 ± 0.03	16.11 ± 0.27		
	F814W	71.2 ± 6.5	9.34 ± 0.03	I_c	9.35 ± 0.03	13.98 ± 0.10	0.2871 ± 0.0050	132.34 ± 0.81
V807 Tau A-B (1998 Dec 5)	F336W	10.4 ± 1.7	13.38 ± 0.02	U	13.56 ± 0.03	16.08 ± 0.18		
	F439W	5.74 ± 0.47	12.80 ± 0.02	B	12.74 ± 0.03	14.59 ± 0.09		
	F555W	5.26 ± 0.18	11.38 ± 0.02	V	11.56 ± 0.02	13.35 ± 0.04		
	F675W	3.66 ± 0.12	10.33 ± 0.02	R_c	10.72 ± 0.02	12.13 ± 0.04		
	F814W	2.008 ± 0.031	9.54 ± 0.03	I_c	9.97 ± 0.04	10.72 ± 0.04		
	F656N	4.38 ± 0.14	9.72 ± 0.02	EW[H α]	-10.4 ± 1.1	-4.1 ± 1.6	0.2992 ± 0.0020	322.87 ± 0.14

Table 3—Continued

Source (Obs Date)	HST Flt	Flux Ratio ^a	System (mag)	Trans- formed to	Primary (mag -or- Å)	Secondary (mag -or- Å)	Mean Sep (arcsec)	Mean PA (degrees)
XZ Tau A-B (1997 Mar 8)	F336W	0.973 ± 0.012	16.12 ± 0.08	<i>U</i>	16.95 ± 0.08	16.92 ± 0.08	0.3006 ± 0.0013	326.45 ± 0.65
	F439W	2.96 ± 0.16	16.22 ± 0.03	<i>B</i>	16.26 ± 0.04	17.44 ± 0.07		
	F555W	5.10 ± 0.18	14.66 ± 0.05	<i>V</i>	14.83 ± 0.05	16.60 ± 0.06		
	F675W	5.81 ± 0.02	13.18 ± 0.02	<i>R_c</i>	13.49 ± 0.03	15.40 ± 0.03		
	F814W	7.000 ± 0.072	11.75 ± 0.03	<i>I_c</i>	11.88 ± 0.03	14.00 ± 0.03		
	F656N	3.096 ± 0.044	11.45 ± 0.04	EW[H α]	-62.3 ± 4.8	-141.8 ± 9.8		
GH Tau A-B (1998 Dec 5)	F336W	1.95 ± 0.12	14.96 ± 0.08	<i>U</i>	15.47 ± 0.09	16.19 ± 0.10	0.3111 ± 0.0013	114.63 ± 0.17
	F439W	1.316 ± 0.056	14.67 ± 0.08	<i>B</i>	15.03 ± 0.09	15.33 ± 0.09		
	F555W	1.171 ± 0.025	13.07 ± 0.10	<i>V</i>	13.72 ± 0.11	13.89 ± 0.11		
	F675W	1.170 ± 0.035	11.77 ± 0.07	<i>R_c</i>	12.57 ± 0.07	12.74 ± 0.14		
	F814W	1.0804 ± 0.0081	10.68 ± 0.14	<i>I_c</i>	11.38 ± 0.14	11.47 ± 0.14		
	F656N	1.889 ± 0.047	10.85 ± 0.04	EW[H α]	-31.3 ± 4.2	-8.3 ± 2.6		
V955 Tau A-B (1997 Mar 3)	F336W	2.342 ± 0.022	18.01 ± 0.29	<i>U</i>	18.47 ± 0.29	19.38 ± 0.29	0.3309 ± 0.0012	204.95 ± 0.18
	F439W	3.419 ± 0.056	17.72 ± 0.05	<i>B</i>	17.81 ± 0.06	19.09 ± 0.06		
	F555W	3.792 ± 0.037	15.76 ± 0.08	<i>V</i>	16.00 ± 0.08	17.45 ± 0.08		
	F675W	3.067 ± 0.043	14.21 ± 0.04	<i>R_c</i>	14.63 ± 0.04	15.86 ± 0.04		
	F814W	1.876 ± 0.023	12.88 ± 0.04	<i>I_c</i>	13.33 ± 0.04	14.02 ± 0.04		
	F656N	4.930 ± 0.094	13.01 ± 0.03	EW[H α]	-44.9 ± 3.8	-17.2 ± 2.5		
UZ Tau Ba-Bb (1994 July 24)	F336W	0.826 ± 0.032	14.91 ± 0.01	<i>U</i>	15.83 ± 0.03	15.62 ± 0.02	0.3678 ± 0.0010	0.05 ± 0.11
	F439W	1.056 ± 0.069	15.13 ± 0.04	<i>B</i>	15.61 ± 0.05	15.67 ± 0.05		
	F555W	1.365 ± 0.049	13.63 ± 0.03	<i>V</i>	14.21 ± 0.03	14.55 ± 0.04		
	F675W	1.484 ± 0.053	12.29 ± 0.02	<i>R_c</i>	12.98 ± 0.03	13.41 ± 0.03		
	F814W	1.309 ± 0.029	11.05 ± 0.02	<i>I_c</i>	11.65 ± 0.02	11.94 ± 0.02		
FV Tau/c A-B (1997 Mar 6)	F336W	> 21	19.69 ± 0.10	<i>U</i>	19.75 ± 0.08	> 23.1	0.7130 ± 0.0018	293.97 ± 0.15
	F439W	> 47	19.70 ± 0.05	<i>B</i>	19.43 ± 0.06	> 23.6		
	F555W	60 ± 22	17.28 ± 0.05	<i>V</i>	17.27 ± 0.05	21.71 ± 0.41		
	F675W	40.3 ± 5.3	15.31 ± 0.04	<i>R_c</i>	15.47 ± 0.05	19.47 ± 0.17		
	F814W	30.1 ± 3.2	13.47 ± 0.03	<i>I_c</i>	13.49 ± 0.03	17.15 ± 0.18		
	F656N	7.24 ± 0.22	14.34 ± 0.05	EW[H α]	-17.3 ± 3.0	-226 ± 42		
FV Tau A-B (1997 Mar 6)	F336W	1.74 ± 0.13	18.83 ± 0.05	<i>U</i>	19.40 ± 0.06	20.01 ± 0.09	0.7130 ± 0.0018	293.97 ± 0.15
	F439W	2.253 ± 0.042	18.56 ± 0.04	<i>B</i>	18.77 ± 0.06	19.62 ± 0.04		

Table 3—Continued

Source (Obs Date)	HST Flt	Flux Ratio ^a	System (mag)	Trans- formed to	Primary (mag -or- Å)	Secondary (mag -or- Å)	Mean Sep (arcsec)	Mean PA (degrees)
	F555W	2.636 ± 0.086	16.07 ± 0.02	<i>V</i>	16.41 ± 0.02	17.46 ± 0.06		
	F675W	2.528 ± 0.022	14.21 ± 0.02	<i>R_c</i>	14.68 ± 0.02	15.70 ± 0.03		
	F814W	2.272 ± 0.011	12.72 ± 0.02	<i>I_c</i>	13.11 ± 0.02	14.00 ± 0.02		
	F656N	1.234 ± 0.010	13.46 ± 0.02	EW[H α]	-5.5 ± 1.0	-41.0 ± 2.6	0.7181 ± 0.0013	272.52 ± 0.14
RW Aur A-B (1994 Nov 9)	F336W	68 ± 16	10.90 ± 0.02	<i>U</i>	10.99 ± 0.02	15.57 ± 0.26		
	F439W	38.4 ± 3.6	11.15 ± 0.01	<i>B</i>	11.02 ± 0.02	14.89 ± 0.10		
	F555W	17.70 ± 0.88	10.46 ± 0.02	<i>V</i>	10.51 ± 0.02	13.63 ± 0.05		
	F675W	12.25 ± 0.48	9.75 ± 0.03	<i>R_c</i>	9.94 ± 0.03	12.69 ± 0.03		
	F814W	8.95 ± 0.26	9.31 ± 0.01	<i>I_c</i>	9.43 ± 0.01	11.80 ± 0.03	1.4175 ± 0.0034	255.459 ± 0.065
GG Tau Ba-Bb (1994 July 25)	F336W	> 8.7	18.92 ± 0.09	<i>U</i>	19.09 ± 0.09	> 21.5		
	F439W	> 8.7	18.78 ± 0.07	<i>B</i>	18.44 ± 0.07	> 20.8		
	F555W	> 8.7	17.03 ± 0.05	<i>V</i>	17.00 ± 0.06	> 19.3		
	F675W	10.9 ± 1.8	15.20 ± 0.03	<i>R_c</i>	15.41 ± 0.03	17.99 ± 0.18		
	F814W	7.50 ± 0.50	13.23 ± 0.02	<i>I_c</i>	13.36 ± 0.02	15.53 ± 0.07	1.4765 ± 0.0065	135.20 ± 0.32
FW Tau A-C (1997 Mar 18)	F336W	> 42	18.22 ± 0.06	<i>U</i>	19.09 ± 0.11	> 23.1		
	F439W	> 112	17.73 ± 0.04	<i>B</i>	17.94 ± 0.13	> 23.1		
	F555W	> 441	16.02 ± 0.03	<i>V</i>	16.64 ± 0.11	> 23.2		
	F675W	217 ± 13	14.94 ± 0.04	<i>R_c</i>	15.06 ± 0.05	20.9 ± 0.5		
	F814W	4066 ± 448	13.07 ± 0.12	<i>I_c</i>	13.07 ± 0.12	22.1 ± 0.6		
	F656N	17.9 ± 1.6	14.14 ± 0.07	EW[H α]	-11.6 ± 3.4	-454 ± 224	2.2945 ± 0.0031	183.756 ± 0.073
UZ Tau A-Ba (1994 July 24)	F336W	3.50 ± 0.27	14.14 ± 0.02	<i>U</i>	14.47 ± 0.02	15.83 ± 0.03		
	F439W	3.02 ± 0.27	14.35 ± 0.02	<i>B</i>	14.42 ± 0.02	15.61 ± 0.05		
	F555W	1.92 ± 0.27	13.07 ± 0.03	<i>V</i>	13.51 ± 0.04	14.21 ± 0.03		
	F675W	1.58 ± 0.21	11.82 ± 0.02	<i>R_c</i>	12.48 ± 0.03	12.98 ± 0.03		
	F814W	1.29 ± 0.22	10.76 ± 0.02	<i>I_c</i>	11.37 ± 0.04	11.65 ± 0.02	3.5395 ± 0.0021	273.099 ± 0.048

^a Flux ratios are calculated as A/B, where A and B are defined in §2.1. This is equivalent to primary/secondary for all pairs except LkHa 332/G1.

^c The optical measurements of FS Tau may be biased because of its extended emission.

^c The brighter component of LkHa 332/G1, listed under the column labeled Primary, is actually the less massive component, but is treated as component A here to avoid confusion with previous measurements (see §2.1).

Table 4. HST/WFPC2 Observations of FS Tau

HST Flt	Total ^a (mag)	Trans- formed to	Total (mag -or- Å)	Binary ^b (mag -or- Å)	Nebula ^c (mag -or- Å)
F336W	17.15 ± 0.25	<i>U</i>	17.21 ± 0.25	18.81 ± 0.15	17.49 ± 0.32
F439W	17.42 ± 0.06	<i>B</i>	17.18 ± 0.07	19.02 ± 0.05	17.40 ± 0.08
F555W	15.81 ± 0.08	<i>V</i>	15.80 ± 0.08	17.53 ± 0.07	16.04 ± 0.11
F675W	14.36 ± 0.09	<i>R_c</i>	14.48 ± 0.09	15.99 ± 0.09	14.80 ± 0.12
F814W	13.11 ± 0.02	<i>I_c</i>	13.10 ± 0.02	14.34 ± 0.05	13.52 ± 0.03
F656N	12.51 ± 0.03	EW[H α]	-37.8 ± 5.7	-72.1 ± 3.5	-40.8 ± 8.0

^a A 4''0 radius is used to determine the Total magnitude (§2.3.3).

^b The Binary magnitudes are calculated from the sum of the component flux densities (Table 3).

^c The Nebula magnitudes are calculated from the differences in the Total and Binary flux densities.

Table 5. Stellar and Circumstellar Properties of Optically Resolved Systems

Source		SpT ^{a,b}	log[T] ^b	SpT	A_v	Mass	EW[H α]	ΔU	$K - L$	Tauri			
				Ref	(mag)	(M_\odot)	(\AA)	(mag)	(mag)	Type ^c			
					$\log[\frac{L}{L_\odot}]$		$\log[\frac{Age}{yr}]$		$\log[\frac{\dot{M}}{M_\odot yr^{-1}}]$				
V773 Tau	A	K2	3.690	1	1.39 ± 0.17	0.276 ± 0.089	1.46 ± 0.10	6.74 ± 0.17	...	< -10	...	W::	
	C	M0	3.588	2	1.39	0.070 ± 0.18	0.70 ± 0.07	< 6.0 ± 0.3	...	0.63	< -8.6	...	W::
FW Tau	A	M5.5±0.5	3.485	3	0.00 ± 0.83	-1.07 ± 0.34	0.12 ± 0.04	6.09 ± 0.41	-11.6	0.86	< -10.6	...	W
	B	M5.5	3.485	2	0.00	-1.12 ± 0.34	0.12 ± 0.08	6.15 ± 0.39	-9.0	0.75	< -10.7	...	W
	C	< -454	C
DF Tau	A	M0.5	3.577	4	0.15 ± 0.80	-0.25 ± 0.32	0.68 ± 0.07	6.27 ± 0.53	...	2.43	-8.0	...	C::
	B	M3	3.533	2	0.15	-0.20 ± 0.32	0.51 ± 0.12	< 6.0 ± 0.3	...	0.85	-9.0	...	C::
FO Tau	A	M2	3.551	4	3.03 ± 0.51	-0.32 ± 0.21	0.60 ± 0.09	6.27 ± 0.27	-117	3.14	-7.9	0.76	C
	B	M2	3.551	2	3.03	-0.35 ± 0.21	0.59 ± 0.09	6.30 ± 0.26	-86	2.68	-8.1	0.25	C
IS Tau	A	K7	3.602	5	3.67 ± 0.50	-0.30 ± 0.20	0.79 ± 0.11	6.52 ± 0.36	-26	2.05	-8.1	0.97	C
	B	M4.5	3.508	2	3.67	-0.72 ± 0.20	0.23 ± 0.11	6.09 ± 0.29	-18	1.99	< -9.0	0.53	W
FS Tau	A	(M1)	(3.569)	4	(2.56 ± 0.56)	(-1.30 ± 0.23)	(0.53 ± 0.08)	(7.89 ± 0.30)	-81	(2.82)	(-9.5)	1.44	C*
	B	(M4)	(3.515)	2	(2.56)	(-1.62 ± 0.23)	(0.20 ± 0.08)	(7.23 ± 0.38)	-38	(2.47)	(-10.1)	1.70	C*
332/G1	A	M1	3.569	6	4.13 ± 0.56	-0.07 ± 0.23	0.67 ± 0.03	< 6.0 ± 0.3	0.0	1.67	< -8.2	0.62	W
	B	K7	3.596	2	4.13	-0.24 ± 0.23	0.75 ± 0.10	6.38 ± 0.40	-2.6	1.35	< -8.5	0.65	W
GG Tau	Aa	K7	3.602	7	1.03 ± 0.50	0.01 ± 0.20	0.76 ± 0.09	6.00 ± 0.35	-57	1.63	-7.9	0.87	C
	Ab	M0.5±0.5	3.577	7	3.28 ± 0.36	-0.11 ± 0.15	0.68 ± 0.02	6.03 ± 0.25	-16	1.64	-8.2	0.80	C
V410 Tau	A	K4	3.663	8	0.67 ± 0.21	0.333 ± 0.085	1.52 ± 0.06	6.36 ± 0.11	...	0.15	< -8.8	0.04	W:
	C	M5.5	3.488	2	0.67	-1.29 ± 0.10	0.13 ± 0.06	6.43 ± 0.38	W::
V807 Tau	A	K7	3.602	6	0.36 ± 0.50	0.03 ± 0.20	0.76 ± 0.11	< 6.0 ± 0.3	-10	0.74	-8.4	0.82	C
	B	M3	3.530	2	0.36	-0.49 ± 0.20	0.40 ± 0.13	6.16 ± 0.27	-4	0.20	< -10.2	0.27	W
XZ Tau	A	M3	3.533	4	1.39 ± 0.81	-0.41 ± 0.32	0.44 ± 0.14	6.11 ± 0.36	-62	1.35	-8.9	1.33	C
	B	(M1.5) ^d	(3.562)	2	(1.39)	(-1.30 ± 0.32)	(0.51 ± 0.08)	(7.80 ± 0.35)	-142/-76 ^e	(3.11)	(-9.3)	1.91	C*
GH Tau	A	M1.5±0.5	3.560	9	0.69 ± 0.21	-0.42 ± 0.10	0.63 ± 0.04	6.50 ± 0.13	-31/-12 ^e	1.31	-8.9	0.70	C
	B	M2±0.5	3.551	9	0.64 ± 0.36	-0.47 ± 0.16	0.56 ± 0.07	6.44 ± 0.18	-8/-15 ^e	0.74	-9.4	0.87	C
V955 Tau	A	K5	3.643	9	3.72 ± 0.24	-0.49 ± 0.10	0.87 ± 0.06	7.27 ± 0.20	-45/-18 ^e	1.77	-8.5	0.88	C
	B	M1	3.570	2	3.72	-0.75 ± 0.10	0.65 ± 0.09	7.06 ± 0.20	-17	2.73	-8.7	0.60	C
UZ Tau	Ba	M2	3.551	6	1.00 ± 0.51	-0.45 ± 0.21	0.56 ± 0.10	6.42 ± 0.25	...	1.61	-8.8	0.87	C:
	Bb	M2	3.549	2	1.00	-0.56 ± 0.21	0.52 ± 0.12	6.51 ± 0.26	...	2.17	-8.7	0.67	C:
	A	M1	3.569	6	0.33 ± 0.56	-0.51 ± 0.23	0.65 ± 0.08	6.71 ± 0.37	...	1.91	-8.7	0.87	C
DD Tau	A	M3	3.533	6	0.39 ± 0.81	-0.89 ± 0.33	0.37 ± 0.12	6.69 ± 0.42	-125	2.16	-9.1	1.25	C
	B	M3	3.533	2	0.39	-0.89 ± 0.33	0.37 ± 0.12	6.69 ± 0.42	-240	1.14	C
T Tau	A	K0	3.720	10	1.46 ± 0.17	0.863 ± 0.070	2.11 ± 0.18	6.24 ± 0.22	-60	0.31	-7.5	1.05	C
	B	3.21	C*
FV Tau/c	A	M3	3.533	6	3.51 ± 0.81	-0.53 ± 0.32	0.41 ± 0.13	6.26 ± 0.37	-17	2.12	< -8.6	0.52	W
	B	(M5)	(3.499)	2	(3.51)	(-1.93 ± 0.33)	(0.13 ± 0.06)	(7.28 ± 0.44)	-224	(3.48)	(-10.2)	1.44	C*
FV Tau	A	K5	3.643	6	5.33 ± 0.24	-0.01 ± 0.10	1.12 ± 0.13	6.57 ± 0.17	-6	2.11	-7.7	0.61	C
	B	K6	3.616	2	5.33	-0.36 ± 0.10	0.89 ± 0.11	6.80 ± 0.22	-41	2.75	-7.9	1.34	C
RW Aur	A	K1±2	3.706	11	0.39 ± 0.33	0.23 ± 0.14	1.34 ± 0.18	6.92 ± 0.31	-76	1.11	-7.5	1.12	C
	B	K5	3.643	12	1.56 ± 0.24	-0.40 ± 0.10	0.93 ± 0.09	7.13 ± 0.18	-43	1.16	-8.8	0.72	C
GG Tau	Ba	M5.5±0.5	3.485	13	0.00 ± 0.83	-1.19 ± 0.34	0.12 ± 0.03	6.26 ± 0.39	-21	1.15	-10.0	0.82	C
	Bb	M7.5±0.5	3.448	13	0.00 ± 0.59	-1.75 ± 0.21	0.042 ± 0.019	< 6.0 ± 0.3	-32	0.85	C
Haro 6-37	A	K7	3.602	6	1.74 ± 0.50	-0.18 ± 0.20	0.78 ± 0.11	6.33 ± 0.35	-22	0.98	C
	B	M1	3.569	6	1.05 ± 0.56	-0.68 ± 0.23	0.65 ± 0.10	6.96 ± 0.35	-184	0.79	C
UX Tau	A	K5	3.643	6	0.26 ± 0.24	-0.04 ± 0.10	1.09 ± 0.13	6.65 ± 0.18	-9.5	0.76	C
	B	M2	3.551	6	0.26 ± 0.51	-0.72 ± 0.21	0.52 ± 0.13	6.77 ± 0.28	-4.5	0.11	W
	C	M5	3.495	14	0.57 ± 1.38	-1.00 ± 0.56	0.16 ± 0.10	6.20 ± 0.61	-8.5	0.38	W
HN Tau	A	(K5)	(3.643)	6	(1.18 ± 0.24)	(-0.65 ± 0.10)	(0.81 ± 0.04)	(7.57 ± 0.22)	-163	(2.08)	(-8.6)	1.41	C*
	B	M4	3.515	6	0.91 ± 1.26	-1.59 ± 0.51	0.20 ± 0.09	7.20 ± 0.62	-87	0.59	C
V710 Tau	A	M0.5	3.577	6	1.80 ± 0.36	-0.29 ± 0.15	0.68 ± 0.06	6.35 ± 0.24	-69	0.44	C

Table 5—Continued

Source	SpT ^{a,b}	log[T] ^b	SpT Ref	A_v (mag)	$\log[\frac{L}{L_\odot}]$	Mass (M_\odot)	$\log[\frac{\text{Age}}{\text{yr}}]$	EW[H α] (\AA)	ΔU (mag)	$\log[\frac{\dot{M}}{M_\odot \text{yr}^{-1}}]$	$K - L$ (mag)	Tauri Type ^c	
HV Tau	B	M2.5	3.551	6	1.82 ± 0.51	-0.20 ± 0.21	0.62 ± 0.08	6.11 ± 0.25	-7.2	0.31	W
	A	M2	3.551	4	1.95 ± 0.51	-0.33 ± 0.21	0.60 ± 0.09	6.27 ± 0.25	-4.3	0.27	W
	C	(K7)	(3.597)	2	(1.95)	(-1.56 ± 0.21)	-15	C*

Note. — The parameters derived for high accretion stars are listed in parentheses and are subject to large uncertainties (§3.1.1).

^a Spectral type uncertainties are one spectral subclass unless otherwise noted.

^b Spectral types and temperatures listed in italics are derived from photometry (§3.1).

^c High accretion stars (C*) are identified using the $K - L$ colors while CTTs (C) and WTTSs (W) are distinguished based on the EW[H α]s or, if the EW[H α] is not available, $K - L$ colors (listed with a colon) or U -band excesses (listed with a double colon; §3.2.2).

^d The veiled optical spectrum of XZ Tau B suggests that its spectral type is cooler than M1 (§2.4.2), which is consistent with the photometric value listed.

^e Multiple EW[H α] measurements are from WFPC2 (§2.2) and FOS (§2.3), respectively; the average value is used in the analysis.

References. — (1) Welty (1995); (2) photometry in §3.1; (3) Briceño et al. (1998); (4) Cohen & Kuhl (1979); (5) Martín (1994); (6) Hartigan et al. (1994); (7) White et al. (1999); (8) Rice & Strassmeier (1996); (9) spectra in §2.3; (10) Basri & Batalha (1990); (11) Mundt & Giampapa (1982); (12) Duchêne et al. (1999b); (13) Luhman (1999); (14) Basri & Marcy (1995).

Table 6. HST Filter Transformations

SpT	<i>U</i> -F336W	<i>B</i> -F439W	<i>V</i> -F555W	<i>R_c</i> -F675W	<i>I_c</i> -F814W	F656N-F675W	Star ID ^a
G8	0.07	-0.14	-0.01	0.10	0.00	-0.24	53, 54
K0	0.07	-0.14	-0.01	0.10	0.00	-0.24	
K1	0.07	-0.15	-0.01	0.10	0.00	-0.24	
K2	0.07	-0.15	-0.01	0.10	0.00	-0.24	
K3	0.07	-0.15	-0.01	0.10	0.00	-0.24	56, 57
K4	0.07	-0.17	-0.01	0.11	0.00	-0.25	
K5	0.08	-0.19	-0.01	0.11	-0.01	-0.27	
K6	0.08	-0.21	-0.01	0.12	-0.01	-0.29	
K7	0.08	-0.23	-0.01	0.13	-0.01	-0.31	63, 64
M0	0.07	-0.24	-0.01	0.13	-0.01	-0.30	61, 65, 66
M1	0.06	-0.24	-0.01	0.13	-0.01	-0.31	
M2	0.06	-0.25	-0.02	0.13	-0.01	-0.33	67
M3	0.06	-0.27	-0.02	0.13	-0.01	-0.34	
M4	0.05	-0.29	-0.03	0.12	-0.01	-0.35	68
M5	0.17	-0.35	-0.03	0.11	0.00	-0.37	
M6	0.28	-0.40	-0.03	0.11	0.00	-0.38	69
M7	0.24	-0.36	-0.04	0.11	-0.02	-0.43	
M8	0.20	-0.31	-0.05	0.11	-0.04	-0.47	70

^a The ID number of the stars from Gunn & Stryker (1983) used to establish the transformations.

Table 7. Single T Tauri Stars in Taurus-Auriga

Source	SpT ^a	EW[H α] (Å)	Ref	A _v (mag)	log[$\frac{L}{L_{\odot}}$]	Mass (M _{\odot)}	log[$\frac{Age}{yr}$]	ΔU (mag)	log[$\frac{\dot{M}}{M_{\odot} yr^{-1}}$]	K - L (mag)
<u>High Accretion T Tauri Stars</u>										
DR Tau	K5	-106	1,2	(0.51)	(-0.017)	(1.11)	(6.60)	(2.45)	(-7.50)	1.47
DG Tau	K6	-84	1,2	(1.41)	(0.062)	(0.88)	(6.12)	(2.48)	(-7.34)	1.68
HL Tau	K7	-55	3,2	(1.82)	(-0.646)	(0.78)	(7.15)	(1.79)	(-8.83)	1.76
<u>Classical T Tauri Stars</u>										
GM Aur	K3	-96	3,2	1.21	0.004	1.22	6.87	0.83	-8.18	0.33
CW Tau	K3	-135	3,2	2.21	-0.120	1.06	7.10	1.31	-7.99	1.20
DS Tau	K5	-59	3,2	0.90	-0.167	1.04	6.87	2.01	-7.94	0.71
LkCa 15	K5	-13	3,2	1.03	-0.131	1.05	6.80	0.59	-8.83	0.57
FY Tau	K5	-48	4,5,2	4.23	0.043	1.14	6.51	2.33	-7.48	0.73
BP Tau	K7	-40	6,2	0.67	-0.083	0.77	6.15	1.88	-7.88	0.57
GK Tau	K7	-22	4,2	1.21	-0.020	0.76	6.03	1.17	-8.19	0.85
AA Tau	K7	-37	3,2	1.13	-0.230	0.78	6.42	1.75	-8.19	0.90
DL Tau	K7	-105	3,2	2.00	0.066	0.77	< 6	2.82	-7.17	1.21
GI Tau	K7	-20	4,2	1.80	-0.052	0.76	6.09	1.43	-8.08	0.96
CI Tau	K7	-102	3,2	1.80	-0.076	0.76	6.12	2.42	-7.59	0.90
DN Tau	M0	-12	3,2	0.49	-0.131	0.70	6.11	0.81	-8.73	0.55
IP Tau	M0	-11	3,2	0.51	-0.353	0.71	6.48	0.44	-9.46	0.89
DO Tau	M0	-100	3,2	2.23	0.023	0.69	< 6	2.44	-7.52	1.21
GO Tau	M0	-81	3,2	2.21	-0.436	0.71	6.61	2.12	-8.42	0.61
FZ Tau	M0	-200	4,5,2	2.72	-0.295	0.70	6.40	3.15	-7.70	1.25
DP Tau	M0.5	-85	3,2	1.26	-0.523	0.68	6.73	2.26	-8.50	0.98
HO Tau	M0.5	-115	3,2	1.13	-0.846	0.67	7.28	2.52	-8.87	0.57
DE Tau	M1	-54	6,2	1.15	0.168	0.66	< 6	2.44	-7.39	0.97
DM Tau	M1	-139	3,2	0.59	-0.610	0.65	6.84	2.34	-8.67	0.83
FM Tau	M1	-62	4,2	0.26	-0.767	0.64	7.09	2.43	-8.87	0.70
CY Tau	M2	-55	6,2	0.03	-0.503	0.55	6.48	1.59	-8.86	0.65
DH Tau	M2	-72	4,2	0.00	-0.638	0.53	6.64	1.80	-8.95	0.63
CX Tau	M2.5	-20	3,2	0.15	-0.480	0.50	6.34	0.78	-9.43	0.58
FP Tau	M4	-38	3,2	0.00	-0.506	0.29	6.00	0.78	-9.45	0.32
LkHa 358	M5.5	-46	3,7	0.12	-2.058	0.087	7.16
MHO-5	M6	-50	7	0.23	-1.329	0.093	6.19
MHO-4	M6	-42	7	1.10	-1.097	0.10	< 6
Anon 13	M6	-41	7,6	4.03	-1.195	0.097	6.00
<u>Weak-lined T Tauri Stars</u>										
LkCa 19	K0	-1	3,2	0.74	0.216	1.24	7.22	-0.01	< -10	0.10
HBC 388	K1	+0.5	8,2	0.00	0.130	1.22	7.18	0.33	< -8.41	0.16
L1551-51	K7	-0.6	8,9,2	0.00	-0.310	0.79	6.54	0.31	< -9.50	0.18
V830 Tau	K7	-3	8,3,2	0.69	-0.101	0.77	6.19	0.44	< -8.97	0.07
V827 Tau	K7	-1.8	8,3,2	1.08	0.037	0.77	6.00	0.62	< -8.53	0.10
HBC 376	K7	-1.4	8,9,2	0.00	-0.434	0.81	6.79	0.63	< -9.30	0.11
LkCa 4	K7	-5	3,2	1.21	-0.020	0.76	6.03	0.52	< -8.73	0.18
Hubble 4	K7	-3.0	6,9,2	1.87	0.167	0.76	< 6	0.79	< -8.16	0.01
V819 Tau	K7	-1.7	6,2	1.64	-0.109	0.77	6.21	0.53	< -8.86	0.21
L1551-55	K7	-0.7	8,3,2	1.03	-0.363	0.80	6.64	0.25	< -9.70	0.17
LkCa 14	M0	-1	3,9,2	0.00	-0.170	0.70	6.17	0.74	< -8.85	0.18
Anon 1	M0	-3	3,9,2	2.08	0.061	0.69	< 6	0.34	< -8.94	0.14
IQ Tau	M0.5	-8	3,2	1.44	-0.143	0.68	6.11	1.45	< -8.32	0.96
X-ray 7	M0.5	-3.3	7,6	8.18	-0.122	0.68	6.08
LkCa 5	M2	-4	3,2	0.15	-0.532	0.54	6.50	-0.10	< 10	0.18
LkCa 1	M4	-4	3,2	0.00	-0.402	0.33	< 6	0.40	< -9.74	0.07
MHO-7	M5	-6.7	7	0.23	-0.981	0.16	6.17
MHO-6	M5	-12	7	0.54	-1.078	0.16	6.31
X-ray 5a	M5.5	-11	7,6	3.36	-0.878	0.13	< 6
X-ray 3	M6	-16	10	0.54	-1.154	0.10	6.00

Note. — The parameters derived for high accretion stars are listed in parentheses and are subject to large uncertainties (§3.1.1).

^a Spectral type uncertainties are one spectral subclass.

References. — (1) Hessman & Guenther (1997); (2) Kenyon & Hartmann (1995); (3) Herbig & Bell (1988); (4) Hartigan et al. (1994); (5) this work; (6) Strom & Strom (1994); (7) Briceño et al. (1998); (8) Walter et al. (1988); (9) Martin (1994); (10) Luhman et al. (1998)